2015

A SUBSYSTEM IDENTIFICATION APPROACH TO MODELING HUMAN CONTROL BEHAVIOR AND STUDYING HUMAN LEARNING

Xingye Zhang
University of Kentucky, xingyezhang86@gmail.com

STUDENT AGREEMENT:

I represent that my thesis or dissertation and abstract are my original work. Proper attribution has been given to all outside sources. I understand that I am solely responsible for obtaining any needed copyright permissions. I have obtained needed written permission statement(s) from the owner(s) of each third-party copyrighted matter to be included in my work, allowing electronic distribution (if such use is not permitted by the fair use doctrine) which will be submitted to UKnowledge as Additional File.

I hereby grant to The University of Kentucky and its agents the irrevocable, non-exclusive, and royalty-free license to archive and make accessible my work in whole or in part in all forms of media, now or hereafter known. I agree that the document mentioned above may be made available immediately for worldwide access unless an embargo applies.

I retain all other ownership rights to the copyright of my work. I also retain the right to use in future works (such as articles or books) all or part of my work. I understand that I am free to register the copyright to my work.

REVIEW, APPROVAL AND ACCEPTANCE

The document mentioned above has been reviewed and accepted by the student's advisor, on behalf of the advisory committee, and by the Director of Graduate Studies (DGS), on behalf of the program; we verify that this is the final, approved version of the student's thesis including all changes required by the advisory committee. The undersigned agree to abide by the statements above.

Xingye Zhang, Student

Dr. Jesse B. Hoagg, Major Professor

Dr. Haluk Karaca, Director of Graduate Studies

A SUBSYSTEM IDENTIFICATION APPROACH TO MODELING HUMAN CONTROL BEHAVIOR AND STUDYING HUMAN LEARNING

DISSERTATION

A dissertation submitted in partial fulfillment of the requirements for the degree of Doctor of Philosophy in the College of Engineering at the University of Kentucky

By

Xingye Zhang

Lexington, Kentucky

Co-Directors: Dr. Jesse B. Hoagg, Professor of Mechanical Engineering
and Dr. T. Michael Seigler, Professor of Mechanical Engineering

Lexington, Kentucky

ABSTRACT OF DISSERTATION

A SUBSYSTEM IDENTIFICATION APPROACH TO MODELING HUMAN CONTROL BEHAVIOR AND STUDYING HUMAN LEARNING

Humans learn to interact with many complex dynamic systems such as helicopters, bicycles, and automobiles. This dissertation develops a subsystem identification method to model the control strategies that human subjects use in experiments where they interact with dynamic systems. This work provides new results on the control strategies that humans learn.

We present a novel subsystem identification algorithm, which can identify unknown linear time-invariant feedback and feedforward subsystems interconnected with a known linear time-invariant subsystem. These subsystem identification algorithms are analyzed in the cases of noiseless and noisy data.

We present results from human-in-the-loop experiments, where human subjects interact with a dynamic system multiple times over several days. Each subject's control behavior is assumed to have feedforward (or anticipatory) and feedback (or reactive) components, and is modeled using experimental data and the new subsystem identification algorithms. The best-fit models of the subjects' behavior suggest that humans learn to control dynamic systems by approximating the inverse of the dynamic system in feedforward. This observation supports the internal model hypothesis in neuroscience. We also examine the impact of system zeros on a human's ability to control a dynamic system, and on the control strategies that humans employ.

KEYWORDS: Human Motor Control, Human Learning, Human-In-The-Loop, Subsystem Identification

Xingye Zhang
December 13, 2015

A Subsystem Identification Approach to Modeling Human Control Behavior and Studying Human Learning

By

Xingye Zhang

Dr. Jesse B. Hoagg

Co-Director of Dissertation

Dr. T. Michael Seigler

Co-Director of Dissertation

Dr. Haluk Karaca

Director of Graduate Studies

December 13, 2015

Acknowledgements

I would like to thank my family for supporting and encouraging me to pursue what I love wholeheartedly.

I would also like to thank my advisor Dr. Hoagg for all the time, effort, support, and encouragement he has given me over the past three and a half years as one of his students. He has been an unbelievable mentor, and I could not have done this without his help and guidance. I also would like to thank Dr. Seigler for all the time, effort, support, and encouragement he has given me on the human learning project. Moreover, I would like to thank Dr. Smith and Dr. Walcott for serving on my committee, and Dr. Adams for serving as the outside examiner.

I am also indebted to all of my friends that I have met over the course of my time including those at Shenyang (China), Beijing (China), Storrs (CT), and Lexington (KY). All of you have been amazing friends and have always been there for me when I needed it most.

Finally, I would like to thank Dr. Sheetz and Mr. Gazula from the Center for Computational Sciences at the University of Kentucky for providing assistance in coding for parallel computation, and thank the Department of Mechanical Engineering, National Science Foundation (award number: CMMI 1405257), and the Kentucky Science and Engineering Foundation (award number: KSEF- 148-502-12-288) for financial support.

Table of Contents

List of Figures

Chapter 1 Introduction

1.1 Motivation

In 1997, the IBM supercomputer Deep Blue beat the world chess champion. In 2011, the newer supercomputer Watson beat human opponents on the quiz show Jeopardy and answered questions using natural conversational language. Both of these supercomputers are able to mimic certain human behavior. However, neither playing chess nor answering questions involves performing physical tasks or interacting with complex dynamic systems.

Robots have been designed to perform some common physical tasks such as pouring water from a bottle into a cup [1], running and kicking a ball [2], and separating a Oreo [3]. However, robots currently cannot compete against humans and win the World Cup Championship in soccer. In contrast to robots, humans learn to perform complex motions with their bodies and learn to interact with complex external dynamic systems.

Humans possess two primary advantages over current automatic control technology. First, humans have an enormous array of sensors and more than 600 actuators. Second, the human brain contains an effective control architecture, which adapts to uncertainty and learns from previous experiences. A human's sensor-and-actuator advantage diminishes when interacting with simple systems or performing simple tasks. In fact, humans' sensors and actuators have poor precision and low bandwidth in comparison to components used in control systems. Thus, tasks that require precision and speed are generally performed by machines. However, humans maintain one

advantage over control systems, namely, the ability to learn and adapt to uncertainty.

Consider a child learning to ride a bicycle. At first, a child has no idea how to ride a bicycle. Yet, after practicing, the child learns to ride. This leads to several questions: (Q1) How do humans control dynamic systems? (Q2) How do humans *learn* to interact with unknown dynamic systems? (Q3) What characteristics make systems difficult for a human to control. Questions (Q1)—(Q3) inspire us to study human motor control and human learning.

An improved understanding of human motor control and human learning has the potential to advance a variety of technologies:

(1) *Control Systems.* No existing control technique can match a human's ability to learn to interact with a wide variety of uncertain dynamic systems. Studying human learning could help us identify human learning mechanisms that are superior to automatic control methods.

(2) *Robotics.* A human's ability to learn to interact with a wide variety of uncertain dynamic systems cannot currently be emulated by robots. Studying human learning offers a chance to improve our understanding of human learning mechanisms and to adopt those mechanisms for robotics.

(3) *Assistive System.* Significant training is necessary for humans to learn to control many dynamic systems such as medical devices, prostheses, aircraft, and automobiles. Studying human learning could lead to techniques that accelerate the learning process.

(4) *Motor Rehabilitation.* Studying human motor control could advance robotic-therapy devices, thus helping people with impaired motor control.

1.2 Human Motor Control and Human Learning

Human motor control and human learning has been a subject of interest in neuroscience for over 30 years. The fundamental question is to determine how the central nervous system (CNS) directs motion. A predominant theory in neuroscience is called the internal model hypothesis (IMH), which proposes that the CNS constructs models of the body and its interactions with the physical world, and these models are continuously updated and used for control. Internal models were first suggested in the 1970s [4, 5]. Subsequent studies provide evidence that support internal models within the cerebellum [6, 7].

Different approaches are used to explore the IMH, including reaching experiments [8–13], grip-force experiments [14–24], sensory-time-delay studies [6, 7, 25–38], and comparisons of experimental data with proposed mathematical models [8, 38–52].

In the reaching experiment [10], a human subject grasps a robot manipulator and moves it to a specified target position. There is a position-and-velocity-dependent external force acting on the robot manipulator, which can be regarded as a change to the subject's arm dynamics. When the external force is zero, subjects tend to move the manipulator in a straight line with a bell-shaped velocity profile [8]. If the position-and-velocity-dependent force is present, then the subjects initially deviate from the straight-line path. However, after a sufficient number of attempts, subjects tend to recover the zero-force straight-line path. If the external force is subsequently removed, then the subjects deviate from the straight-line path in a manner that mirrors the initial deviations. The results of reaching experiments are often interpreted with internal models.

In the grip-force experiments [15, 16], human subjects are asked to hold an object using their thumb and index finger, and lift the object vertically. The grip force is normal to the surface, where the tips of the fingers contact the object, and the load

force is tangential to that surface. When lifting the object, a subjects' grip force is adjusted in concert with the load force such that the grip force is slightly larger than the minimum required force to prevent slipping. One explanation for the relationship between grip force and load force is that the subjects construct internal models of the object and the lifting process [22].

The CNS relies primarily on feedback from the cutaneous mechanoreceptors in the fingertips to regulate grip pressure [16–21]. In [23, 24], a subject was initially trained on griping an object with their fingers and moving the object up and down vertically. Then, the subject's hands were anesthetized to remove sensory feedback and the grip-force experiment was repeated. The subject's grip force with anesthesia was larger than their grip force without anesthesia. Moreover, the subject's grip forces with and without anesthesia are modulated in concert with load force. One possible explanation for the relationship between grip force and load force is that an internal model enables the anesthetized subject to alter the grip force as required despite the lack of sensory feedback.

From the viewpoint of sensory time delays, it is argued that time delays (30–50 ms) in sensory feedback are too large to allow for rapid control of muscles based solely on feedback [6, 7]. In [30–32], healthy subjects perform a grip-force experiment during rapid arm movement. The subjects' grip force was modulated in concert with fluctuations in load force, which is acceleration dependent [30–32]. The relationship between grip force and load force, that is, the absence of lag between grip force and load force, can be explained by the existence of internal models [22].

The human optical system is another example where sensory delay is used as evidence of internal models. There is approximately 100 ms of delay between retinal stimulus and perception in the human optical system [33–35]. This has led to the study of saccades, which are rapid eye movements used to track a target. There is an initial delay in eye movement of 90–120 ms when tracking a moving target.

Thus, continuous eye movement cannot immediately catch the target, and a saccade is initiated to catch up [48]. Due to the slow response of the optical system, it is believed that saccades do not rely solely on feedback, and thus, an internal model is required [36–38].

In [8,38–52], the IMH is explored by comparing the results of human control experiments with proposed mathematical models constructed using the IMH. The mathematical models include predictor models, state estimators, forward models, and inverse models. For example, in [44], healthy subjects performed in-the-dark arm movements both with and without constant forcing. The crucial finding from this study is that the position errors are larger with constant external forcing. Assuming proprioception (i.e., sensory feedback from the muscles, limbs, and joints) is not affected by external forcing, this indicates that the CNS alters sensory feedback. The errors between a subject's estimated position and the actual position agreed qualitatively with the behavior of a Kalman filter. The authors of [44] conclude that the experiment supports the existence of an observer, which implies the existence of an internal model.

Although evidence has been given in support of the IMH, other possibilities exist. Many of the results discussed thus far have other interpretations [53–59]. The equilibrium point hypothesis, also called the $\lambda-$model, is another theory. The equilibrium point hypothesis proposes that voluntary movements arise from changes in the CNS's equilibrium state, resulting from motor apparatus, external force, and sensory interactions.

1.3 Human-In-The-Loop Control Experiments

In this dissertation, we design and conduct human-in-the-loop (HITL) experiments, where human subjects learn to interact with unknown dynamic systems, which are simulated by a computer. A subject's dominant hand is used to manipulate a single-

degree-of-freedom joystick, which affects the motion of an object displayed on a computer screen as shown in Figure 1.1(a). The controlled objects position and the joystick position are functions of time and are related to each other by a dynamic system. A reference object also moves on the computer screen. The subject's objective is to manipulate the joystick in a manner that makes the controlled object and the reference object have the same position at each instant of time. Thus, these experiments examine a human's approach to command following. Figure 1.1(b) shows a subject performing the experiment.

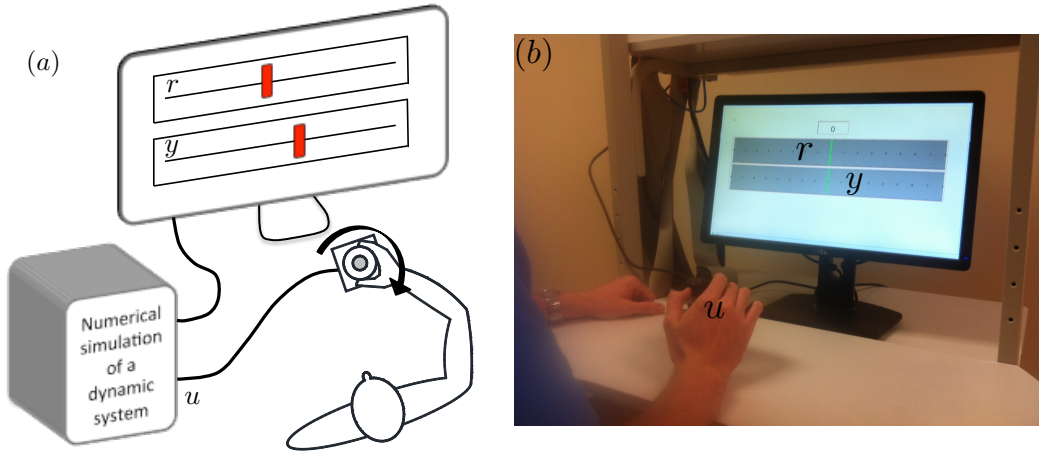

Figure 1.1: Figure (a) shows a human subject using a joystick to affect the motion of an object on a computer screen. The object's position y represents the output of a dynamic system that is simulated by a computer, and the joystick position u represents the input to the system. A reference object is also displayed on the screen and its position is r. Figure (b) shows a subject performing the experiment.

The human subject's joystick position u is the input to a dynamic system, which is programed into the computer. The controlled object's position y is the output of this dynamic system, and the reference object's position r is an exogenous signal. Together, the human and the computer-simulated dynamic system comprise a closed-loop HITL dynamic system as shown in Figure 1.2.

We record the time-domain data r, u, and y, where u and y contain information of the human subject's behavior. Our objective is to construct a model of a human

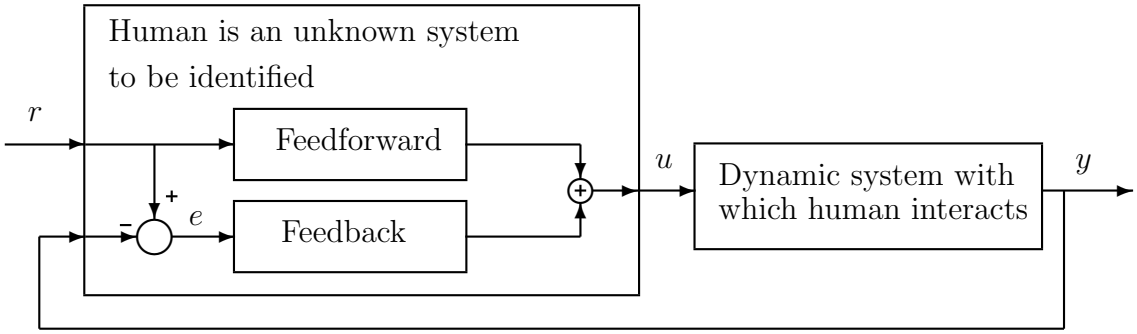

Figure 1.2: Modeling a human's control strategy can be viewed as an SSID problem, where r and y are measured and the dynamic system with which the human interacts is assumed to be known.

subject's behavior using the experimental data—this is a subsystem identification problem.

1.4 Modeling Human Control Behavior Using Subsystem Identification

System identification is the process of building empirical models of an unknown dynamic system by using measured input and output data [60–62]. In contrast, subsystem identification (SSID) is the process of building empirical models of unknown dynamic subsystems, which are interconnected with known dynamic subsystems. These connections can be series, parallel, or feedback. SSID relies on measured data to identify the unknown subsystems. However, not all input and output signals to the unknown subsystems are necessarily accessible, that is, available for measurement.

Consider the HITL experiment in Figure 1.1, where a human interacts with a dynamic system by using feedback y and external information r (e.g., a command) to generate a control u as shown in Figure 1.2. In this scenario, the human is an unknown subsystem, which can include both feedback and feedforward. The feedback-feedforward architecture is a general structure to model human's behavior. See [6] for a physiological interpretation of this architecture.

Modeling the human's control strategy can be viewed as a closed-loop SSID prob-

lem, where r and y are measured and the dynamic system with which the human interacts is assumed to be known. Note that the control u may also be measured. However, u is the sum of feedback and feedforward terms, but each individual term is inaccessible.

Closed-loop SSID is distinct from the well-studied problem of system identification in closed loop [62–65]. A distinguishing feature of closed-loop SSID is that the unknown subsystems have inputs and outputs that are inaccessible.

There is interest in modeling HITL behavior for applications such as aircraft [66–69] and automobiles [70–72]. In addition, SSID methods can be used to model human behavior in motor control experiments [73–76].

SSID also has applications in biology and physics. For example, many biological systems are modeled by the interconnection of subsystems [77], which may be unknown and have inaccessible inputs and outputs. Similarly, physical systems are often modeled by a composition of subsystems, which are based on either physical laws or empirical information. For example, in [78], a large-scale physics-based model of the global ionosphere-thermosphere is improved by using measured data to estimate thermal conductivity, which can be regarded as an unknown feedback subsystem. In this application, the output of the unknown subsystem is inaccessible.

Existing methods for SSID are given in [78–90]. Specifically, [79–81] present methods for static subsystems, while [78, 82–90] present methods for dynamic subsystems. In the dynamic SSID literature, the approaches in [82–86] are restricted to open-loop SSID, that is, identification of subsystems interconnected without feedback. We note that [85, 86] use open-loop SSID to model the dynamics of human subsystems. Specifically, [85] identifies a transfer function that models a human's precision grip force dynamics, whereas [86] identifies two transfer functions that together model a human's oculomotor subsystem.

In contrast to [79–86], the work in this dissertation focuses on dynamic closed-loop

SSID, that is, identification of dynamic subsystems with feedback. Existing dynamic closed-loop SSID methods include [78, 87–90]. In particular, [87] identifies a transfer function that models the behavior of a human subject interacting in feedback with a mechanical system. However, the method in [87] applies to systems with feedback only, that is, systems without feedforward. Note that the methods in [78, 87–90] are time-domain techniques and yield identified models that may not result in an asymptotically stable closed-loop system.

In this dissertation, we present closed-loop SSID techniques that: i) identify feedback and feedforward subsystems, and ii) ensure asymptotic stability of the identified closed-loop transfer function. Characteristics i) and ii) of the SSID algorithm are motivated by the application to modeling human control behavior. First, humans generally use both anticipatory (feedforward) and reactive (feedback) control [6, 7], which motivates i). Second, if a HITL system has a bounded output, then it is desirable to identify subsystems that result in an asymptotically stable closed-loop transfer function, thus motivating ii). In addition, human control behavior is band limited; specifically, humans cannot produce motion with arbitrarily high frequency. Thus, models over a limited frequency range are to be identified, which motivates the development of new SSID techniques in the frequency domain.

1.5 Overview of Dissertation

Chapter 2. We present a frequency-domain SSID algorithm, which identifies unknown feedback and feedforward subsystems that are interconnected with a known subsystem. This method requires only accessible input and output measurements, applies to linear time-invariant (LTI) subsystems, and uses a candidate-pool approach to ensure asymptotic stability of the identified closed-loop transfer function. The algorithm is analyzed in the cases of noiseless and noisy data. The main analytic result of this chapter shows that the coefficients of the identified feedback and feed-

forward transfer functions are arbitrarily close to the true coefficients if the data noise is sufficiently small and the candidate pool is sufficiently dense.

The new contributions of this chapter are: i) an SSID method that identifies both feedback and feedforward controllers and guarantees the stability of the identified closed-loop transfer function; and ii) an analysis of the SSID algorithm in the cases of noiseless and noisy data.

Chapter 3. We present results from a HITL experiment in which human subjects learn to control an unknown dynamic system over 40 trials. For each trial, the SSID algorithm in Chapter 2 is used to estimate each subject's feedforward control and feedback control. Over the 40 trials, the magnitudes of the identified feedback controllers do not change significantly, whereas the identified feedforward controllers do change significantly. By the last trial, the average identified feedforward controller approximates the inverse of the dynamic system. This observation provides evidence that a fundamental component of human learning is updating the anticipatory control until it models the inverse dynamics, which supports the IMH.

The new contribution of this chapter is the use of SSID to model human control behavior in a HITL experiment. The identified models of the human behavior provide evidence in support of the IMH.

Chapter 4. The SSID algorithm from Chapter 2 is extended to address multivariable feedback and feedforward subsystems that are interconnected with a known subsystem, where the feedback does not have to be measured. This method requires only accessible input and output measurements, applies to multivariable discrete-time LTI subsystems, and uses a candidate-pool approach to ensure asymptotic stability of the identified closed-loop transfer function. The algorithm is analyzed in the cases of noiseless and noisy data. The main analytic result shows that the coefficients of the identified feedback and feedforward transfer functions are arbitrarily close to the true coefficients if the data noise is sufficiently small and the candidate pool is sufficiently

dense.

The new contributions of this chapter are: i) an SSID method that identifies multivariable LTI feedback and feedforward controllers and guarantees the stability of the identified closed-loop transfer function; and ii) an analysis of the multivariable SSID algorithm in the cases of noiseless and noisy data.

Chapter 5. We present results from a HITL experiment in which human subjects learn to control 3 different unknown dynamic systems over 40 trials. One of the dynamic systems has a minimum-phase zero, one has a nonminimum-phase zero, and one has a slower (i.e., closer to the imaginary axis) nonminimum-phase zero. For each dynamic system, the command-following error tends to decrease over 40 trials. The average command-following error for the minimum-phase system is smaller than that for the nonminimum-phase system, which is smaller than that for the system with the slower nonminimum-phase zero. Thus, the systems with a nonminimum-phase zeros are harder to control than the minimum-phase system.

For the minimum-phase and nonminimum-phase system, we use the SSID algorithm in Chapter 4 to model each subject's feedback and feedforward control on each trial. For both systems, the average identified feedforward controllers approximate the inverse of the dynamic system. This observation supports the IMH. However, the average identified feedforward controller for the minimum-phase system is closer to the inverse dynamics than the one for the nonminimum-phase system. We discuss why this result as well as other factors may help explain why nonminimum-phase zeros make systems difficult for humans to control.

The new contribution of this chapter is the use of SSID to model human control behavior when interacting with a nonminimum-phase system. The identified models of the human behavior provide evidence in support of the IMH. Another new contribution is the exploration on the impact of system zeros on human motor control and human learning.

In this dissertation, the notation is defined and valid within each chapter.

Chapter 2 Subsystem Identification for Single-Input Single-Output Subsystems

In this chapter, we present a frequency-domain subsystem identification algorithm that identifies unknown feedback and feedforward subsystems that are interconnected with a known subsystem. This method requires only accessible input and output measurements, applies to linear time-invariant subsystems, and uses a candidate-pool approach to ensure asymptotic stability of the identified closed-loop transfer function. The algorithm is analyzed in the cases of noiseless and noisy data. The main analytic result of this chapter shows that the coefficients of the identified feedback and feedforward transfer functions are arbitrarily close to the true coefficients if the data noise is sufficiently small and the candidate pool is sufficiently dense. This subsystem identification approach has application to modeling the control behavior of humans interacting with and receiving feedback from a dynamic system. The methods and results of this chapter are published in [91, 92].

2.1 Introduction

Consider a scenario where a human interacts with a dynamic system by using feedback y and external information r (e.g., a command) to generate a control u as shown in Figure 2.1. In this scenario, the human is an unknown subsystem, which can include both feedback and feedforward. Modeling the human's control strategy can be viewed as a subsystem identification (SSID) problem, where r and y are measured and the dynamic system with which the human interacts is assumed to be

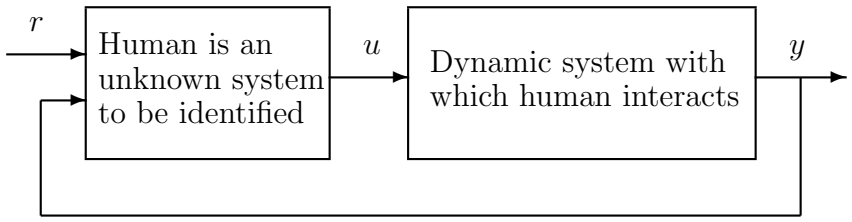

Figure 2.1: Modeling a human's control strategy can be viewed as an SSID problem, where r and y are measured and the dynamic system with which the human interacts is assumed to be known.

known. The internal signals that the human uses to construct u are inaccessible (i.e., unmeasurable). For example, if u is the sum of feedback and feedforward terms, then these individual terms are inaccessible.

Existing methods for SSID are given in [78–90]. Specifically, [79–81] present methods for static subsystems, while [78, 82–90] present methods for dynamic subsystems. In the dynamic SSID literature, the approaches in [82–86] are restricted to open-loop SSID, that is, identification of subsystems interconnected without feedback.

In contrast to [79–86], the work in this dissertation focuses on dynamic closed-loop SSID, that is, identification of dynamic subsystems with feedback. Existing dynamic closed-loop SSID methods include [78, 87–90]. In particular, [87] identifies a transfer function that models the behavior of a human subject interacting in feedback with a mechanical system. However, the method in [87] applies to systems with feedback only, that is, systems without feedforward. Note that the methods in [78, 87–90] are time-domain techniques and yield identified models that may not result in an asymptotically stable closed-loop system.

This chapter presents a new closed-loop SSID technique that: i) identifies feedback and feedforward subsystems, and ii) ensures asymptotic stability of the identified closed-loop transfer function. A closed-loop SSID method that addresses both i) and ii) is a new contribution of this chapter. The method relies on a candidate-pool approach to accomplish ii). Another contribution of this chapter is an analysis of the properties of the SSID algorithm in the cases of noiseless and noisy data. Our main

analytic result shows that the coefficients of the identified feedback and feedforward transfer functions are arbitrarily close to the true coefficients if the data noise is sufficiently small and the candidate pool is sufficiently dense.

Characteristics i) and ii) of the SSID algorithm are motivated by the application to modeling human control behavior. First, humans generally use both anticipatory (feedforward) and reactive (feedback) control [6, 7], which motivates i). Second, if a human-in-the-loop system has a bounded output, then it is desirable to identify subsystems that result in an asymptotically stable closed-loop transfer function, thus motivating ii). In addition, human control behavior is band limited; specifically, humans cannot produce motion with arbitrarily high frequency. Thus, models over a limited frequency range are to be identified, which motivates the development of a new SSID technique in the frequency domain.

2.2 Problem Formulation

Consider the linear time-invariant system shown in Figure 2.2, where r, y, σ_r, and σ_y are the Laplace transforms of the input, output, input noise, and output noise, respectively, and for $G_{\mathrm{ff}}, G_{\mathrm{fb}}, G_{\mathrm{p}} \colon \mathbb{C} \to \mathbb{C}$ is a real rational transfer function. If $\sigma_r = 0$

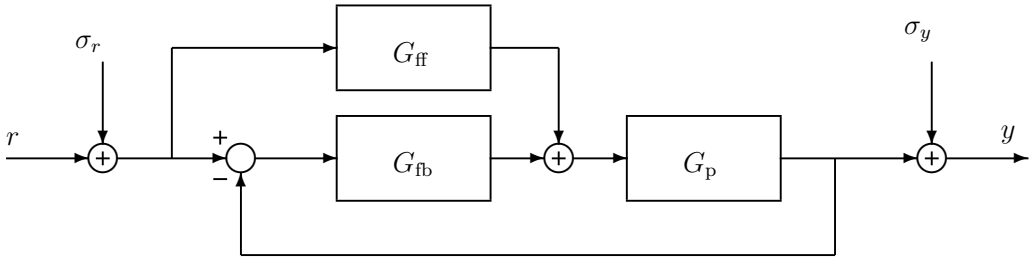

Figure 2.2: The input r and output y of this linear time-invariant system are measured, but all internal signals are inaccessible.

and $\sigma_y = 0$, then the closed-loop transfer function from r to y is given by

$$\tilde{G}(s) \triangleq \frac{G_{\mathrm{p}}(s)G_{\mathrm{ff}}(s) + G_{\mathrm{p}}(s)G_{\mathrm{fb}}(s)}{1 + G_{\mathrm{p}}(s)G_{\mathrm{fb}}(s)}. \tag{2.1}$$

Next, let N be a positive integer, and define $\mathcal{N} \triangleq \{1, 2, \ldots, N\}$. For all $k \in \mathcal{N}$, let $\omega_k \in (0, \infty)$, where $\omega_1 < \cdots < \omega_N$. Furthermore, for all $k \in \mathcal{N}$, define the *closed-loop frequency response data*

$$H(\omega_k) \triangleq \frac{y(\jmath\omega_k)}{r(\jmath\omega_k)} = \tilde{G}(\jmath\omega_k) + \sigma(\jmath\omega_k), \tag{2.2}$$

where $\sigma(s) \triangleq [\tilde{G}(s)\sigma_r(s) + \sigma_y(s)]/r(s)$. If $\sigma(\jmath\omega_k) \equiv 0$, then $\{H(\omega_k)\}_{k=1}^N$ is noiseless. In contrast, if $\sigma(\jmath\omega_k) \not\equiv 0$, then $\{H(\omega_k)\}_{k=1}^N$ is noisy.

We present a method to identify G_{ff} and G_{fb}, provided that G_{p} and $\{H(\omega_k)\}_{k=1}^N$ are known and $G_{\mathrm{p}} \neq 0$. In this case, the closed-loop frequency response data $\{H(\omega_k)\}_{k=1}^N$ can be obtained from the accessible signals r and y and does not depend on the internal signals, which are not assumed to be measured.

Note that $G_{\mathrm{ff}}, G_{\mathrm{fb}}, G_{\mathrm{p}}$ can be expressed as

$$G_{\mathrm{ff}}(s) = \frac{N_{\mathrm{ff}}(s)}{D_{\mathrm{ff}}(s)}, \qquad G_{\mathrm{fb}}(s) = \frac{N_{\mathrm{fb}}(s)}{D_{\mathrm{fb}}(s)}, \qquad G_{\mathrm{p}}(s) = \frac{N_{\mathrm{p}}(s)}{D_{\mathrm{p}}(s)},$$

where N_{ff} and D_{ff}, N_{fb} and D_{fb}, and N_{p} and D_{p} are coprime, and $D_{\mathrm{ff}}, D_{\mathrm{fb}}, D_{\mathrm{p}}$ are monic. Define

$$n_{\mathrm{ff}} \triangleq \deg N_{\mathrm{ff}}, d_{\mathrm{ff}} \triangleq \deg D_{\mathrm{ff}}, n_{\mathrm{fb}} \triangleq \deg N_{\mathrm{fb}}, d_{\mathrm{fb}} \triangleq \deg D_{\mathrm{fb}}, n_{\mathrm{p}} \triangleq \deg N_{\mathrm{p}}, d_{\mathrm{p}} \triangleq \deg D_{\mathrm{p}}.$$

Thus, (2.1) can be expressed as

$$\tilde{G}(s) = \frac{N_{\mathrm{p}}(s)\left[D_{\mathrm{fb}}(s)N_{\mathrm{ff}}(s) + D_{\mathrm{ff}}(s)N_{\mathrm{fb}}(s)\right]}{D_{\mathrm{ff}}(s)\left[D_{\mathrm{p}}(s)D_{\mathrm{fb}}(s) + N_{\mathrm{p}}(s)N_{\mathrm{fb}}(s)\right]}.$$

We make the following assumptions:

(A2.1) d_{ff}, d_{fb}, n_{ff}, and n_{fb} are known.

(A2.2) $d_{\mathrm{p}} + d_{\mathrm{fb}} > n_{\mathrm{p}} + n_{\mathrm{fb}}$.

(A2.3) $N > d_{\mathrm{p}} + d_{\mathrm{ff}} + d_{\mathrm{fb}} + n_{\mathrm{p}} + \max\{n_{\mathrm{ff}} + d_{\mathrm{fb}}, n_{\mathrm{fb}} + d_{\mathrm{ff}}\}$.

(A2.4) If $\lambda \in \mathbb{C}$ and $D_{\mathrm{ff}}(\lambda)\,[D_{\mathrm{p}}(\lambda)D_{\mathrm{fb}}(\lambda) + N_{\mathrm{p}}(\lambda)N_{\mathrm{fb}}(\lambda)] = 0$, then $\operatorname{Re}\lambda < 0$.

Assumption (A2.1) can be replaced by the assumption that upper bounds on d_{ff}, d_{fb}, n_{ff}, and n_{fb} are known. However, (A2.1) is invoked for clarity of the presentation. Assumption (A2.2) states that the loop transfer function $G_{\mathrm{p}}G_{\mathrm{fb}}$ is strictly proper. Assumption (A2.3) implies that the number N of frequency response data points is sufficiently large. This assumption ensures that the minimization problem solved in the SSID has a unique solution. Assumption (A2.4) implies that $\tilde{G}$ is asymptotically stable, that is, the poles of $\tilde{G}$ are in the open-left-half complex plane.

Define $d \triangleq d_{\mathrm{ff}} + d_{\mathrm{fb}} + n_{\mathrm{fb}} + 1$, and for all nonnegative integers j, let $\Gamma_j : \mathbb{C} \to \mathbb{C}^{j+1}$ be given by $\Gamma_j(s) \triangleq \begin{bmatrix} s^j & s^{j-1} & \cdots & s & 1 \end{bmatrix}^{\mathrm{T}}$. Consider the functions $\mathcal{N}_{\mathrm{ff}} \colon \mathbb{C} \times \mathbb{R}^{n_{\mathrm{ff}}+1} \to \mathbb{C}$ and $\mathcal{D}_{\mathrm{ff}}, \mathcal{N}_{\mathrm{fb}}, \mathcal{D}_{\mathrm{fb}} \colon \mathbb{C} \times \mathbb{R}^{d} \to \mathbb{C}$ given by

$$\mathcal{N}_{\mathrm{ff}}(s,\beta) \triangleq \Gamma_{n_{\mathrm{ff}}}^{\mathrm{T}}(s)\beta, \qquad \mathcal{D}_{\mathrm{ff}}(s,\phi) \triangleq s^{d_{\mathrm{ff}}} + \Gamma_{d_{\mathrm{ff}}-1}^{\mathrm{T}}(s)E_1\phi,$$
$$\mathcal{N}_{\mathrm{fb}}(s,\phi) \triangleq \Gamma_{n_{\mathrm{fb}}}^{\mathrm{T}}(s)E_2\phi, \qquad \mathcal{D}_{\mathrm{fb}}(s,\phi) \triangleq s^{d_{\mathrm{fb}}} + \Gamma_{d_{\mathrm{fb}}-1}^{\mathrm{T}}(s)E_3\phi,$$

where $\beta \in \mathbb{R}^{n_{\mathrm{ff}}+1}$, $\phi \in \mathbb{R}^{d}$, and

$$E_1 \triangleq \begin{bmatrix} I_{d_{\mathrm{ff}}} & 0_{d_{\mathrm{ff}} \times (d_{\mathrm{fb}}+n_{\mathrm{fb}}+1)} \end{bmatrix} \in \mathbb{R}^{d_{\mathrm{ff}} \times d},$$
$$E_2 \triangleq \begin{bmatrix} 0_{(n_{\mathrm{fb}}+1) \times d_{\mathrm{ff}}} & I_{n_{\mathrm{fb}}+1} & 0_{(n_{\mathrm{fb}}+1) \times d_{\mathrm{fb}}} \end{bmatrix} \in \mathbb{R}^{(n_{\mathrm{fb}}+1) \times d},$$
$$E_3 \triangleq \begin{bmatrix} 0_{d_{\mathrm{fb}} \times (d_{\mathrm{ff}}+n_{\mathrm{fb}}+1)} & I_{d_{\mathrm{fb}}} \end{bmatrix} \in \mathbb{R}^{d_{\mathrm{fb}} \times d}.$$

Next, consider the functions $\mathcal{G}_{\mathrm{ff}} \colon \mathbb{C} \times \mathbb{R}^{n_{\mathrm{ff}}+1} \times \mathbb{R}^{d} \to \mathbb{C}$ and $\mathcal{G}_{\mathrm{fb}} \colon \mathbb{C} \times \mathbb{R}^{d} \to \mathbb{C}$ given by

$$\mathcal{G}_{\mathrm{ff}}(s,\beta,\phi) \triangleq \frac{\mathcal{N}_{\mathrm{ff}}(s,\beta)}{\mathcal{D}_{\mathrm{ff}}(s,\phi)}, \qquad \mathcal{G}_{\mathrm{fb}}(s,\phi) \triangleq \frac{\mathcal{N}_{\mathrm{fb}}(s,\phi)}{\mathcal{D}_{\mathrm{fb}}(s,\phi)},$$

which, for each $\beta \in \mathbb{R}^{n_{\mathrm{ff}}+1}$ and $\phi \in \mathbb{R}^{d}$, are real rational transfer functions.

Our objective is to determine β and ϕ such that $\mathcal{G}_{\mathrm{ff}}$ and $\mathcal{G}_{\mathrm{fb}}$ approximate G_{ff} and G_{fb}, respectively. To achieve this objective, consider the cost function

$$J(\beta,\phi) \triangleq \sum_{k=1}^{N} \left| \frac{N_{\mathrm{p}}(\jmath\omega_k)\left[\mathcal{D}_{\mathrm{fb}}(\jmath\omega_k,\phi)\mathcal{N}_{\mathrm{ff}}(\jmath\omega_k,\beta)+\mathcal{D}_{\mathrm{ff}}(\jmath\omega_k,\phi)\mathcal{N}_{\mathrm{fb}}(\jmath\omega_k,\phi)\right]}{\mathcal{D}_{\mathrm{ff}}(\jmath\omega_k,\phi)\left[D_{\mathrm{p}}(\jmath\omega_k)\mathcal{D}_{\mathrm{fb}}(\jmath\omega_k,\phi)+N_{\mathrm{p}}(\jmath\omega_k)\mathcal{N}_{\mathrm{fb}}(\jmath\omega_k,\phi)\right]} - H(\omega_k) \right|^2, \tag{2.3}$$

which is a measure of the difference between the frequency response data $\{H(\omega_k)\}_{k=1}^{N}$ and the closed-loop transfer function obtained from the estimates $\mathcal{G}_{\mathrm{ff}}$ and $\mathcal{G}_{\mathrm{fb}}$. Note that J is nonlinear and nonconvex in (β,ϕ).

Let $\beta_* \in \mathbb{R}^{n_{\mathrm{ff}}+1}$ and $\phi_* \in \mathbb{R}^d$ be such that, for all $s \in \mathbb{C}$, $N_{\mathrm{ff}}(s) = \mathcal{N}_{\mathrm{ff}}(s,\beta_*)$, $D_{\mathrm{ff}}(s) = \mathcal{D}_{\mathrm{ff}}(s,\phi_*)$, $N_{\mathrm{fb}}(s) = \mathcal{N}_{\mathrm{fb}}(s,\phi_*)$, and $D_{\mathrm{fb}}(s) = \mathcal{D}_{\mathrm{fb}}(s,\phi_*)$.

If $\sigma(\jmath\omega_k) \equiv 0$, then $J(\beta_*,\phi_*) = 0$, which implies that the true parameters β_* and ϕ_* minimize the cost function (2.3) if the closed-loop frequency response data $\{H(\omega_k)\}_{k=1}^{N}$ is noiseless.

2.3 Subsystem Identification

We now develop an SSID algorithm to obtain estimates of β_* and ϕ_*, and thus estimates of G_{ff} and G_{fb}. Consider the function $\tilde{\mathcal{G}}\colon \mathbb{C}\times\mathbb{R}^{n_{\mathrm{ff}}+1}\times\mathbb{R}^d \to \mathbb{C}$ defined by

$$\tilde{\mathcal{G}}(s,\beta,\phi) \triangleq \frac{\tilde{\mathcal{N}}_1(s,\phi)\beta + \tilde{\mathcal{N}}_2(s,\phi)}{\tilde{\mathcal{D}}(s,\phi)}, \tag{2.4}$$

where

$$\tilde{\mathcal{D}}(s,\phi) \triangleq \mathcal{D}_{\mathrm{ff}}(s,\phi)\left[D_{\mathrm{p}}(s)\mathcal{D}_{\mathrm{fb}}(s,\phi)+N_{\mathrm{p}}(s)\mathcal{N}_{\mathrm{fb}}(s,\phi)\right], \tag{2.5}$$

$$\tilde{\mathcal{N}}_1(s,\phi) \triangleq N_{\mathrm{p}}(s)\mathcal{D}_{\mathrm{fb}}(s,\phi)\Gamma_{n_{\mathrm{ff}}}^{\mathrm{T}}(s), \tag{2.6}$$

$$\tilde{\mathcal{N}}_2(s,\phi) \triangleq N_{\mathrm{p}}(s)\mathcal{D}_{\mathrm{ff}}(s,\phi)\mathcal{N}_{\mathrm{fb}}(s,\phi). \tag{2.7}$$

Note that $\tilde{\mathcal{G}}(s,\beta,\phi)$ is the closed-loop transfer function obtained using β and ϕ. It follows from (2.3)–(2.7) that

$$J(\beta,\phi)=\sum_{k=1}^{N}|\tilde{\mathcal{G}}(\jmath\omega_k,\beta,\phi)-H(\omega_k)|^2. \tag{2.8}$$

Next, define

$$\Omega_0(\phi)\triangleq\sum_{k=1}^{N}\left|\frac{\tilde{\mathcal{N}}_2(\jmath\omega_k,\phi)}{\tilde{\mathcal{D}}(\jmath\omega_k,\phi)}-H(\omega_k)\right|^2\in\mathbb{R}, \tag{2.9}$$

$$\Omega_1(\phi)\triangleq 2\mathrm{Re}\sum_{k=1}^{N}\left[\frac{\tilde{\mathcal{N}}_1(\jmath\omega_k,\phi)}{\tilde{\mathcal{D}}(\jmath\omega_k,\phi)}\right]^*\left[\frac{\tilde{\mathcal{N}}_2(\jmath\omega_k,\phi)}{\tilde{\mathcal{D}}(\jmath\omega_k,\phi)}-H(\omega_k)\right]\in\mathbb{R}^{n_{\mathrm{ff}}+1}, \tag{2.10}$$

$$\Omega_2(\phi)\triangleq \mathrm{Re}\sum_{k=1}^{N}\left[\frac{\tilde{\mathcal{N}}_1(\jmath\omega_k,\phi)}{\tilde{\mathcal{D}}(\jmath\omega_k,\phi)}\right]^*\left[\frac{\tilde{\mathcal{N}}_1(\jmath\omega_k,\phi)}{\tilde{\mathcal{D}}(\jmath\omega_k,\phi)}\right]\in\mathbb{R}^{(n_{\mathrm{ff}}+1)\times(n_{\mathrm{ff}}+1)}, \tag{2.11}$$

where $[\,\cdot\,]^*$ denotes the complex conjugate transpose. Thus, (2.8) can be expressed as

$$J(\beta,\phi)=\beta^{\mathrm{T}}\Omega_2(\phi)\beta+\Omega_1^{\mathrm{T}}(\phi)\beta+\Omega_0(\phi), \tag{2.12}$$

which is convex in β, because, for each $\phi\in\mathbb{R}^d$, $\Omega_2(\phi)$ is positive semidefinite.

Define the set of $\phi\in\mathbb{R}^d$ such that $\tilde{\mathcal{G}}(s,\beta,\phi)$ is asymptotically stable, which is given by $\mathcal{S}\triangleq\{\phi\in\mathbb{R}^d\colon\tilde{\mathcal{D}}(s,\phi)\text{ is Hurwitz}\}$.

The following result provides sufficient conditions such that $\Omega_2(\phi)$ is positive definite.

Proposition 2.1. Consider Ω_2 given by (2.11), and assume (A2.1)–(A2.3) are satisfied. Let $\phi\in\mathcal{S}$. Then, $\Omega_2(\phi)$ is positive definite.

Proof. Let $\phi\in\mathcal{S}$. It follows from (2.11) that $\Omega_2(\phi)$ is well defined and positive semidefinite. Next, assume for contradiction that $\Omega_2(\phi)$ is not positive definite. Thus, there exists a nonzero $x\in\mathbb{R}^{n_{\mathrm{ff}}+1}$ such that $x^{\mathrm{T}}\Omega_2(\phi)x=0$, and it follows from (2.11)

that

$$0 = x^{\mathrm{T}}\Omega_2(\phi)x = \sum_{k=1}^{N}\left|\frac{\tilde{\mathcal{N}}_1(\jmath\omega_k,\phi)x}{\tilde{\mathcal{D}}(\jmath\omega_k,\phi)}\right|^2.$$

Thus, for all $k \in \mathcal{N}$, $\tilde{\mathcal{N}}_1(\jmath\omega_k,\phi)x = 0$. Next, it follows from (A2.3) that $N > d_{\mathrm{p}} + d_{\mathrm{ff}} + d_{\mathrm{fb}} + n_{\mathrm{p}} + \max\{n_{\mathrm{ff}} + d_{\mathrm{fb}}, n_{\mathrm{fb}} + d_{\mathrm{ff}}\} \geq d_{\mathrm{fb}} + n_{\mathrm{p}} + n_{\mathrm{ff}}$. Since, $\tilde{\mathcal{N}}_1(\jmath\omega_1,\phi)x = \cdots = \tilde{\mathcal{N}}_1(\jmath\omega_N,\phi)x = 0$, $\tilde{\mathcal{N}}_1(s,\phi)x$ is a degree $d_{\mathrm{fb}} + n_{\mathrm{p}} + n_{\mathrm{ff}}$ polynomial, and $N > d_{\mathrm{fb}} + n_{\mathrm{p}} + n_{\mathrm{ff}}$, it follows that $\tilde{\mathcal{N}}_1(s,\phi)x \equiv 0$. Moreover, since $\tilde{\mathcal{N}}_1(s,\phi)x \equiv 0$, $N_{\mathrm{p}}(s) \not\equiv 0$ and $s^{d_{\mathrm{fb}}} + \Gamma^{\mathrm{T}}_{d_{\mathrm{fb}}-1}(s)E_3\phi \not\equiv 0$, it follows from (2.6) that $\Gamma^{\mathrm{T}}_{n_{\mathrm{ff}}}(s)x \equiv 0$. Thus, $x = 0$, which is a contradiction. Therefore, $\Omega_2(\phi)$ is positive definite. □

For each $\phi \in \mathcal{S}$, the following result provides the global minimizer of $J(\beta,\phi)$.

Proposition 2.2. Consider J given by (2.12), and assume (A2.1)–(A2.3) are satisfied. Let $\phi \in \mathcal{S}$, and let $\beta \in \mathbb{R}^{n_{\mathrm{ff}}+1}\backslash\{-\frac{1}{2}\Omega_2^{-1}(\phi)\Omega_1(\phi)\}$. Then,

$$J\left(-\frac{1}{2}\Omega_2^{-1}(\phi)\Omega_1(\phi),\phi\right) = \Omega_0(\phi) - \frac{1}{4}\Omega_1^{\mathrm{T}}(\phi)\Omega_2^{-1}(\phi)\Omega_1(\phi) < J(\beta,\phi).$$

Proof. Let $\phi \in \mathcal{S}$, and Proposition 2.1 implies that $\Omega_2(\phi)$ is positive definite. Define $x \triangleq -\frac{1}{2}\Omega_2^{-1}(\phi)\Omega_1(\phi) \in \mathbb{R}^{n_{\mathrm{ff}}+1}$, and let $\beta \in \mathbb{R}^{n_{\mathrm{ff}}+1}$ be such that $\beta \neq x$. Thus, (2.12) implies that

$$J(\beta,\phi) = \beta^{\mathrm{T}}\Omega_2(\phi)\beta + \Omega_1^{\mathrm{T}}(\phi)\beta + \Omega_0(\phi) = [\beta - x]^{\mathrm{T}}\,\Omega_2(\phi)\,[\beta - x] + J(x,\phi). \quad (2.13)$$

Since $\Omega_2(\phi)$ is positive definite, it follows that $[\beta - x]^{\mathrm{T}}\Omega_2(\phi)[\beta - x] > 0$, and (2.13) confirms the result. □

Next, let M be a positive integer, and let $\Phi \subseteq \mathcal{S}$ be a set with M elements. We call Φ the *candidate pool*. Define $\mathcal{M} \triangleq \{1, 2, \ldots, M\}$. Now, create a candidate sequence using the M elements in the candidate pool Φ. For $i, j \in \mathcal{M}$, let $\phi_i, \phi_j \in \Phi$ be such

that if $i \neq j$, then $\phi_i \neq \phi_j$. The sequence $\{\phi_i\}_{i=1}^M$ is not unique; however, the order of the sequence is selected arbitrarily.

Now, for all $i \in \mathcal{M}$, define the quadratic cost function

$$\mathcal{J}_i(\beta) \triangleq J(\beta, \phi)\Big|_{\phi=\phi_i} = \beta^{\mathrm{T}}\Omega_2(\phi_i)\beta + \Omega_1^{\mathrm{T}}(\phi_i)\beta + \Omega_0(\phi_i). \tag{2.14}$$

Since $\phi_1, \ldots, \phi_M \in \Phi \subseteq \mathcal{S}$, Proposition 2.1 implies that $\Omega_2(\phi_1), \ldots, \Omega_2(\phi_M)$ are positive definite. The following result is a consequence of Proposition 2.2 and provides the unique global minimizer of $\mathcal{J}_i$ for each $i \in \mathcal{M}$.

Proposition 2.3. Consider $\mathcal{J}_i$ given by (2.14), assume (A2.1)–(A2.3) are satisfied, and assume $\Phi \subseteq \mathcal{S}$. Let $i \in \mathcal{M}$, and let $\beta \in \mathbb{R}^{n_{\mathrm{ff}}+1} \backslash \{-\frac{1}{2}\Omega_2^{-1}(\phi_i)\Omega_1(\phi_i)\}$. Then,

$$\mathcal{J}_i\left(-\frac{1}{2}\Omega_2^{-1}(\phi_i)\Omega_1(\phi_i)\right) = \Omega_0(\phi_i) - \frac{1}{4}\Omega_1^{\mathrm{T}}(\phi_i)\Omega_2^{-1}(\phi_i)\Omega_1(\phi_i) < \mathcal{J}_i(\beta).$$

Proposition 2.3 implies that for each $i \in \mathcal{M}$, $\beta_i \triangleq -\frac{1}{2}\Omega_2^{-1}(\phi_i)\Omega_1(\phi_i)$ is the global minimizer of $\mathcal{J}_i$. Next, let $\ell \in \mathcal{M}$ be the smallest integer such that

$$\mathcal{J}_\ell(\beta_\ell) = \min_{i \in \mathcal{M}} \mathcal{J}_i(\beta_i).$$

Then, the identified parameters are $\beta^+ \triangleq \beta_\ell$ and $\phi^+ \triangleq \phi_\ell$, and the identified transfer functions are

$$G_{\mathrm{ff}}^+(s) \triangleq \mathcal{G}_{\mathrm{ff}}(s, \beta^+, \phi^+) \qquad G_{\mathrm{fb}}^+(s) \triangleq \mathcal{G}_{\mathrm{fb}}(s, \phi^+).$$

Note that $\arg\min_{i \in \mathcal{M}} \mathcal{J}_i(\beta_i)$ is not necessarily unique. In this case, $\ell \in \mathcal{M}$ is the smallest integer such that $\mathcal{J}_\ell(\beta_\ell) = \min_{i \in \mathcal{M}} \mathcal{J}_i(\beta_i)$. However, in practice, $\arg\min_{i \in \mathcal{M}} \mathcal{J}_i(\beta_i)$ is generally unique. This SSID method is summarized by the following algorithm.

Algorithm 2.1. Consider the closed-loop transfer function (2.1), where G_{p} is

known. Assume $\{H(\omega_k)\}_{k=1}^N$ is known, and (A2.1)–(A2.4) are satisfied. Then, the subsystem identification algorithm is as follows:

Step 1. Generate the candidate pool $\Phi \subseteq \mathcal{S}$ and candidate sequence $\{\phi_i\}_{i=1}^M$.

Step 2. For each $i \in \mathcal{M}$, find $\beta_i \triangleq -\frac{1}{2}\Omega_2^{-1}(\phi_i)\Omega_1(\phi_i)$, which is the unique global minimizer of $\mathcal{J}_i$.

Step 3. Find the smallest integer $\ell \in \mathcal{M}$ such that $\mathcal{J}_\ell(\beta_\ell) = \min_{i\in\mathcal{M}} \mathcal{J}_i(\beta_i)$.

Step 4. The identification results are $\beta^+ = \beta_\ell$, $\phi^+ = \phi_\ell$, $G_{\mathrm{ff}}^+(s) = \mathcal{G}_{\mathrm{ff}}(s, \beta^+, \phi^+)$, and $G_{\mathrm{fb}}^+(s) = \mathcal{G}_{\mathrm{fb}}(s, \phi^+)$.

In the next two sections, Algorithm 2.1 is analyzed. Specifically, we analyze how the identified parameters β^+ and ϕ^+ relate to the true parameters β_* and ϕ_*.

2.4 Analysis with Noiseless Frequency Response Data

In this section, Algorithm 2.1 is analyzed under the assumption of noiseless frequency response data. We assume that for all $k \in \mathcal{N}$, $\sigma(\jmath\omega_k) = 0$, which implies that for all $k \in \mathcal{N}$, $H(\omega_k) = \tilde{G}(\jmath\omega_k)$. The following result relates β_* and ϕ_* if $\sigma(\jmath\omega_k) \equiv 0$.

Proposition 2.4. Assume (A2.1)–(A2.4) are satisfied, and assume for all $k \in \mathcal{N}$, $\sigma(\jmath\omega_k) = 0$. Then, $\beta_* = -\frac{1}{2}\Omega_2^{-1}(\phi_*)\Omega_1(\phi_*)$ and $J(\beta_*, \phi_*) = 0$.

Proof. Since for all $k \in \mathcal{N}$, $\sigma(\jmath\omega_k) = 0$, it follows that $H(\omega_k) = \tilde{G}(\jmath\omega_k) = \tilde{\mathcal{G}}(\jmath\omega_k, \beta_*, \phi_*)$. Thus, it follows from (2.4) that for all $k \in \mathcal{N}$,

$$\frac{\tilde{\mathcal{N}}_2(\jmath\omega_k, \phi_*)}{\tilde{\mathcal{D}}(\jmath\omega_k, \phi_*)} - H(\omega_k) = \frac{\tilde{\mathcal{N}}_2(\jmath\omega_k, \phi_*)}{\tilde{\mathcal{D}}(\jmath\omega_k, \phi_*)} - \tilde{\mathcal{G}}(\jmath\omega_k, \beta_*, \phi_*) = -\frac{\tilde{\mathcal{N}}_1(\jmath\omega_k, \phi_*)\beta_*}{\tilde{\mathcal{D}}(\jmath\omega_k, \phi_*)}. \tag{2.15}$$

Next, substituting (2.15) into (2.10), and using (2.11) yields $\Omega_1(\phi_*) = -2\Omega_2(\phi_*)\beta_*$. Since $\phi_* \in \mathcal{S}$, Proposition 2.1 implies that $\Omega_2(\phi_*)$ is positive definite, and thus, $\beta_* = -\frac{1}{2}\Omega_2^{-1}(\phi_*)\Omega_1(\phi_*)$. Moreover, (2.8) implies that $J(\beta_*, \phi_*) = \sum_{k=1}^N |\tilde{\mathcal{G}}(\jmath\omega_k, \beta_*, \phi_*) - H(\omega_k)|^2 = 0$. □

The following result provides sufficient conditions on $\beta \in \mathbb{R}^{n_{\mathrm{ff}}+1}$ and $\phi \in \mathcal{S}$ such that $\tilde{\mathcal{G}}(s,\beta,\phi) \equiv \tilde{G}(s)$.

Proposition 2.5. Let $\beta \in \mathbb{R}^{n_{\mathrm{ff}}+1}$ and $\phi \in \mathbb{R}^{d}$. Assume (A2.3) is satisfied, and assume $\sum_{k=1}^{N} |\tilde{\mathcal{G}}(\jmath\omega_k,\beta,\phi) - \tilde{G}(\jmath\omega_k)| = 0$. Then, for all $s \in \mathbb{C}$, $\tilde{\mathcal{G}}(s,\beta,\phi) = \tilde{G}(s)$.

Proof. Let $\beta \in \mathbb{R}^{n_{\mathrm{ff}}+1}$ and $\phi \in \mathcal{S}$. Since $\sum_{k=1}^{N} |\tilde{\mathcal{G}}(\jmath\omega_k,\beta,\phi) - \tilde{G}(\jmath\omega_k)| = 0$, it follows that for all $k \in \mathcal{N}$, $\tilde{\mathcal{G}}(\jmath\omega_k,\beta,\phi) = \tilde{G}(\jmath\omega_k)$. Define $\tilde{\mathcal{N}}(s) \triangleq \tilde{\mathcal{N}}_1(s,\phi)\beta + \tilde{\mathcal{N}}_2(s,\phi)$, $\tilde{\mathcal{N}}_*(s) \triangleq \tilde{\mathcal{N}}_1(s,\phi_*)\beta_* + \tilde{\mathcal{N}}_2(s,\phi_*)$, and $\psi(s) \triangleq \tilde{\mathcal{D}}(s,\phi_*)\tilde{\mathcal{N}}(s) - \tilde{\mathcal{D}}(s,\phi)\tilde{\mathcal{N}}_*(s)$. Since $\deg \tilde{\mathcal{N}} \leq n_{\mathrm{p}} + \max\{n_{\mathrm{ff}} + d_{\mathrm{fb}}, n_{\mathrm{fb}} + d_{\mathrm{ff}}\}$, $\deg \tilde{\mathcal{N}}_* \leq n_{\mathrm{p}} + \max\{n_{\mathrm{ff}} + d_{\mathrm{fb}}, n_{\mathrm{fb}} + d_{\mathrm{ff}}\}$, and $\deg \tilde{\mathcal{D}}(s,\phi) = \deg \tilde{\mathcal{D}}(s,\phi_*) = d_{\mathrm{p}} + d_{\mathrm{ff}} + d_{\mathrm{fb}}$, it follows that $\deg \psi \leq d_{\mathrm{p}} + d_{\mathrm{ff}} + d_{\mathrm{fb}} + n_{\mathrm{p}} + \max\{n_{\mathrm{ff}} + d_{\mathrm{fb}}, n_{\mathrm{fb}} + d_{\mathrm{ff}}\}$. Since for all $k \in \mathcal{N}$, $\tilde{\mathcal{G}}(\jmath\omega_k,\beta,\phi) = \tilde{G}(\jmath\omega_k)$, it follows that for all $k \in \mathcal{N}$, $\psi(\jmath\omega_k) = 0$. Next, it follows from (A2.3) that $\deg \psi < N$. Since for all $k \in \mathcal{N}$, $\psi(\jmath\omega_k) = 0$, and $\deg \psi < N$, it follows that $\psi(s) \equiv 0$, which implies that $\tilde{\mathcal{D}}(s,\phi_*)\tilde{\mathcal{N}}(s) \equiv \tilde{\mathcal{D}}(s,\phi)\tilde{\mathcal{N}}_*(s)$. Thus, $\tilde{\mathcal{G}}(s,\beta,\phi) \equiv \tilde{\mathcal{G}}(s,\beta_*,\phi_*) \equiv \tilde{G}(s)$. □

Proposition 2.5 provides sufficient conditions such that $\tilde{\mathcal{G}}(s,\beta,\phi) \equiv \tilde{G}(s) \equiv \tilde{\mathcal{G}}(s,\beta_*,\phi_*)$; however, these conditions are not sufficient to conclude that $\left[\begin{array}{cc} \beta^{\mathrm{T}} & \phi^{\mathrm{T}} \end{array}\right]$ equals $\left[\begin{array}{cc} \beta_*^{\mathrm{T}} & \phi_*^{\mathrm{T}} \end{array}\right]$. The following example demonstrates this case.

Example 2.1. Consider the closed-loop transfer function (2.1), where

$$G_{\mathrm{p}}(s) = \frac{1}{s+2}, \qquad G_{\mathrm{ff}}(s) = \frac{s+3}{s+1}, \qquad G_{\mathrm{fb}}(s) = 1.$$

Note that $\beta_* = \left[\begin{array}{cc} 1 & 3 \end{array}\right]^{\mathrm{T}}$, $\phi_* = \left[\begin{array}{cc} 1 & 1 \end{array}\right]^{\mathrm{T}}$, and $\tilde{G}(s) = (2s+4)/(s^2+4s+3)$. Let $\beta = \left[\begin{array}{cc} 3 & 7 \end{array}\right]^{\mathrm{T}} \neq \beta_*$ and $\phi = \left[\begin{array}{cc} 3 & -1 \end{array}\right]^{\mathrm{T}} \neq \phi_*$, and it follows that $\tilde{\mathcal{G}}(s,\beta,\phi) \equiv \tilde{G}(s) \equiv \tilde{\mathcal{G}}(s,\beta_*,\phi_*)$. △

Example 2.1 shows that there can exist $\beta \in \mathbb{R}^{n_{\mathrm{ff}}+1}$ and $\phi \in \mathcal{S}$ such that $\left[\begin{array}{cc} \beta^{\mathrm{T}} & \phi^{\mathrm{T}} \end{array}\right] \neq \left[\begin{array}{cc} \beta_*^{\mathrm{T}} & \phi_*^{\mathrm{T}} \end{array}\right]$ and $\tilde{\mathcal{G}}(s,\beta,\phi) \equiv \tilde{\mathcal{G}}(s,\beta_*,\phi_*)$. In this case, the SSID problem is not well

posed, because J does not have a unique minimizer, and (β_*, ϕ_*) cannot be determined uniquely from the noiseless closed-loop frequency response data $\{H(\omega_k)\}_{k=1}^N$.

Now, we impose an additional assumption to ensure that if $\tilde{\mathcal{G}}(s, \beta, \phi) \equiv \tilde{G}(s)$, then $\beta = \beta_*$ and $\phi = \phi_*$. First, let $\Psi \subseteq \mathbb{R}^d$ be a compact and perfect (i.e., closed with no isolated point) set containing ϕ_*. Note that Ψ can be selected sufficiently large to ensure $\phi_* \in \Psi$. Assume Ψ is known. In practice, Ψ is used to generate the candidate pool. For the remainder of this chapter, we impose the following assumption:

(A2.5) If $\beta \in \mathbb{R}^{n_{\mathrm{ff}}+1}$, $\phi \in \Psi \cap \mathcal{S}$, and $\tilde{\mathcal{G}}(s, \beta, \phi) \equiv \tilde{G}(s)$, then $\beta = \beta_*$ and $\phi = \phi_*$.

Assumption (A2.5) implies that $\left[\begin{array}{cc} \beta_*^{\mathrm{T}} & \phi_*^{\mathrm{T}} \end{array}\right]^{\mathrm{T}}$ is the only element in $\mathbb{R}^{n_{\mathrm{ff}}+1} \times (\Psi \cap \mathcal{S})$ that yields the closed-loop transfer function $\tilde{G}$.

2.4.1 ϕ_* in the candidate pool Φ

The following result provides sufficient conditions such that the identified transfer functions G_{ff}^+ and G_{fb}^+ are equal to G_{ff} and G_{fb}, respectively.

Theorem 2.1. Consider the closed-loop transfer function (2.1), where G_{p} is known. Assume $\{H(\omega_k)\}_{k=1}^N$ is known, (A2.1)–(A2.5) are satisfied, and for all $k \in \mathcal{N}$, $\sigma(\jmath\omega_k) = 0$. Furthermore, consider Algorithm 2.1 with the candidate pool $\Phi \subseteq (\Psi \cap \mathcal{S})$, and assume $\phi_* \in \Phi$. Let β^+ and ϕ^+ denote the identified parameters obtained from Algorithm 2.1. Then, $\beta^+ = \beta_*$ and $\phi^+ = \phi_*$.

Proof. Since $\phi_* \in \Phi$, it follows that there exists $m \in \mathcal{M}$ such that $\phi_m = \phi_*$. Next, since for all $k \in \mathcal{N}$, $\sigma(\jmath\omega_k) = 0$, it follows from Proposition 2.3 and Proposition 2.4 that $\beta_m = -\frac{1}{2}\Omega_2^{-1}(\phi_m)\Omega_1(\phi_m) = -\frac{1}{2}\Omega_2^{-1}(\phi_*)\Omega_1(\phi_*) = \beta_*$. Thus, (2.14) and Proposition 2.4 imply that $\mathcal{J}_m(\beta_m) = J(\beta_m, \phi_m) = J(\beta_*, \phi_*) = 0$.

Since for all $i \in \mathcal{M}$, $\mathcal{J}_i(\beta_i) \geq 0$ and $\mathcal{J}_m(\beta_m) = 0$, it follows that $J(\beta^+, \phi^+) = \min_{i \in \mathcal{M}} \mathcal{J}_i(\beta_i) = \mathcal{J}_m(\beta_m) = 0$. Since for all $k \in \mathcal{N}$, $H(\omega_k) = \tilde{G}(\jmath\omega_k)$, it follows from (2.8) that $0 = J(\beta^+, \phi^+) = \sum_{k=1}^N |\tilde{\mathcal{G}}(\jmath\omega_k, \beta^+, \phi^+) - \tilde{G}(\jmath\omega_k)|^2$. Thus, Proposition 2.5

implies that $\tilde{\mathcal{G}}(s, \beta^+, \phi^+) \equiv \tilde{G}(s)$. Since, in addition, $\phi^+ \in \Phi \subseteq (\Psi \cap \mathcal{S})$, (A2.5) implies that $\beta^+ = \beta_*$ and $\phi^+ = \phi_*$. □

2.4.2 ϕ_* not necessarily in the candidate pool Φ

Now, the analysis in the previous section is extended to address the case where ϕ_* is not necessarily in the candidate pool. It follows from Proposition 2.1 that for all $\phi \in \mathcal{S}$, $\Omega_2(\phi)$ is positive definite, which implies that $\theta \colon \mathcal{S} \to \mathbb{R}^{n_{\mathrm{ff}}+1}$ given by

$$\theta(\phi) \triangleq -\frac{1}{2}\Omega_2^{-1}(\phi)\Omega_1(\phi) \tag{2.16}$$

is well defined on $\mathcal{S}$. Define $Q \colon \mathcal{S} \to [0, \infty)$ by

$$Q(\phi) \triangleq J(\theta(\phi), \phi). \tag{2.17}$$

The following result addresses continuity of θ and Q.

Proposition 2.6. Assume (A2.1)–(A2.3) are satisfied. Then, θ and Q are continuous on $\mathcal{S}$.

Proof. Let $\phi \in \mathcal{S}$, and it follows that $\tilde{\mathcal{D}}(s, \phi)$ is Hurwitz. Thus, for all $k \in \mathcal{N}$, $\tilde{\mathcal{D}}(\jmath\omega_k, \phi) \neq 0$, and it follows from (2.9)–(2.11) that Ω_0, Ω_1, and Ω_2 are well defined and continuous on $\mathcal{S}$.

Next, it follows from Proposition 2.1 that $\Omega_2(\phi)$ is positive definite. Since Ω_2 is continuous on $\mathcal{S}$, it follows that each element of Ω_2 is continuous on $\mathcal{S}$, which implies that the adjugate of Ω_2, denoted by $\operatorname{adj}\Omega_2$, and the determinant of Ω_2, denoted by $\det\Omega_2$, are continuous on $\mathcal{S}$. Since Ω_2 is invertible on $\mathcal{S}$ and $\Omega_2^{-1} = \frac{1}{\det\Omega_2}\operatorname{adj}\Omega_2$, it follows that Ω_2^{-1} is continuous on $\mathcal{S}$.

Since Ω_2^{-1} and Ω_1 are continuous on $\mathcal{S}$, it follows from (2.16) that θ is continuous on $\mathcal{S}$. Moreover, it follows from (2.12) that J is continuous on $\mathbb{R}^{n_{\mathrm{ff}}+1} \times \mathcal{S}$. Since, in

addition, θ is continuous on $\mathcal{S}$, it follows from (2.17) that Q is continuous on $\mathcal{S}$. $\square$

It follows from (A2.4) that $\tilde{\mathcal{D}}(s, \phi_*)$ is Hurwitz. Thus, there exists $\rho < 0$ such that if $\lambda \in \mathbb{C}$ and $\tilde{\mathcal{D}}(\lambda, \phi_*) = 0$, then $\operatorname{Re} \lambda < \rho$. Assume ρ is known. Note that $\rho < 0$ can be selected such that $|\rho|$ is arbitrarily small, which ensures that $\mathcal{S}_\rho \triangleq \{\phi \in \mathbb{R}^d \colon \tilde{\mathcal{D}}(s + \rho, \phi) \text{ is Hurwitz}\}$ contains ϕ_*. In practice, $\mathcal{S}_\rho$ is used to generate the candidate pool.

The following propositions are needed for the main result of this section. The proofs are in Appendix A. Note that $\overline{\Psi \cap \mathcal{S}_\rho}$ denotes the closure of $\Psi \cap \mathcal{S}_\rho$.

Proposition 2.7. $\Psi \cap \mathcal{S}_\rho$ is bounded and contains no isolated points.

Proposition 2.8. $\overline{\Psi \cap \mathcal{S}_\rho} \subseteq \mathcal{S}$ is compact.

Let $\mathbb{Z}^+$ denote the set of positive integers, let $n \in \mathbb{Z}^+$, and define the *open ball of radius* $\epsilon > 0$ *centered at* $c \in \mathbb{R}^n$ by $\mathbb{B}_\epsilon(c) \triangleq \{x \in \mathbb{R}^n \colon \|x - c\| < \epsilon\}$. We now define a convergent sequence of finite sets.

Definition 2.1. Let $n \in \mathbb{Z}^+$, and let $\Delta \subseteq \mathbb{R}^n$ be bounded and contain no isolated points. For all $j \in \mathbb{Z}^+$, let $\Delta_j \subseteq \Delta$ be a finite set. Then, $\{\Delta_j\}_{j=1}^\infty$ *converges to* Δ if for each $x \in \Delta$, there exists a sequence $\{x_j \colon x_j \in \Delta_j\}_{j=1}^\infty$ such that for all $\epsilon > 0$, there exists $L \in \mathbb{Z}^+$ such that for $j > L$, $x_j \in \mathbb{B}_\epsilon(x)$.

The following result considers Algorithm 2.1 with a sequence of candidate pools that converges to $\Psi \cap \mathcal{S}_\rho$. This result demonstrates that a sufficiently dense candidate pool yields identified parameters β^+ and ϕ^+ that are arbitrarily close to β_* and ϕ_*.

Theorem 2.2. Consider the closed-loop transfer function (2.1), where G_{p} is known. Assume $\{H(\omega_k)\}_{k=1}^N$ is known, (A2.1)–(A2.5) are satisfied, and for all $k \in \mathcal{N}$, $\sigma(\jmath\omega_k) = 0$. For all $j \in \mathbb{Z}^+$, let $\Lambda_j \subseteq (\Psi \cap \mathcal{S}_\rho)$ be a finite set such that $\{\Lambda_j\}_{j=1}^\infty$ converges to $\Psi \cap \mathcal{S}_\rho$. For each $j \in \mathbb{Z}^+$, let β_j^+ and ϕ_j^+ denote the identified parameters obtained from Algorithm 2.1 with the candidate pool $\Phi = \Lambda_j$. Then, for all $\epsilon > 0$, there exists $L \in \mathbb{Z}^+$ such that if $j > L$, then $\beta_j^+ \in \mathbb{B}_\epsilon(\beta_*)$ and $\phi_j^+ \in \mathbb{B}_\epsilon(\phi_*)$.

Proof. Let $\epsilon > 0$. Since θ is continuous on $\mathcal{S}$ and $\phi_* \in \mathcal{S}$, it follows that there exists $\delta > 0$ such that for all $x \in \mathbb{B}_\delta(\phi_*)$, $\theta(x) \in \mathbb{B}_\epsilon(\theta(\phi_*))$.

Define $\epsilon_1 \triangleq \min\{\epsilon, \delta\}$, $\Lambda_{\mathrm{c}} \triangleq \overline{\Psi \cap \mathcal{S}_\rho}$, and

$$\Lambda_{\epsilon_1} \triangleq \Lambda_{\mathrm{c}} \backslash \mathbb{B}_{\epsilon_1}(\phi_*) = \Lambda_{\mathrm{c}} \cap \{x \in \mathbb{R}^d \colon \|x - \phi_*\| \geq \epsilon_1\}. \tag{2.18}$$

It follows from Proposition 2.8 that $\Lambda_{\mathrm{c}} \subseteq \mathcal{S}$ is compact. Since Λ_{c} is compact, and $\{x \in \mathbb{R}^d \colon \|x - \phi_*\| \geq \epsilon_1\}$ is closed, it follows from (2.18) that Λ_{ϵ_1} is compact.

Proposition 2.6 implies that Q is continuous on $\Lambda_{\epsilon_1} \subseteq \Lambda_{\mathrm{c}} \subseteq \mathcal{S}$. Next, define $Q_{\epsilon_1} \triangleq \min_{x \in \Lambda_{\epsilon_1}} Q(x)$, which exists because Q is continuous on the compact set Λ_{ϵ_1} [93, Theorem 7.7]. Assume for contradiction that $Q_{\epsilon_1} = 0$. Thus, there exists $\phi \in \Lambda_{\epsilon_1}$ such that $Q(\phi) = 0$. Since for all $k \in \mathcal{N}$, $H(\omega_k) = \tilde{G}(\jmath\omega_k)$, it follows from (2.8) and (2.17) that $0 = Q(\phi) = J(\theta(\phi), \phi) = \sum_{k=1}^N |\tilde{\mathcal{G}}(\jmath\omega_k, \theta(\phi), \phi) - \tilde{G}(\jmath\omega_k)|^2$. Thus, Proposition 2.5 implies that $\tilde{\mathcal{G}}(s, \theta(\phi), \phi) \equiv \tilde{G}(s)$, and it follows from (A2.5) that $\phi = \phi_* \notin \Lambda_{\epsilon_1}$, which is a contradiction. Thus, $Q_{\epsilon_1} > 0$.

Next, since for all $k \in \mathcal{N}$, $\sigma(\jmath\omega_k) = 0$, it follows from Proposition 2.4, (2.16), and (2.17) that $\beta_* = \theta(\phi_*)$ and $Q(\phi_*) = J(\beta_*, \phi_*) = 0$. Furthermore, since Q is continuous on Λ_{c}, it follows that there exists $\delta_1 > 0$ such that for all $x \in \Lambda_{\mathrm{c}} \cap \mathbb{B}_{\delta_1}(\phi_*)$, $Q(x) < Q_{\epsilon_1}$. Since $\{\Lambda_j\}_{j=1}^\infty$ converges to $(\Psi \cap \mathcal{S}_\rho) \subseteq \Lambda_{\mathrm{c}}$, it follows from Definition 2.1 that there exists a sequence $\{\phi_j \colon \phi_j \in \Lambda_j\}_{j=1}^\infty$ and $L \in \mathbb{Z}^+$ such that for all $j > L$, $\phi_j \in \mathbb{B}_{\min\{\epsilon_1, \delta_1\}}(\phi_*) \subseteq \mathbb{B}_{\delta_1}(\phi_*)$. Thus, for all $j > L$, $Q(\phi_j) < Q_{\epsilon_1}$.

Let $j \in \mathbb{Z}^+$ be such that $j > L$. It follows from Algorithm 2.1, (2.16), and (2.17) that $Q(\phi_j^+) \leq Q(\phi_j) < Q_{\epsilon_1}$. Assume for contradiction that $\phi_j^+ \notin \mathbb{B}_{\epsilon_1}(\phi_*)$. Therefore, $\phi_j^+ \in \Lambda_{\epsilon_1}$, which implies that $Q_{\epsilon_1} \leq Q(\phi_j^+)$, which is a contradiction. Thus, $\phi_j^+ \in \mathbb{B}_{\epsilon_1}(\phi_*) \subseteq \mathbb{B}_\epsilon(\phi_*)$. Since $\phi_j^+ \in \mathbb{B}_{\epsilon_1}(\phi_*) \subseteq \mathbb{B}_\delta(\phi_*)$, it follows that $\beta_j^+ = \theta(\phi_j^+) \in \mathbb{B}_\epsilon(\theta(\phi_*)) = \mathbb{B}_\epsilon(\beta_*)$. □

2.5 Analysis with Noisy Frequency Response Data

In this section, Algorithm 2.1 is analyzed under the assumption of noisy frequency response data. Define $\hat{\Omega}_0 \colon \mathcal{S} \times \mathbb{C}^N \to \mathbb{R}$ and $\hat{\Omega}_1 \colon \mathcal{S} \times \mathbb{C}^N \to \mathbb{R}^{n_{\mathrm{ff}}+1}$ by

$$\hat{\Omega}_0(\phi, \eta) \triangleq \sum_{k=1}^{N} \left| \frac{\tilde{\mathcal{N}}_2(\jmath\omega_k, \phi)}{\tilde{\mathcal{D}}(\jmath\omega_k, \phi)} - \tilde{G}(\jmath\omega_k) - \eta_k \right|^2, \tag{2.19}$$

$$\hat{\Omega}_1(\phi, \eta) \triangleq 2\mathrm{Re} \sum_{k=1}^{N} \left[\frac{\tilde{\mathcal{N}}_1(\jmath\omega_k, \phi)}{\tilde{\mathcal{D}}(\jmath\omega_k, \phi)} \right]^* \left[\frac{\tilde{\mathcal{N}}_2(\jmath\omega_k, \phi)}{\tilde{\mathcal{D}}(\jmath\omega_k, \phi)} - \tilde{G}(\jmath\omega_k) - \eta_k \right], \tag{2.20}$$

where $\eta_1, \ldots, \eta_N \in \mathbb{C}$ and $\eta \triangleq \left[\begin{array}{ccc} \eta_1 & \ldots & \eta_N \end{array} \right]^{\mathrm{T}}$. Define $\sigma_* \triangleq \left[\begin{array}{ccc} \sigma(\jmath\omega_1) & \cdots & \sigma(\jmath\omega_N) \end{array} \right]^{\mathrm{T}} \in \mathbb{C}^N$, and note that $\hat{\Omega}_0(\phi, \sigma_*) = \Omega_0(\phi)$ and $\hat{\Omega}_1(\phi, \sigma_*) = \Omega_1(\phi)$. Thus, $\hat{\Omega}_0$ and $\hat{\Omega}_1$ are extensions of Ω_0 and Ω_1. Specifically, $\hat{\Omega}_0$ and $\hat{\Omega}_1$ are functions not only of the parameter ϕ but also the noise η.

Define $\hat{J} \colon \mathbb{R}^{n_{\mathrm{ff}}+1} \times \mathcal{S} \times \mathbb{C}^N \to [0, \infty)$, $\hat{\theta} \colon \mathcal{S} \times \mathbb{C}^N \to \mathbb{R}^{n_{\mathrm{ff}}+1}$, and $\hat{Q} \colon \mathcal{S} \times \mathbb{C}^N \to [0, \infty)$ by

$$\hat{J}(\beta, \phi, \eta) \triangleq \sum_{k=1}^{N} \left| \tilde{\mathcal{G}}(\jmath\omega_k, \beta, \phi) - \tilde{G}(\jmath\omega_k) - \eta_k \right|^2, \tag{2.21}$$

$$\hat{\theta}(\phi, \eta) \triangleq -\frac{1}{2} \Omega_2^{-1}(\phi) \hat{\Omega}_1(\phi, \eta), \tag{2.22}$$

$$\hat{Q}(\phi, \eta) \triangleq \hat{J}(\hat{\theta}(\phi, \eta), \phi, \eta). \tag{2.23}$$

Note that $\hat{J}(\beta, \phi, \sigma_*) = J(\beta, \phi)$, $\hat{\theta}(\phi, \sigma_*) = \theta(\phi)$, and $\hat{Q}(\phi, \sigma_*) = Q(\phi)$. Thus, $\hat{J}$, $\hat{\theta}$, and $\hat{Q}$ are extensions of J, θ, and Q. Specifically, $\hat{J}$, $\hat{\theta}$, and $\hat{Q}$ are functions not only of the parameters β and ϕ but also of the noise η.

It follows from (2.4), (2.11), and (2.19)–(2.21) that

$$\hat{J}(\beta, \phi, \eta) = \beta^{\mathrm{T}} \Omega_2(\phi) \beta + \hat{\Omega}_1^{\mathrm{T}}(\phi, \eta) \beta + \hat{\Omega}_0(\phi, \eta). \tag{2.24}$$

Furthermore, it follows from (2.16), (2.17), (2.21)–(2.23), and Proposition 2.4 that

$$\hat{\theta}(\phi_*, 0) = -\frac{1}{2}\Omega_2^{-1}(\phi_*)\hat{\Omega}_1(\phi_*, 0) = \beta_*, \tag{2.25}$$

$$\hat{Q}(\phi_*, 0) = \hat{J}(\beta_*, \phi_*, 0) = 0. \tag{2.26}$$

The following result is an extension of Proposition 2.6.

Proposition 2.9. Assume (A2.1)–(A2.3) are satisfied. Then, $\hat{\theta}$ and $\hat{Q}$ are continuous on $\mathcal{S} \times \mathbb{C}^N$.

Proof. It follows (2.19) and (2.20) that $\hat{\Omega}_0$ and $\hat{\Omega}_1$ are continuous on $\mathcal{S} \times \mathbb{C}^N$. Also, it follows from (2.11) that Ω_2 is continuous on $\mathcal{S}$.

Next, it follows from Proposition 2.1 that $\Omega_2(\phi)$ is positive definite. Since Ω_2 is continuous on $\mathcal{S}$, it follows that each element of Ω_2 is continuous on $\mathcal{S}$, which implies that the adjugate of Ω_2, denoted by $\operatorname{adj}\Omega_2$, and the determinant of Ω_2, denoted by $\det\Omega_2$, are continuous on $\mathcal{S}$. Since Ω_2 is invertible on $\mathcal{S}$ and $\Omega_2^{-1} = \frac{1}{\det\Omega_2}\operatorname{adj}\Omega_2$, it follows that Ω_2^{-1} is continuous on $\mathcal{S}$.

Therefore, it follows from (2.22) and (2.24) that $\hat{J}$ is continuous on $\mathbb{R}^{n_{\mathrm{ff}}+1} \times \mathcal{S} \times \mathbb{C}^N$ and $\hat{\theta}$ is continuous on $\mathcal{S} \times \mathbb{C}^N$. Thus, it follows from (2.23) that $\hat{Q}$ is continuous on $\mathcal{S} \times \mathbb{C}^N$. □

2.5.1 ϕ_* in the candidate pool Φ

The following result provides sufficient conditions such that the identified parameter ϕ^+ equals ϕ_*. This result also shows that if the norm of the noise σ_* is sufficiently small, then the identified parameter β^+ is arbitrarily close to β_*.

Theorem 2.3. Consider the closed-loop transfer function (2.1), where G_{p} is known. Assume $\{H(\omega_k)\}_{k=1}^N$ is known and (A2.1)–(A2.5) are satisfied. Furthermore, consider Algorithm 2.1 with the candidate pool $\Phi \subseteq (\Psi \cap \mathcal{S})$, and assume $\phi_* \in \Phi$. Let β^+ and

ϕ^+ denote the identified parameters obtained from Algorithm 2.1. Then, there exists $\delta_0 > 0$ such that if $\|\sigma_*\| < \delta_0$, then $\phi^+ = \phi_*$. Furthermore, for all $\epsilon > 0$, there exists $\delta \in (0, \delta_0)$ such that if $\|\sigma_*\| < \delta$, then $\beta^+ \in \mathbb{B}_\epsilon(\beta_*)$.

Proof. Let $\phi \in \Phi \backslash \{\phi_*\}$, and assume for contradiction that $\hat{Q}(\phi, 0) = 0$. It follows from (2.21) and (2.23) that

$$0 = \hat{Q}(\phi, 0) = \hat{J}(\hat{\theta}(\phi, 0), \phi, 0) = \sum_{k=1}^{N} |\tilde{\mathcal{G}}(\jmath\omega_k, \hat{\theta}(\phi, 0), \phi) - \tilde{G}(\jmath\omega_k)|^2.$$

Thus, Proposition 2.5 implies that $\tilde{\mathcal{G}}(s, \hat{\theta}(\phi, 0), \phi) \equiv \tilde{G}(s)$, and it follows from (A2.5) that $\phi = \phi_*$, which is a contradiction. Therefore, $\hat{Q}(\phi, 0) > 0$.

Define $U \triangleq \min_{x \in \Phi \backslash \{\phi_*\}} \hat{Q}(x, 0) > 0$. Since $\hat{Q}$ is continuous on $\mathcal{S} \times \mathbb{C}^N$, it follows that for each $i \in \mathcal{M}$, $\hat{Q}(\phi_i, \cdot)$ is continuous on $\mathbb{C}^N$. Thus, for each $i \in \mathcal{M}$, there exists $\delta_i > 0$ such that for all $\eta \in \{x \in \mathbb{C}^N \colon \|x\| < \delta_i\}$,

$$|\hat{Q}(\phi_i, \eta) - \hat{Q}(\phi_i, 0)| < U/2. \tag{2.27}$$

Define $\delta_0 \triangleq \min_{i \in \mathcal{M}} \delta_i > 0$, and assume that $\|\sigma_*\| < \delta_0$. Since $\phi_* \in \Phi$, it follows that there exists $m \in \mathcal{M}$ such that $\phi_m = \phi_*$. Since $\hat{Q}(\phi_m, 0) = \hat{Q}(\phi_*, 0) = 0$, it follows from (2.27) that $\hat{Q}(\phi_m, \sigma_*) = |\hat{Q}(\phi_m, \sigma_*) - \hat{Q}(\phi_m, 0)| < U/2$. Let $j \in \mathcal{M} \backslash \{m\}$. It follows from (2.27) that $-U/2 < \hat{Q}(\phi_j, \sigma_*) - \hat{Q}(\phi_j, 0)$, which implies that $\hat{Q}(\phi_j, \sigma_*) > \hat{Q}(\phi_j, 0) - U/2$. Since, in addition, $\hat{Q}(\phi_j, 0) \geq U$, it follows that $\hat{Q}(\phi_j, \sigma_*) > U/2$. Therefore, $\hat{Q}(\phi_m, \sigma_*) < \hat{Q}(\phi_j, \sigma_*)$, which implies that $Q(\phi_m) < Q(\phi_j)$. Thus, (2.14), (2.16), (2.17), and Proposition 2.3 imply that $\mathcal{J}_m(\beta_m) < \mathcal{J}_j(\beta_j)$. Therefore, it follows from Algorithm 2.1 that $\phi^+ = \phi_m = \phi_*$ and

$$\beta^+ = \beta_m = \theta(\phi_*) = \hat{\theta}(\phi_*, \sigma_*). \tag{2.28}$$

Let $\epsilon > 0$. Since $\hat{\theta}$ is continuous on $\mathcal{S} \times \mathbb{C}^N$, it follows that $\hat{\theta}(\phi_*, \cdot)$ is continuous

on $\mathbb{C}^N$. Therefore, there exists $\delta \in (0, \delta_0)$ such that for all $\eta \in \{x \in \mathbb{C}^N \colon \|x\| < \delta\}$, $\hat{\theta}(\phi_*, \eta) \in \mathbb{B}_\epsilon(\hat{\theta}(\phi_*, 0))$. Finally, assume $\|\sigma_*\| < \delta$, and (2.25) and (2.28) imply that $\beta^+ \in \mathbb{B}_\epsilon(\beta_*)$. □

2.5.2 ϕ_* not necessarily in the candidate pool Φ

Now, the analysis in the previous section is extended to address the case where ϕ_* is not necessarily in the candidate pool. The following result considers Algorithm 2.1 with a sequence of candidate pools that converges to $\Psi \cap \mathcal{S}_\rho$. This result demonstrates that a sufficiently dense candidate pool and sufficiently small noise σ_* yield identified parameters β^+ and ϕ^+ that are arbitrarily close to β_* and ϕ_*.

Theorem 2.4. Consider the closed-loop transfer function (2.1), where G_{p} is known. Assume $\{H(\omega_k)\}_{k=1}^N$ is known and (A2.1)–(A2.5) are satisfied. For all $j \in \mathbb{Z}^+$, let $\Lambda_j \subseteq (\Psi \cap \mathcal{S}_\rho)$ be a finite set such that $\{\Lambda_j\}_{j=1}^\infty$ converges to $\Psi \cap \mathcal{S}_\rho$. For each $j \in \mathbb{Z}^+$, let β_j^+ and ϕ_j^+ denote the identified parameters obtained from Algorithm 2.1 with the candidate pool $\Phi = \Lambda_j$. Then, for all $\epsilon > 0$, there exist $\delta > 0$ and $L \in \mathbb{Z}^+$ such that if $\|\sigma_*\| < \delta$ and $j > L$, then $\beta_j^+ \in \mathbb{B}_\epsilon(\beta_*)$ and $\phi_j^+ \in \mathbb{B}_\epsilon(\phi_*)$.

Proof. Let $\epsilon > 0$. Since $\hat{\theta}$ is continuous on $\mathcal{S} \times \mathbb{C}^N$ and $\phi_* \in \mathcal{S}$, it follows that there exists $\delta_0 > 0$ such that for all $\phi \in \mathbb{B}_{\delta_0}(\phi_*)$ and all $\eta \in \{x \in \mathbb{C}^N \colon \|x\| < \delta_0\}$,

$$\hat{\theta}(\phi, \eta) \in \mathbb{B}_\epsilon(\hat{\theta}(\phi_*, 0)). \tag{2.29}$$

Define $\epsilon_1 \triangleq \min\{\epsilon, \delta_0\}$, $\Lambda_{\mathrm{c}} \triangleq \overline{\Psi \cap \mathcal{S}_\rho}$, and

$$\Lambda_{\epsilon_1} \triangleq \Lambda_{\mathrm{c}} \backslash \mathbb{B}_{\epsilon_1}(\phi_*) = \Lambda_{\mathrm{c}} \cap \{x \in \mathbb{R}^d \colon \|x - \phi_*\| \geq \epsilon_1\}. \tag{2.30}$$

It follows from Proposition 2.8 that $\Lambda_{\mathrm{c}} \subseteq \mathcal{S}$ is compact. Since Λ_{c} is compact, and $\{x \in \mathbb{R}^d \colon \|x - \phi_*\| \geq \epsilon_1\}$ is closed, it follows from (2.30) that Λ_{ϵ_1} is compact.

Let $v > \delta_0$, and define $V \triangleq \{x \in \mathbb{C}^N \colon \|x\| \leq v\}$. Since $\Lambda_{\epsilon_1} \subseteq \Lambda_{\mathrm{c}} \subseteq \mathcal{S}$ and $V \subseteq \mathbb{C}^N$, it follows from Proposition 2.9 that $\hat{Q}$ is continuous on $\Lambda_{\epsilon_1} \times V$. Next, define $\Theta \colon V \to [0, \infty)$ by $\Theta(\eta) \triangleq \min_{\phi \in \Lambda_{\epsilon_1}} \hat{Q}(\phi, \eta)$, which exist because Λ_{ϵ_1} is compact and $\hat{Q}$ is continuous on $\Lambda_{\epsilon_1} \times V$ [93, Theorem 7.7].

Assume for contradiction that $\Theta(0) = 0$. Thus, there exists $z \in \Lambda_{\epsilon_1}$ such that $\hat{Q}(z, 0) = 0$, and it follows from (2.21) and (2.23) that

$$0 = \hat{J}(\hat{\theta}(z,0), z, 0) = \sum_{k=1}^{N} |\tilde{\mathcal{G}}(\jmath\omega_k, \hat{\theta}(z,0), z) - \tilde{G}(\jmath\omega_k)|^2.$$

Thus, Proposition 2.5 implies that $\tilde{\mathcal{G}}(s, \hat{\theta}(z,0), z) \equiv \tilde{G}(s)$, and it follows from (A2.5) that $z = \phi_* \notin \Lambda_{\epsilon_1}$, which is a contradiction. Thus, $\Theta(0) > 0$.

Since $\hat{Q}$ is continuous on $\Lambda_{\epsilon_1} \times V$, and Λ_{ϵ_1} and V are compact, it follows from [94, Theorem 9.14] that Θ is continuous on V. Furthermore, since $\hat{Q}$ is continuous on $\mathcal{S} \times \mathbb{C}^N$, it follows that $\hat{Q}(\phi_*, \cdot)$ is continuous on V. Thus, $W \colon V \to \mathbb{R}$ defined by $W(\eta) \triangleq \Theta(\eta) - \hat{Q}(\phi_*, \eta)$ is continuous on V. It follows from (2.26) that $W(0) = \Theta(0) - \hat{Q}(\phi_*, 0) = \Theta(0) > 0$. Since, in addition, W is continuous on V, it follows that there exists $\delta_1 \in (0, v)$ such that for all $\eta \in \{x \in \mathbb{C}^N \colon \|x\| < \delta_1\}$, $W(\eta) > 0$. Define $\delta \triangleq \min\{\delta_0, \delta_1\} > 0$ and assume $\|\sigma_*\| < \delta$.

Since $W(\sigma_*) > 0$ and Proposition 2.9 implies that $\hat{Q}(\cdot, \sigma_*)$ is continuous on Λ_{c}, it follows from the continuity of $\hat{Q}(\cdot, \sigma_*)$ that there exists $\delta_2 > 0$ such that for all $\phi \in (\Lambda_{\mathrm{c}} \cap \mathbb{B}_{\delta_2}(\phi_*))$, $|\hat{Q}(\phi, \sigma_*) - \hat{Q}(\phi_*, \sigma_*)| < W(\sigma_*)$. Thus, for all $\phi \in (\Lambda_{\mathrm{c}} \cap \mathbb{B}_{\delta_2}(\phi_*))$, $\hat{Q}(\phi, \sigma_*) - \hat{Q}(\phi_*, \sigma_*) \leq |\hat{Q}(\phi, \sigma_*) - \hat{Q}(\phi_*, \sigma_*)| < W(\sigma_*) = \Theta(\sigma_*) - \hat{Q}(\phi_*, \sigma_*)$, which implies that

$$\hat{Q}(\phi, \sigma_*) < \Theta(\sigma_*). \tag{2.31}$$

Since $\{\Lambda_j\}_{j=1}^{\infty}$ converges to $(\Psi \cap \mathcal{S}_\rho) \subseteq \Lambda_{\mathrm{c}}$, it follows from Definition 2.1 that there exists a sequence $\{\phi_j \colon \phi_j \in \Lambda_j\}_{j=1}^{\infty}$ and $L \in \mathbb{Z}^+$ such that for all $j > L$, $\phi_j \in$

$\mathbb{B}_{\min\{\epsilon_1,\delta_2\}}(\phi_*)$. Thus, it follows from (2.31) that for all $j > L$, $\hat{Q}(\phi_j, \sigma_*) < \Theta(\sigma_*)$.

Let $j \in \mathbb{Z}^+$ be such that $j > L$. It follows from Algorithm 2.1, (2.16), and (2.17) that $Q(\phi_j^+) \leq Q(\phi_j)$. Therefore, (2.31) implies that $\hat{Q}(\phi_j^+, \sigma_*) \leq \hat{Q}(\phi_j, \sigma_*) < \Theta(\sigma_*)$. Assume for contradiction that $\phi_j^+ \notin \mathbb{B}_{\epsilon_1}(\phi_*)$. Therefore, $\phi_j^+ \in \Lambda_{\epsilon_1}$, which implies that $\Theta(\sigma_*) = \min_{\phi \in \Lambda_{\epsilon_1}} \hat{Q}(\phi, \sigma_*) \leq \hat{Q}(\phi_j^+, \sigma_*)$, which is a contradiction. Thus, $\phi_j^+ \in \mathbb{B}_{\epsilon_1}(\phi_*) \subseteq \mathbb{B}_{\epsilon}(\phi_*)$. Since $\phi_j^+ \in \mathbb{B}_{\epsilon_1}(\phi_*) \subseteq \mathbb{B}_{\delta_0}(\phi_*)$, it follows from (2.25) and (2.29) that $\beta_j^+ = \hat{\theta}(\phi_j^+, \sigma_*) \in \mathbb{B}_{\epsilon}(\hat{\theta}(\phi_*, 0)) = \mathbb{B}_{\epsilon}(\beta_*)$. □

2.6 Numerical Examples

For all examples in this section, let

$$G_{\mathrm{p}}(s) = \frac{4}{s+2}, \qquad G_{\mathrm{ff}}(s) = \frac{2.1s+3}{s+6.5}, \qquad G_{\mathrm{fb}}(s) = \frac{5.4}{s+7.1},$$

which implies that $\beta_* = [\ 2.1 \quad 3\ ]^{\mathrm{T}}$ and $\phi_* = [\ 6.5 \quad 5.4 \quad 7.1\ ]^{\mathrm{T}}$. Let $\Psi = [-8, 8] \times [-8, 8] \times [-8, 8]$, which is a compact and perfect set containing ϕ_*. It can be shown that this example satisfies (A2.5). Let $\beta = [\ u_1 \quad u_2\ ]^{\mathrm{T}} \in \mathbb{R}^2$ and $\phi = [\ v_1 \quad v_2 \quad v_3\ ]^{\mathrm{T}} \in \mathbb{R}^3$, and assume $\tilde{\mathcal{G}}(s, \beta, \phi) \equiv \tilde{G}(s)$, where $\tilde{G}$ is given by (2.1). It follows that

$$\tilde{\mathcal{G}}(s, \beta, \phi) = \frac{4\left[(u_1 s + u_2)(s + v_3) + v_2(s + v_1)\right]}{(s + v_1)\left[(s+2)(s+v_3) + 4v_2\right]} = \frac{4(2.1s^2 + 23.31s + 56.4)}{(s+6.5)(s^2 + 9.1s + 35.8)}. \quad (2.32)$$

Since the roots of $s^2 + 9.1s + 35.8$ are complex, (2.32) implies that $v_1 = 6.5$ and $(s+2)(s+v_3)+4v_2 = s^2+9.1s+35.8$, or equivalently, $v_3 = 7.1$ and $v_2 = 5.4$. Moreover, the numerator of (2.32) implies that $(u_1 s+u_2)(s+v_3)+v_2(s+v_1) = 2.1s^2+23.31s+56.4$, or equivalently, $u_1 = 2.1$ and $u_2 = 3$. Thus, $\beta = \beta_*$ and $\phi = \phi_*$.

For all examples in this chapter, let $N = 20$ and $\omega_k = 0.2\pi k$, where $k \in \mathcal{N}$.

Example 2.2. *Noiseless data and* $\phi_* \in \Phi$. Assume $\sigma(\jmath\omega_k) \equiv 0$. Consider

$$\Pi_0 \triangleq \left\{\phi \in \mathbb{R}^3 \colon E_1\phi, E_2\phi, E_3\phi \in \{-8 + 0.1k\}_{k=0}^{160}\right\} \subseteq \Psi,$$

define $\Lambda_0 \triangleq \Pi_0 \cap \mathcal{S}$, and note that $\phi_* \in \Lambda_0$. Algorithm 2.1 is used with the candidate pool $\Phi = \Lambda_0$ to obtain β^+ and ϕ^+. The identified parameters are $\beta^+ = \beta_* = [\ 2.1 \quad 3\ ]^{\mathrm{T}}$ and $\phi^+ = \phi_* = [\ 6.5 \quad 5.4 \quad 7.1\ ]^{\mathrm{T}}$, which agrees with Theorem 2.1. $\triangle$

Example 2.3. *Noiseless data and* $\phi_* \notin \Phi$. Assume $\sigma(\jmath\omega_k) \equiv 0$. For $j = 1, \ldots, 25$, consider

$$\Pi_j \triangleq \left\{\phi \in \mathbb{R}^3 \colon E_1\phi, E_2\phi, E_3\phi \in \left\{-8 + \frac{16}{5 + 10(j-1)}k\right\}_{k=0}^{5+10(j-1)}\right\} \subseteq \Psi,$$

define $\Lambda_j \triangleq \Pi_j \cap \mathcal{S}_\rho$, where $\rho = -0.001$, and note that for $j = 1, \ldots, 25$, $\phi_* \notin \Lambda_j$.

For $j = 1, \ldots, 25$, Algorithm 2.1 is used with the candidate pool $\Phi = \Lambda_j$ to obtain the identified parameters β_j^+ and ϕ_j^+. Figure 2.3 demonstrates that $\|\beta_j^+ - \beta_*\|_2$ and $\|\phi_j^+ - \phi_*\|_2$ are arbitrarily small for sufficient large j, which agrees with Theorem 2.2. Note that $\|\beta_j^+ - \beta_*\|_2$ and $\|\phi_j^+ - \phi_*\|_2$ do not decrease monotonically. The Bode plots of G_{ff}^+ and G_{fb}^+ with $\Phi = \Lambda_1, \Phi = \Lambda_2$, and $\Phi = \Lambda_{25}$ are shown in Figure 2.4. The identified transfer functions G_{ff}^+ and G_{fb}^+ with $\Phi = \Lambda_{25}$ approximate G_{ff} and G_{fb} better than those with $\Phi = \Lambda_1$ and $\Phi = \Lambda_2$. $\triangle$

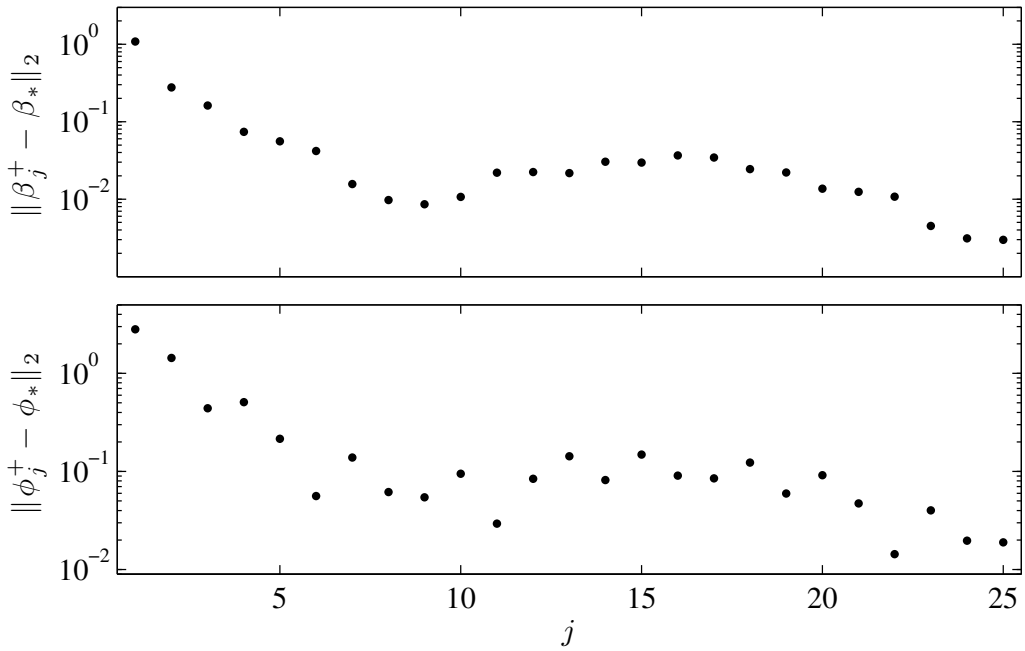

Figure 2.3: *Noiseless data and* $\phi_* \notin \Phi$. For $j = 1, \ldots, 25$, Algorithm 2.1 is used with the candidate pool Λ_j to obtain the identified parameters β_j^+ and ϕ_j^+. Note that $\|\beta_j^+ - \beta_*\|_2$ and $\|\phi_j^+ - \phi_*\|_2$ can be made arbitrarily small if the candidate pool is sufficiently dense.

Example 2.4. *Noisy data and* $\phi_* \in \Phi$. For $i = 1, \ldots, 20$, let $n_{r,i}(t)$ and $n_{y,i}(t)$ be zero-mean Gaussian white-noise realizations with variance of 4^{-i}. Moreover, for $i = 1, \ldots, 20$, let $\sigma_{r,i}(\jmath\omega)$ and $\sigma_{y,i}(\jmath\omega)$ be the Fourier transforms of $n_{r,i}$ and $n_{y,i}$, respectively. For $i = 1, \ldots, 20$, the noisy closed-loop frequency response data is $H_i(\omega_k) \triangleq \tilde{G}(\jmath\omega_k) + \sigma_i(\jmath\omega_k)$, where $\sigma_i(\jmath\omega_k) \triangleq [\tilde{G}(\jmath\omega_k)\sigma_{r,i}(\jmath\omega_k) + \sigma_{y,i}(\jmath\omega_k)]/r(\jmath\omega_k)$. For $i = 1, \ldots, 20$, define

$$R_i \triangleq \frac{1}{N} \sum_{k=1}^{N} \left| \frac{\sigma_i(\jmath\omega_k)}{\tilde{G}(\jmath\omega_k)} \right|,$$

which is the frequency-averaged noise-to-signal ratio. In this example, for $i = 1, \ldots, 20$, $R_i \in (0, 24)$. Specifically, $R_1 = 23.8$, $R_5 = 1.39$, $R_{10} = 4.49 \times 10^{-2}$, $R_{12} = 9.53 \times 10^{-3}$, and $R_{20} = 4.36 \times 10^{-5}$.

For $i = 1, \ldots, 20$, Algorithm 2.1 is used with the candidate pool $\Phi = \Lambda_0$ and data

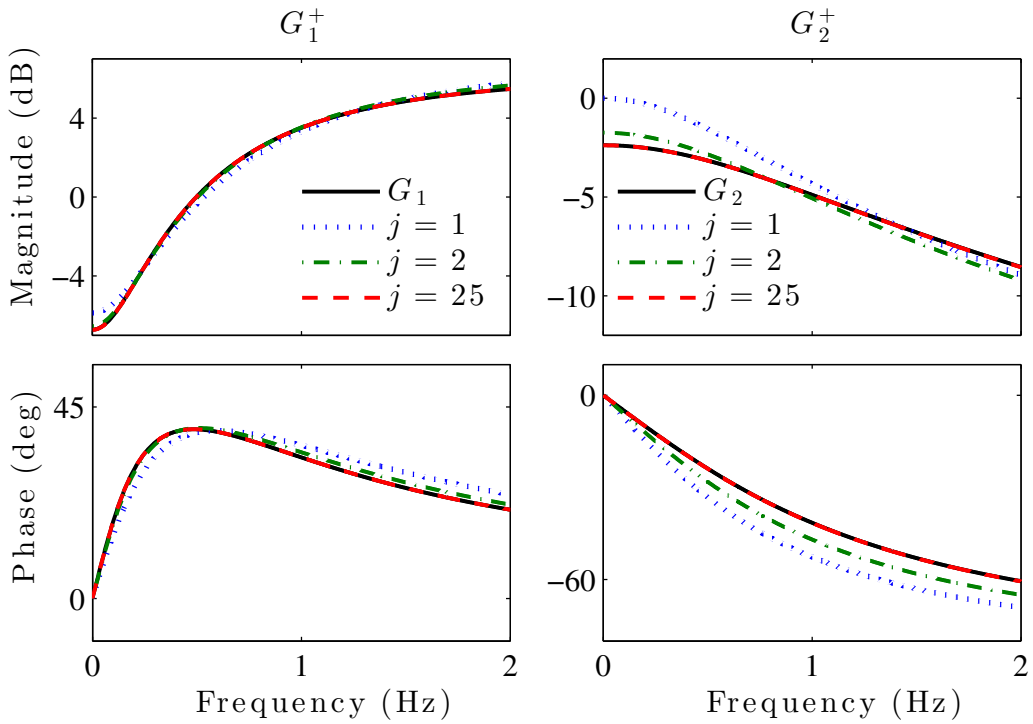

Figure 2.4: *Noiseless data and* $\phi_* \notin \Phi$. For $j = 1, 2, 25$, Algorithm 2.1 is used with the candidate pool Λ_j to obtain G_{ff}^+ and G_{fb}^+. Note that G_{ff}^+ and G_{fb}^+ with candidate pool Λ_{25} approximate G_{ff} and G_{fb} better than those with candidate pools Λ_1 and Λ_2.

$\{H_i(\omega_k)\}_{k=1}^N$ to obtain the identified parameters β_i^+ and ϕ_i^+. Figure 2.5 demonstrates that for $i \geq 14$, $\phi_i^+ = \phi_*$ and for sufficiently large i, $\|\beta_i^+ - \beta_*\|_2$ is arbitrarily small, which agrees with Theorem 2.3. The Bode plots of G_{ff}^+ and G_{fb}^+ with data $\{H_5(\omega_k)\}_{k=1}^N$, $\{H_{10}(\omega_k)\}_{k=1}^N$, and $\{H_{20}(\omega_k)\}_{k=1}^N$ are shown in Figure 2.6. The identified transfer functions G_{ff}^+ and G_{fb}^+ with data $\{H_{20}(\omega_k)\}_{k=1}^N$ approximate G_{ff} and G_{fb} better than those with data $\{H_5(\omega_k)\}_{k=1}^N$ and $\{H_{10}(\omega_k)\}_{k=1}^N$. The identified transfer function G_{fb}^+ with data $\{H_{20}(\omega_k)\}_{k=1}^N$ is $G_{\text{fb}}^+ = G_{\text{fb}}$. △

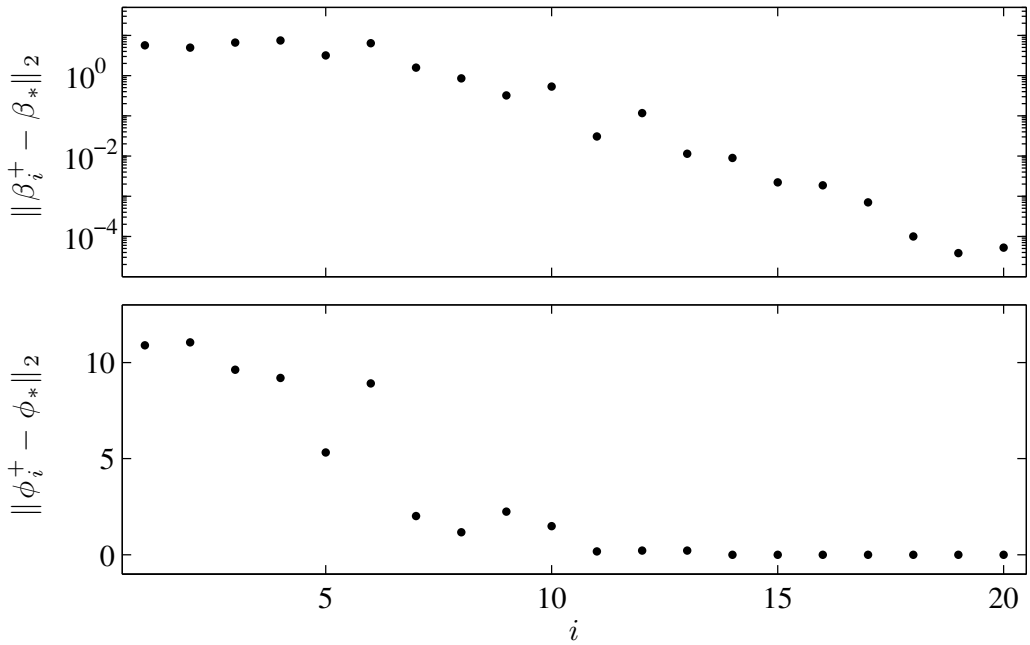

Figure 2.5: *Noisy data and* $\phi_* \in \Phi$. For $i = 1, \ldots, 20$, Algorithm 2.1 is used with the candidate pool Λ_0 and data $\{H_i(\omega_k)\}_{k=1}^N$ to obtain the identified parameters β_i^+ and ϕ_i^+. For $i \geq 14$, $\phi_i^+ = \phi_*$. Note that $\|\beta_i^+ - \beta_*\|_2$ can be made arbitrarily small if the norm of the noise σ_* is sufficiently small.

Example 2.5. *Noisy data and* $\phi_* \notin \Phi$. Consider the noisy closed-loop frequency response data $\{H_5(\omega_k)\}_{k=1}^N$, $\{H_{10}(\omega_k)\}_{k=1}^N$, $\{H_{12}(\omega_k)\}_{k=1}^N$, and $\{H_{20}(\omega_k)\}_{k=1}^N$ given in Example 2.4. Moreover, consider $\Lambda_1, \ldots, \Lambda_{25}$ given in Example 2.3. For $i = 5, 10, 12, 20$, and $j = 1, \ldots, 25$, Algorithm 2.1 is used with the candidate pool $\Phi = \Lambda_j$ and data $\{H_i(\omega_k)\}_{k=1}^N$ to obtain $\beta_{j,i}^+$ and $\phi_{j,i}^+$. Figure 2.7 demonstrates that $\|\beta_{j,i}^+ - \beta_*\|_2$ and $\|\phi_{j,i}^+ - \phi_*\|_2$ are arbitrarily small for sufficient large j and i, which agrees with Theorem 2.4. $\triangle$

2.7 Conclusions

In this chapter, we present a frequency-domain SSID algorithm for identifying unknown feedback and feedforward subsystems interconnected with a known subsystem. This SSID method ensures asymptotic stability of the identified closed-loop transfer

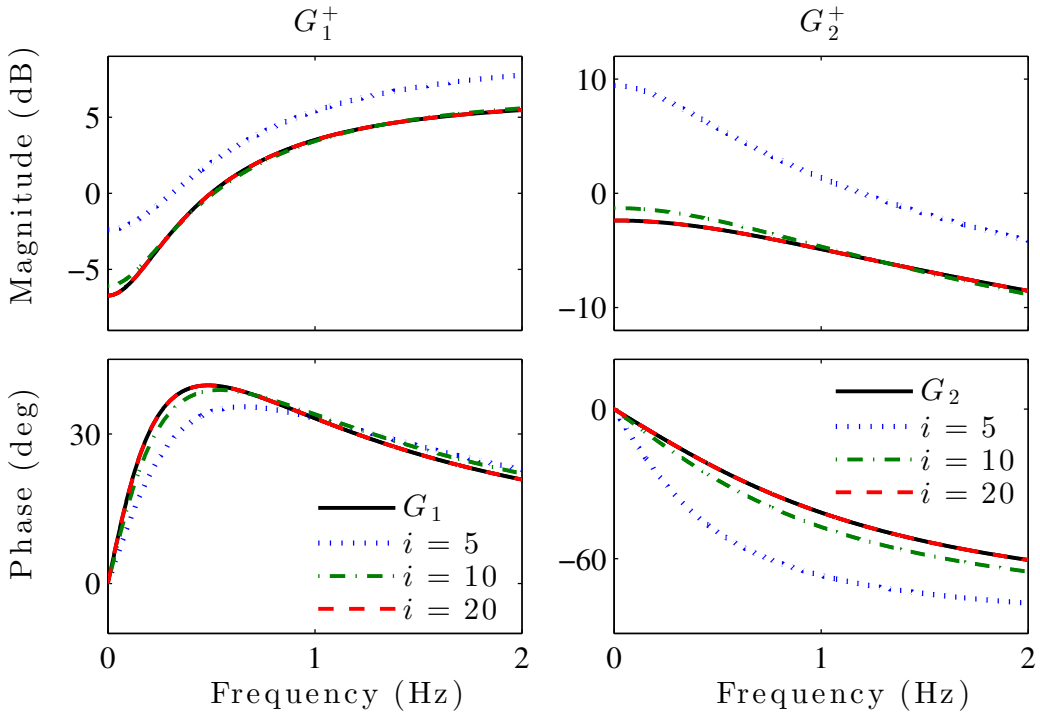

Figure 2.6: *Noisy data and* $\phi_* \in \Phi$. For $i = 5, 10, 20$, Algorithm 2.1 is used with the candidate pool Λ_0 and data $\{H_i(\omega_k)\}_{k=1}^N$ to obtain $G_{\rm ff}^+$ and $G_{\rm fb}^+$. Note that $G_{\rm ff}^+$ and $G_{\rm fb}^+$ with $\{H_{20}(\omega_k)\}_{k=1}^N$ approximate $G_{\rm ff}$ and $G_{\rm fb}$ better than those with $\{H_5(\omega_k)\}_{k=1}^N$ and $\{H_{10}(\omega_k)\}_{k=1}^N$.

function. The method has application to modeling human control behavior (both feedback and feedforward). The main analytic results of the chapter are Theorems 2.1–2.4, which describe the properties of the SSID algorithm. In particular, Theorem 2.4 shows that the coefficients of the identified feedback and feedforward transfer functions are arbitrarily close to the true coefficients if the candidate pool is sufficiently dense and the data noise is sufficiently small.

In the next chapter, the SSID Algorithm 2.1 is used to model human control behavior in a human-in-the-loop experiment.

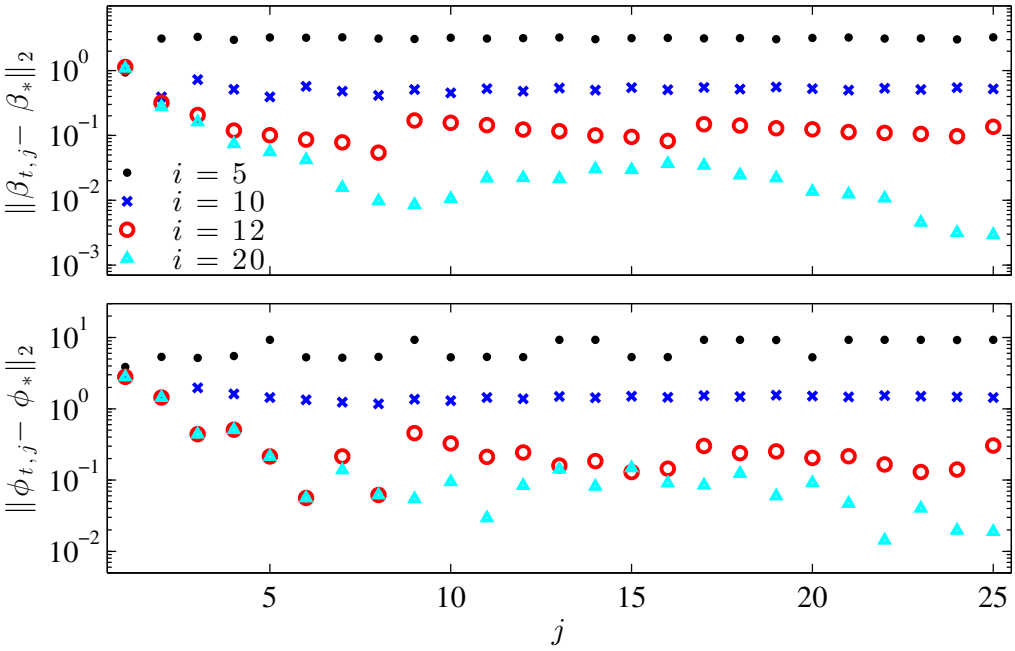

Figure 2.7: *Noisy data and* $\phi_* \notin \Phi$. For $i = 5, 10, 12, 20$, and $j = 1, \ldots, 25$, Algorithm 2.1 is used with the candidate pool Λ_j and data $\{H_i(\omega_k)\}_{k=1}^N$ to obtain $\beta_{j,i}^+$ and $\phi_{j,i}^+$. Note that $\|\beta_{j,i}^+ - \beta_*\|_2$ and $\|\phi_{j,i}^+ - \phi_*\|_2$ are small for large j and i.

Chapter 3 The Roles of Feedback and Feedforward in Human Learning

We present results from a human-in-the-loop (HITL) experiment in which human subjects learn to control an unknown dynamic system over 40 trials. For each trial, the subsystem identification (SSID) algorithm in Chapter 2 is used to estimate each subject's feedforward (or anticipatory) control and feedback (or reactive) control. Over the 40 trials, the magnitudes of the identified feedback controllers do not change significantly, whereas the identified feedforward controllers do change significantly. By the last trial, the average identified feedforward controller approximates the inverse of the dynamic system. This observation provides evidence that a fundamental component of human learning is updating the anticipatory control until it models the inverse dynamics. The results in this chapter have been submitted for publication in [95].

3.1 Introduction

Humans learn to control a wide range of complex dynamic systems, including bicycles, kites, and hula hoops. The strategies used by humans to control these systems are unclear [96]. The internal model hypothesis proposes that the brain constructs models of the body's interactions with the physical world and that those models are used for control [6, 7, 97]. Suggested uses of internal models include prediction, state estimation, model-based control, and feedforward model inversion [10, 98–104].

The internal model hypothesis has been explored by comparing the results of human control experiments with mathematical models of proposed human control ar-

chitectures [8, 38–50, 52, 105]. These models reproduce certain qualitative features observed in the experiments. However, vastly different control strategies can yield similar dynamic behavior. Thus, a model that reproduces qualitative features of an experiment does not necessarily provide an accurate representation of the human's control strategy.

In contrast to the approaches in [8,38–50,52,105], SSID is used to obtain feedforward and feedback controllers that are the best fit to data obtained from a human control experiment. Other studies that use system identification approaches to model human responses include [74, 75, 85, 86, 106–108]. Specifically, [85] identifies models of a human's precision grip force and [86] identifies models of a human's oculomotor system. However, the human systems investigated in [85, 86] are modeled without feedback. In [106–108], identification methods are used to model the behavior of human pilots; however, these models include error feedback only and thus, do not incorporate feedforward control. In [74, 75], feedforward and feedback controllers are estimated for humans performing ramp-tracking tasks. However, these feedforward and feedback models rely on an assumed control strategy, specifically, the feedforward models are assumed to include the inverse system dynamics. In contrast to [74,75,85,86,106–108], the present chapter uses SSID to model a human's response with both feedforward and feedback control without assuming *a priori* a specific feedforward or feedback control strategy.

3.2 Experimental Methods

Subjects in this experiment use a single-degree-of-freedom joystick to affect the motion of an object on a computer screen as shown in Figure 3.1. The controlled object's position y and the joystick position u are functions of time t and are related to each other by a dynamic system. A reference object, whose position r is independent of the joystick position u, also moves on the computer screen. The subject's objective

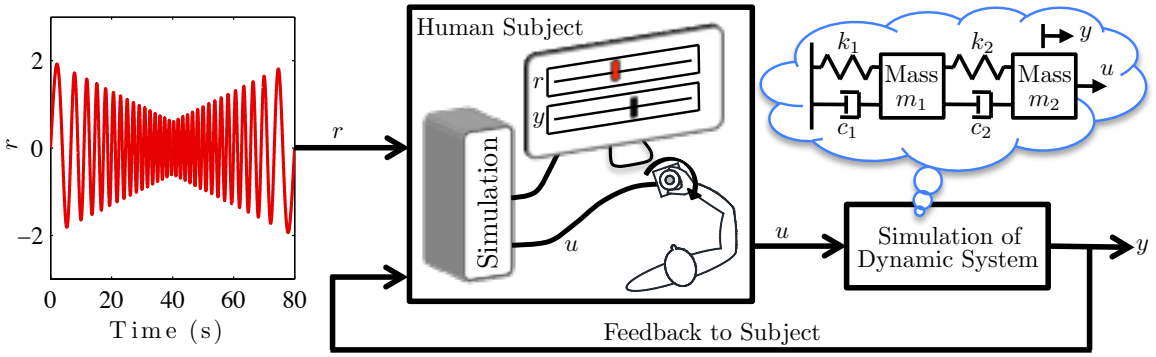

Figure 3.1: Subjects use a joystick to affect the motion of an object on a computer screen. The object's position y represents the position of a mass in a mass-spring-damper system that is simulated by a computer, and the joystick position u represents the force applied to the mass. A reference object is also displayed on the screen, and its position r is an 80-s chirp signal.

is to manipulate the joystick in a manner that makes the controlled object and the reference object have the same position at each instant of time. Specifically, the objective is to generate a control u that minimizes the magnitude of the command-following error $e = r - y$. Prior to performing the experiment, a subject has no knowledge of the reference object's motion r or the dynamic system relating u and y.

The controlled object's position y satisfies the differential equation

$$M \begin{bmatrix} \ddot{x} \\ \ddot{y} \end{bmatrix} + C \begin{bmatrix} \dot{x} \\ \dot{y} \end{bmatrix} + K \begin{bmatrix} x \\ y \end{bmatrix} = Bu, \tag{3.1}$$

where M, C, and K are real 2×2 matrices, B is a real 2×1 matrix, and the initial conditions are zero. Many physical systems such as aircraft, bicycles, and haptic interfaces can be modeled by (3.1). In this experiment, (3.1) models the mass-spring-damper system shown in Figure 3.1, where y represents the position of the second mass, and u represents the force applied to the second mass. In this case, the matrices

M, C, K, and B are given by

$$M = \begin{bmatrix} m_1 & 0 \\ 0 & m_2 \end{bmatrix}, \qquad C = \begin{bmatrix} c_1 + c_2 & -c_2 \\ -c_2 & c_2 \end{bmatrix}, \tag{3.2}$$

$$K = \begin{bmatrix} k_1 + k_2 & -k_2 \\ -k_2 & k_2 \end{bmatrix}, \qquad B = \begin{bmatrix} 0 \\ 1 \end{bmatrix}, \tag{3.3}$$

where m_1 and m_2 are the masses, k_1 and k_2 are the spring stiffnesses, and c_1 and c_2 are the damping constants shown in Figure 3.1. The input-output response of (3.1)–(3.3) is written in the Laplace domain as $\hat{y}(s) = G(s)\hat{u}(s)$, where

$$G(s) = B^{\mathrm{T}}(s^2M + sC + K)^{-1}B$$

is the transfer function from u to y, and $\hat{u}(s)$ and $\hat{y}(s)$ are the Laplace transforms of u and y. Since all of the physical parameters m_1, m_2, c_1, c_2, k_1, and k_2 are positive, the transfer function G is asymptotically stable (that is, the poles of G are in the open-left-half complex plane) and minimum phase (that is, the zeros of G are in the open-left-half complex plane). Specifically, the transfer function is

$$G(s) = \frac{m_1s^2 + c_1s + c_2s + k_1 + k_2}{(m_1s^2 + c_1s + k_1)(m_2s^2 + c_2s + k_2) + m_2c_2s^3 + m_2k_2s^2},$$

and the parameters are $m_1 = 1$, $m_2 = 0.5$, $c_1 = 0.56\pi$, $c_2 = 0.5\pi$, $k_1 = 0.16\pi^2$, and $k_2 = 0.5\pi^2$.

A total of 10 people voluntarily participated in this study. At the time of the experiment, these 10 subjects had no known neurological or motor control disorders and were 18–35 years of age. Each subject performed 40 trials of the experiment in a period of 14 days. A trial is an 80-second time period during which a subject operates a joystick. Each subject's 40 trials were divided into 8 sessions, and each

session consisted of 5 trials. Each session was completed within a period of 20 minutes. No subject participated in more than one session within a 12-hour period. For each session, subjects are placed in an isolated area free from distraction. Subjects sit in a chair facing a computer screen. A subject's dominant hand is used to manipulate a single-degree-of-freedom joystick. Prior to their first trial, the subjects are told that manipulating the joystick moves an object that is displayed on the computer screen, as shown in Figure 3.1. A reference object is also displayed on the computer screen. Participants are instructed to manipulate the joystick such that the controlled object and the reference object have the same position at each instant of time. The subjects possess no initial knowledge of the reference object's motion or the dynamics G from the joystick motion to object's motion.

This experiment satisfies the U.S. Department of Health and Human Services Code of Federal Regulation for human subject research (45 CFR 46) and was approved by the University of Kentucky Institutional Review Board (IRB number 12-0816-P4S).

For each trial, the joystick position u is the real-time input to a computer simulation of the dynamic system (3.1)–(3.3), which determines the controlled object's motion on the computer screen. The reference object's position r is an 80-second chirp signal with frequency content between 0.1 and 0.4 Hz, specifically,

$$r(t) = \begin{cases} (2 - 0.035t)\sin\left(0.2\pi t + 0.015\pi t^2\right), & \text{if } t \in [0, 40], \\ (0.8 - 0.035t)\sin\left(0.2\pi(80 - t) + 0.015\pi(80 - t)^2\right), & \text{if } t \in (40, 80]. \end{cases}$$

3.3 Experimental Results in the Time Domain

Each trial of the experiment lasts for $T = 80$s. For each trial of the experiment, we record data r and y with the sampling time $T_\mathrm{s} = 0.002$s and obtain the sequences $r(iT_\mathrm{s})$, $y(iT_\mathrm{s})$, and $e(iT_\mathrm{s})$, where $i = 0, 1, 2, \ldots, 40000$. For each trial, we define time-

averaged magnitude of the error is

$$\|e\| = \frac{1}{40001} \sum_{i=0}^{40000} |e(iT_s)|.$$

Figure 3.2(a) shows the reference r and output y for one subject's Trials 1 and 40. For this subject, the error e for Trial 40 is smaller than that for Trial 1. Figure 3.2(b)

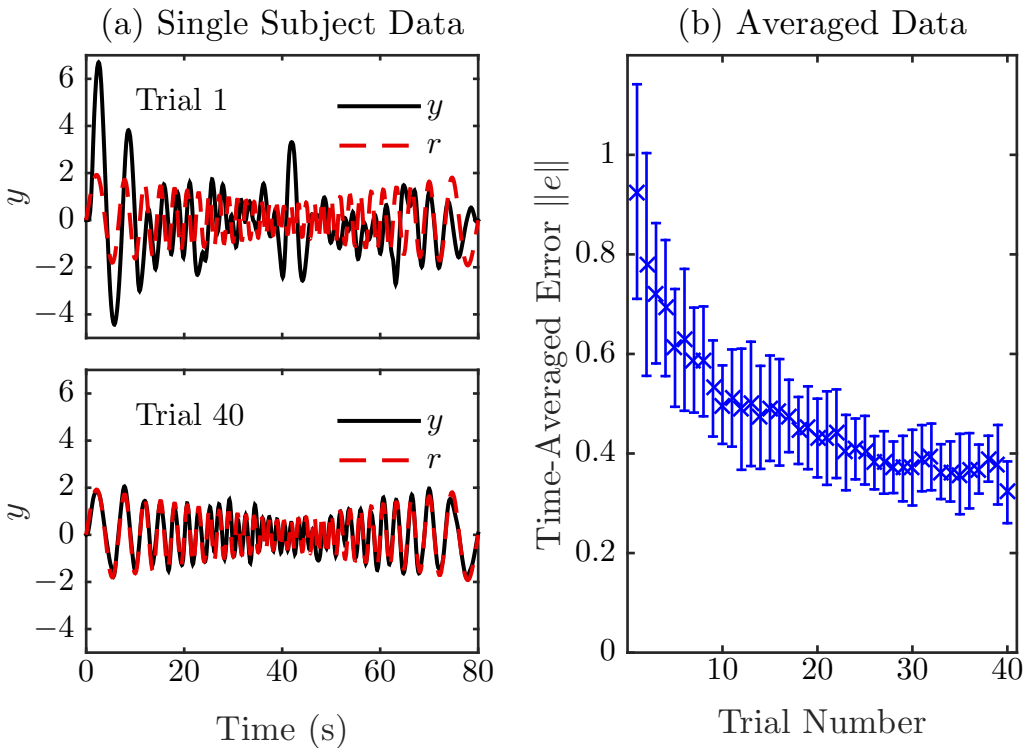

Figure 3.2: Figure (a) shows the position y and reference r for a single subject on the first and last trial. The subject's error $e = r - y$ is smaller on the last trial than on the first trial, indicating that the subject learned to control the dynamic system. Figure (b) shows the time-averaged magnitude of the error $\|e\|$ of the 10 subjects for each of the 40 trials. The $\times$ indicates the mean of the 10 subjects and the vertical lines show one standard deviation. The mean $\|e\|$ improves over the trials.

shows the time-averaged magnitude of the error $\|e\|$ of the 10 subjects for each of the 40 trials. The mean $\|e\|$ improves over the trials.

3.4 Discussion of Potential Control Strategies

The linear time-invariant control architecture shown in Figure 3.3 is used to model each subject's control strategy. See [6] for a physiological interpretation of this archi-

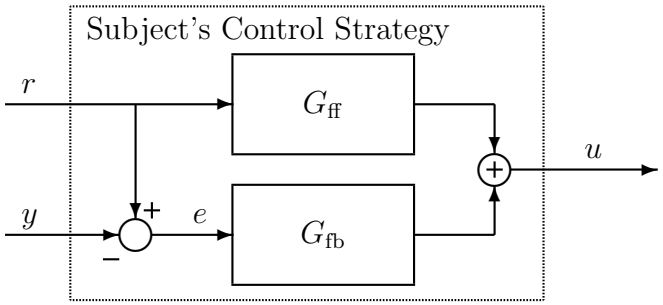

Figure 3.3: Each subject's control strategy is modeled using a feedback controller G_{fb} and a feedforward controller G_{ff}.

tecture. A subject's control strategy is modeled by

$$\hat{u}(s) = G_{\text{fb}}(s)\hat{e}(s) + G_{\text{ff}}(s)\hat{r}(s), \tag{3.4}$$

where $\hat{e}(s)$ and $\hat{r}(s)$ are the Laplace transforms of e and r, and the real rational transfer functions G_{fb} and G_{ff} are the feedback and feedforward controllers. Feedback is the reactive control determined from the observed error e, whereas feedforward is the anticipatory control determined solely from the reference r. The closed-loop response is $\hat{e}(s) = \tilde{G}_{er}(s)\hat{r}(s)$, where

$$\tilde{G}_{er}(s) \triangleq \frac{1 - G_{\text{ff}}(s)G(s)}{1 + G_{\text{fb}}(s)G(s)} \tag{3.5}$$

is the closed-loop transfer function from r to e. The frequency response of $\tilde{G}_{er}$ is the complex-valued function $\tilde{G}_{er}(\jmath\omega)$, where ω is the frequency.

To ensure that the error e is bounded, the controllers G_{ff} and G_{fb} must be such that the closed-loop transfer function $\tilde{G}_{er}$ is asymptotically stable (that is, the poles of $\tilde{G}_{er}$ are in the open-left-half complex plane). To make the error e small, G_{ff} and

G_{fb} must make the magnitude of $\tilde{G}_{er}(\jmath\omega)$ small at frequencies coinciding with the 0.1-to-0.4 Hz frequency content of the reference r.

Now, we consider control strategies that could be used to achieve good command following. One control strategy is to use high gain in feedback. It follows from (3.5) that the magnitude of $\tilde{G}_{er}(\jmath\omega)$ is small if the magnitude of $G_{\text{fb}}(\jmath\omega)$ is large. Therefore, as long as $\tilde{G}_{er}$ is asymptotically stable, the magnitude of e is decreased by increasing the magnitude of $G_{\text{fb}}(\jmath\omega)$ at the frequencies of r. Figure 3.4(a) shows that using high gain in feedback can make the magnitude of e small even if there is no feedforward control. High-gain feedback makes the magnitude of e small by making the closed-loop transfer function from r to y

$$\tilde{G}_{yr}(s) \triangleq 1 - \tilde{G}_{er}(s) = \frac{G(s)[G_{\text{ff}}(s) + G_{\text{fb}}(s)]}{1 + G(s)G_{\text{fb}}(s)}$$

close to 1 over the 0-to-0.5 Hz frequency range. Note that humans cannot use arbitrarily high gain in feedback due to delay in a human's reaction as well as the physical limitations of a human's speed and range of motion.

Another control strategy is to use the inverse dynamics G^{-1} in feedforward. If $G_{\text{ff}} \approx G^{-1}$, then it follows from (3.5) that $\tilde{G}_{er} \approx 0$, which implies that the command-following error is small, that is, $e \approx 0$. In this case, the human must learn to approximate the inverse dynamics G^{-1} in feedforward. Figure 3.4(b) shows that using the approximate inverse dynamics in feedforward can make the magnitude of e small even if there is no feedback control. Other control strategies also make the magnitude of e small. For example, high gain in feedback and approximate inverse dynamics in feedforward can be combined across the frequency range of r.

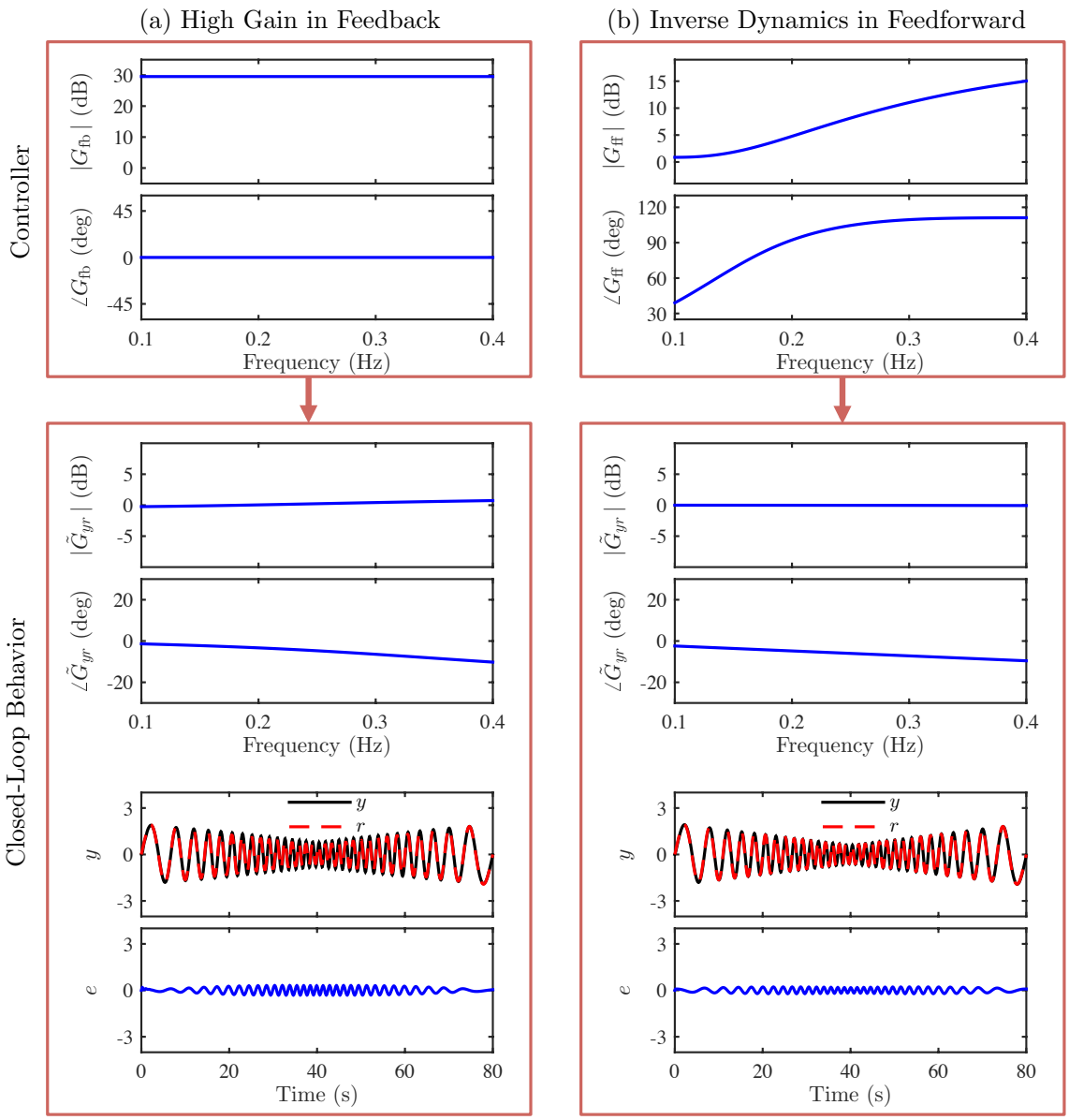

Figure 3.4: Two control strategies that make the magnitude of the error e small are high gain in feedback and approximate inverse dynamics in feedforward. Figure (a) shows the high-gain control strategy with the proportional feedback controller $G_{\text{fb}} = 30$ and with no feedforward controller (i.e., $G_{\text{ff}} = 0$). Figure (b) shows the control strategy of approximating the inverse dynamics in feedforward. The feedforward controller is $G_{\text{ff}}(s) = 900G^{-1}(s)/(s+30)^2$, which is a proper approximation of G^{-1} across the frequency range. There is no feedback controller (i.e., $G_{\text{fb}} = 0$). In both cases, the closed-loop transfer function $\tilde{G}_{yr}$ is approximately 1 (i.e., 0 decibels magnitude and 0 degrees phase) across the frequency range and the magnitude of e is small.

3.5 Modeling Human Control Behavior

We review the SSID algorithm in Chapter 2 in a simplified form and use it to identify the feedback and feedforward controllers used by humans in the experiment. For each trial, a subject's control strategy is modeled using the linear time-invariant control structure 3.4 shown in Figure 3.3. We also present the details how we generated the candidate pool used in the SSID algorithm.

3.5.1 Summary of Subsystem Identification Algorithm

The time-domain signals $\{r(iT_{\mathrm{s}})\}_{i=0}^{40000}$ and $\{y(iT_{\mathrm{s}})\}_{i=0}^{40000}$ are divided into two segments of 40 s. For each segment, the discrete Fourier transform is calculated at the frequencies $\omega_k = 2\pi\,(0.1 + 0.025(k-1))$ rad/s, where $k = 1, 2 \ldots, N = 13$. The ratio of the discrete Fourier transforms from the two segments are averaged to obtain the frequency response data $\{H(\omega_k)\}_{k=1}^{N}$.

Our objective is to determine G_{ff} and G_{fb} such that the modeled frequency response $\{\tilde{G}_{yr}(\jmath\omega_k)\}_{k=1}^{N}$ approximates the data $\{H(\omega_k)\}_{k=1}^{N}$. To achieve this objective, we seek to find G_{ff} and G_{fb} that minimize the cost $J(G_{\mathrm{ff}}, G_{\mathrm{fb}})$, given by (3.6), subject to the constraint that $\tilde{G}_{yr}$ is asymptotically stable.

$$\begin{aligned} J(G_{\mathrm{ff}}, G_{\mathrm{fb}}) &= \sum_{k=1}^{N} \left| \tilde{G}_{yr}(\jmath\omega_k) - H(\omega_k) \right|^2 \\ &= \sum_{k=1}^{N} \left| \frac{G(\jmath\omega_k)\,[G_{\mathrm{ff}}(\jmath\omega_k) + G_{\mathrm{fb}}(\jmath\omega_k)]}{1 + G_{\mathrm{fb}}(\jmath\omega_k)G(\jmath\omega_k)} - H(\omega_k) \right|^2, \end{aligned} \tag{3.6}$$

We parameterize the feedback and feedforward controllers by their numerator and denominator coefficients and cast the SSID problem in terms of these coefficients. Let n_{ff} and n_{fb} be nonnegative integers that denote the degrees of the numerator polynomials of G_{ff} and G_{fb}. Similarly, let d_{ff} and d_{fb} be nonnegative integers that denote the degrees of the denominator polynomials of G_{ff} and G_{fb}. Define $d \triangleq$

$d_{\mathrm{ff}} + d_{\mathrm{fb}} + n_{\mathrm{fb}} + 1$, and consider the functions $\mathcal{N}_{\mathrm{ff}} \colon \mathbb{C} \times \mathbb{R}^{n_{\mathrm{ff}}+1} \to \mathbb{C}$, $\mathcal{D}_{\mathrm{ff}} \colon \mathbb{C} \times \mathbb{R}^{d} \to \mathbb{C}$, $\mathcal{N}_{\mathrm{fb}} \colon \mathbb{C} \times \mathbb{R}^{d} \to \mathbb{C}$, and $\mathcal{D}_{\mathrm{fb}} \colon \mathbb{C} \times \mathbb{R}^{d} \to \mathbb{C}$ given by

$$\begin{aligned} \mathcal{N}_{\mathrm{ff}}(s, \beta) &\triangleq \nu_{\mathrm{ff}}(s)\beta, & \mathcal{D}_{\mathrm{ff}}(s, \phi) &\triangleq s^{d_{\mathrm{ff}}} + \mu_{\mathrm{ff}}(s)\phi, \\ \mathcal{N}_{\mathrm{fb}}(s, \phi) &\triangleq \nu_{\mathrm{fb}}(s)\phi, & \mathcal{D}_{\mathrm{fb}}(s, \phi) &\triangleq s^{d_{\mathrm{fb}}} + \mu_{\mathrm{fb}}(s)\phi, \end{aligned}$$

where $\nu_{\mathrm{ff}} : \mathbb{C} \to \mathbb{C}^{1 \times (n_{\mathrm{ff}}+1)}$ and $\mu_{\mathrm{ff}}, \nu_{\mathrm{fb}}, \mu_{\mathrm{fb}} : \mathbb{C} \to \mathbb{C}^{1 \times d}$ are given by

$$\begin{aligned} \nu_{\mathrm{ff}}(s) &\triangleq \begin{bmatrix} s^{n_{\mathrm{ff}}} & s^{n_{\mathrm{ff}}-1} & \cdots & s & 1 \end{bmatrix}, \\ \mu_{\mathrm{ff}}(s) &\triangleq \begin{bmatrix} s^{d_{\mathrm{ff}}-1} & s^{d_{\mathrm{ff}}-2} & \cdots & s & 1 & 0_{1 \times (d_{\mathrm{fb}}+n_{\mathrm{fb}}+1)} \end{bmatrix}, \\ \nu_{\mathrm{fb}}(s) &\triangleq \begin{bmatrix} 0_{1 \times d_{\mathrm{ff}}} & s^{n_{\mathrm{fb}}} & s^{n_{\mathrm{fb}}-1} & \cdots & s & 1 & 0_{1 \times d_{\mathrm{fb}}} \end{bmatrix}, \\ \mu_{\mathrm{fb}}(s) &\triangleq \begin{bmatrix} 0_{1 \times (d_{\mathrm{ff}}+n_{\mathrm{fb}}+1)} & s^{d_{\mathrm{fb}}-1} & s^{d_{\mathrm{fb}}-2} & \cdots & s & 1 \end{bmatrix}. \end{aligned}$$

We consider the functions $\mathcal{G}_{\mathrm{ff}} \colon \mathbb{C} \times \mathbb{R}^{n_{\mathrm{ff}}+1} \times \mathbb{R}^{d} \to \mathbb{C}$ and $\mathcal{G}_{\mathrm{fb}} \colon \mathbb{C} \times \mathbb{R}^{d} \to \mathbb{C}$ given by

$$\mathcal{G}_{\mathrm{ff}}(s, \beta, \phi) \triangleq \frac{\mathcal{N}_{\mathrm{ff}}(s, \beta)}{\mathcal{D}_{\mathrm{ff}}(s, \phi)}, \qquad \mathcal{G}_{\mathrm{fb}}(s, \phi) \triangleq \frac{\mathcal{N}_{\mathrm{fb}}(s, \phi)}{\mathcal{D}_{\mathrm{fb}}(s, \phi)},$$

where β contains the numerator coefficients of $\mathcal{G}_{\mathrm{ff}}$, and ϕ contains the denominator coefficients of $\mathcal{G}_{\mathrm{ff}}$ as well as the numerator and denominator coefficients of $\mathcal{G}_{\mathrm{fb}}$.

The real rational transfer function G can be expressed as $G(s) = N_{\mathrm{p}}(s)/D_{\mathrm{p}}(s)$, where N_{p} and D_{p} are coprime polynomials. Next, consider the cost function $\mathcal{J} \colon \mathbb{R}^{n_{\mathrm{ff}}+1} \times \mathbb{R}^{d} \to [0, \infty)$ given by

$$\mathcal{J}(\beta, \phi) \triangleq J(\mathcal{G}_{\mathrm{ff}}(s, \beta, \phi), \mathcal{G}_{\mathrm{fb}}(s, \phi)) = \beta^{\mathrm{T}} \Omega_2(\phi) \beta + \Omega_1^{\mathrm{T}}(\phi)\beta + \Omega_0(\phi),$$

where

$$\Omega_0(\phi) \triangleq \sum_{k=1}^{N} \left| \frac{\tilde{\mathcal{N}}_2(\jmath\omega_k, \phi)}{\tilde{\mathcal{D}}(\jmath\omega_k, \phi)} - H(\omega_k) \right|^2,$$

$$\Omega_1(\phi) \triangleq 2\mathrm{Re} \sum_{k=1}^{N} \left[\frac{\tilde{\mathcal{N}}_2(\jmath\omega_k, \phi)}{\tilde{\mathcal{D}}(\jmath\omega_k, \phi)} - H(\omega_k) \right] \frac{\tilde{\mathcal{N}}_1^{\mathrm{T}}(-\jmath\omega_k, \phi)}{\tilde{\mathcal{D}}(-\jmath\omega_k, \phi)},$$

$$\Omega_2(\phi) \triangleq \mathrm{Re} \sum_{k=1}^{N} \frac{\tilde{\mathcal{N}}_1^{\mathrm{T}}(-\jmath\omega_k, \phi)\tilde{\mathcal{N}}_1(\jmath\omega_k, \phi)}{\left| \tilde{\mathcal{D}}(\jmath\omega_k, \phi) \right|^2},$$

and

$$\tilde{\mathcal{N}}_2(s, \phi) \triangleq N_{\mathrm{p}}(s)\mathcal{D}_{\mathrm{ff}}(s, \phi)\mathcal{N}_{\mathrm{fb}}(s, \phi),$$

$$\tilde{\mathcal{N}}_1(s, \phi) \triangleq N_{\mathrm{p}}(s)\mathcal{D}_{\mathrm{fb}}(s, \phi)\nu_{\mathrm{ff}}(s),$$

$$\tilde{\mathcal{D}}(s, \phi) \triangleq [D_{\mathrm{p}}(s)\mathcal{D}_{\mathrm{fb}}(s, \phi) + N_{\mathrm{p}}(s)\mathcal{N}_{\mathrm{fb}}(s, \phi)]\mathcal{D}_{\mathrm{ff}}(s, \phi).$$

For each $\phi \in \mathbb{R}^d$, $\Omega_0(\phi) \in \mathbb{R}$, $\Omega_1(\phi) \in \mathbb{R}^{n_{\mathrm{ff}}+1}$, and $\Omega_2(\phi) \in \mathbb{R}^{(n_{\mathrm{ff}}+1)\times(n_{\mathrm{ff}}+1)}$ is positive semidefinite.

We restrict our attention to $\phi \in \mathbb{R}^d$ contained in

$$\mathcal{S} \triangleq \{\phi \in \mathbb{R}^d \colon \tilde{\mathcal{D}}(s, \phi) \text{ is Hurwitz}\},$$

which is the set of parameters that yield asymptotically stable closed-loop transfer functions. Let M be a positive integer, and let $\Phi \subset \mathcal{S}$ be a set with M elements. We call Φ the *candidate pool*. Next, we create a candidate sequence using the M elements in the candidate pool Φ. Specifically, for $i, j = 1, 2, \ldots, M$, let $\phi_i, \phi_j \in \Phi$ such that if $i \neq j$, then $\phi_i \neq \phi_j$. The sequence $\{\phi_i\}_{i=1}^{M}$ is not unique; however, the order of the sequence is selected arbitrarily.

Define $\mathcal{M} \triangleq \{1, 2, \ldots, M\}$, and for all $i \in \mathcal{M}$, define the quadratic cost function

$$\mathcal{J}_i(\beta) \triangleq \mathcal{J}(\beta, \phi_i) = \beta^{\mathrm{T}}\Omega_2(\phi_i)\beta + \Omega_1^{\mathrm{T}}(\phi_i)\beta + \Omega_0(\phi_i).$$

If the number N of frequency response data is sufficiently large, then $\Omega_2(\phi_1), \ldots, \Omega_2(\phi_M)$ are positive definite and thus nonsingular. In this case, for each $i = 1, \ldots, N$, define

$$\beta_i \triangleq -\frac{1}{2}\Omega_2^{-1}(\phi_i)\Omega_1(\phi_i),$$

which is the unique global minimizer of $\mathcal{J}_i$. Specifically, for each $i \in \mathcal{M}$ and for all $\beta \in \mathbb{R}^{n_{\mathrm{ff}}+1} \backslash \{\beta_i\}$,

$$\mathcal{J}_i(\beta_i) < \mathcal{J}_i(\beta).$$

Let $\ell \in \mathcal{M}$ be the smallest integer such that $\mathcal{J}_\ell(\beta_\ell) = \min_{i \in \mathcal{M}} \mathcal{J}_i(\beta_i)$. Thus, the identified parameters are β_ℓ and ϕ_ℓ and the identified transfer functions are

$$G_{\mathrm{ff}}(s) \triangleq \frac{\mathcal{N}_{\mathrm{ff}}(s, \beta_\ell)}{\mathcal{D}_{\mathrm{ff}}(s, \phi_\ell)}, \qquad G_{\mathrm{fb}}(s) \triangleq \frac{\mathcal{N}_{\mathrm{fb}}(s, \phi_\ell)}{\mathcal{D}_{\mathrm{fb}}(s, \phi_\ell)}. \tag{3.7}$$

The linear feedback-and-feedforward control (3.4) with are estimates of the unknown subsystem. We now summarize this SSID method.

Algorithm 3.1. Consider the known transfer function G and the known closed-loop frequency response data $\{H(\omega_k)\}_{k=1}^N$. Then, the subsystem identification algorithm is as follows:

Step 1. Generate the candidate pool $\Phi \subset \mathcal{S}$ and candidate sequence $\{\phi_i\}_{i=1}^M$.

Step 2. For each $i \in \mathcal{M}$, find $\beta_i \triangleq -\frac{1}{2}\Omega_2^{-1}(\phi_i)\Omega_1(\phi_i)$, which is the unique global minimizer of $\mathcal{J}_i$.

Step 3. Find the smallest $\ell \in \mathcal{M}$ such that $\mathcal{J}_\ell(\beta_\ell) = \min_{i \in \mathcal{M}} \mathcal{J}_i(\beta_i)$.

Step 4. The identified parameters are β_ℓ and ϕ_ℓ.

Step 5. The identified feedforward and feedback transfer functions are G_{ff} and G_{fb} given by (3.7).

3.5.2 Application of SSID Algorithm to Experimental Data

For each of the 400 trials, we identify a second-order strictly proper feedback controller and a second-order improper feedforward controller (i.e., $n_{\text{fb}} = 1$, $n_{\text{ff}} = 4$, $d_{\text{fb}} = 2$, $d_{\text{ff}} = 2$). These controller orders allow for high gain feedback as well as approximate feedforward model inversion, or combinations of these control approaches.

The candidate pool Φ is designed to capture a wide range of behavior over the 0.1-to-0.4 Hz frequency range. The candidate pool Φ is constructed subject to the following conditions:

C1) If $\phi \in \Phi$, $\lambda \in \mathbb{C}$, and $\mathcal{D}_{\text{ff}}(\lambda, \phi) = 0$, then $|\lambda| \leq 25$.

C2) If $\phi \in \Phi$, $\lambda \in \mathbb{C}$, and $\mathcal{D}_{\text{fb}}(\lambda, \phi) = 0$, then $|\lambda| \leq 25$.

C3) If $\phi \in \Phi$, $\lambda \in \mathbb{C}$, and $\mathcal{N}_{\text{fb}}(\lambda, \phi) = 0$, then $|\lambda| \leq 25$.

C4) If $\phi \in \Phi$, then $\max_{\omega \in [0.2\pi, 0.8\pi]} |\mathcal{G}_{\text{fb}}(\jmath\omega, \phi)| \leq 30.5$.

C5) If $\phi \in \Phi$, $\lambda \in \mathbb{C}$, and $\tilde{\mathcal{D}}(\lambda, \phi) = 0$, then $\operatorname{Re} \lambda < -0.1$.

Conditions C1)–C3) constrain Φ to include only elements that have a significant impact on controller dynamics over the 0.1-to-0.4 Hz frequency range. Specifically, C1)–C3) state that for each $\phi \in \Phi$, the poles of the feedforward controller, the poles of the feedback controller, and the zeros of the feedback controller have absolute value between 0 and 25 rad/s. This condition arises because the data $\{H(\omega_k)\}_{k=1}^N$ is at frequencies $\omega_1, \ldots, \omega_N \in [0.2\pi, 0.8\pi]$ rad/s, which corresponds to the the frequency range of the chirp signal r. Thus, we seek to identify G_{ff} and G_{fb} on the interval $[0.2\pi, 0.8\pi]$ rad/s. The upper limit 25 rad/s on the magnitude of the poles and zeros

is one decade above the 0.8π rad/s limit on the chirp frequency (i.e., $(10)(0.8\pi) \approx 25$). Moreover, a pole or zero with magnitude greater than 25 rad/s has negligible effect on the Bode plot over the frequency range $[0.2\pi, 0.8\pi]$ rad/s. Thus, the candidate pool is restricted to contain elements that correspond to poles and zeros with absolute value between 0 and 25 rad/s.

Conditions C4) states that for each $\phi \in \Phi$, the peak magnitude of the feedback controller $\mathcal{G}_{\text{fb}}(s, \phi)$ over the frequency range $[0.2\pi, 0.8\pi]$ rad/s is no more than 30.5 (or approximately 30 dB). An upper limit on the magnitude of the feedback controller is imposed, because a human cannot use arbitrarily high gain in feedback. The 30 dB upper limit is determined from another experiment with 10 subjects, where each subject was asked to follow a single-frequency sinusoid using only error feedback (i.e., feedforward of the command signal was not available). In this experiment, the peak magnitude of the feedback controller used by the subjects is approximately 30 dB, suggesting that 30 dB is the peak gain that a human can use in feedback.

Conditions C5) states that for each $\phi \in \Phi$, the real parts of the roots of $\tilde{\mathcal{D}}(s, \phi)$ are bounded away from the imaginary axis, specifically, less than -0.1. This condition guarantees that $\Phi \subset \mathcal{S}$ (i.e., for all $\phi \in \Phi$, the roots of $\tilde{\mathcal{D}}(s, \phi)$ are in the open-left-half complex plane). A pole with -0.1 real part has a settling time of approximately 40 s. Thus, C5) restricts the candidate pool to elements that result in closed-loop transfer functions with settling times less than 40 s. Note that the behavior observed in this experiment exhibits settling times significantly less than 40 s.

The candidate pool contains approximately 160 billion elements, and more details of the candidate pool is present in Appendix B.

The SSID algorithm is implemented using parallel computation on a supercomputer. Algorithm 3.1 is coded in C++ for parallel computation and implemented on the Lipscomb High Performance Computing Cluster at the University of Kentucky. For each trial, Algorithm 3.1 is run on 2 compute nodes of the Lipscomb cluster; each

node has a 16 Intel E5-2670 @ 2.6 GHz cores. For each trial, it takes approximately 3.5 hours to run Algorithm 3.1 using 2 compute nodes and the candidate pool Φ given above. Thus, performing SSIDs for all 400 trials requires approximately 2,800 compute node hours.

3.6 Subsystem Identification Results

For each of the 400 trials, the second-order feedback controller G_{fb} and second-order feedforward controller G_{ff} that minimize J are identified. Figure 3.5 shows the Bode plots of the identified G_{fb} and G_{ff} for the first and last trials of one subject. The identified G_{ff} for the first trial does not approximate G^{-1}, whereas the identified G_{ff} for the last trial is a better approximation of G^{-1}. Similarly results are observed for the other 9 subjects.

Figure 3.6(a) shows that the average magnitude of the identified feedback controller G_{fb} does not change significantly over the 40 trials. This observation contrasts the results of [109], which suggests that higher feedback gains are used during the learning period (i.e., the early trials). Figure 3.6(a) also shows that the difference between the identified feedforward controller G_{ff} and the inverse dynamics G^{-1} decreases over the 40 trials. The metrics $\|G_{\text{fb}}\|$ and $\|G_{\text{ff}} - G^{-1}\|$ are the frequency-averaged magnitudes of G_{fb} and $G_{\text{ff}} - G^{-1}$, which are given by

$$\|G_{\text{fb}}\| = \frac{1}{\omega_N - \omega_1} \int_{\omega_1}^{\omega_N} |G_{\text{fb}}(\jmath\omega)| \, \mathrm{d}\omega,$$
$$\|G_{\text{ff}} - G^{-1}\| = \frac{1}{\omega_N - \omega_1} \int_{\omega_1}^{\omega_N} |G_{\text{ff}}(\jmath\omega) - G^{-1}(\jmath\omega)| \, \mathrm{d}\omega,$$

where $\omega_1 = 0.2\pi$ radians per second and $\omega_N = 0.8\pi$ radians per second. Figure 3.6(b) compares the command-following error on all 400 trials to how closely the identified G_{ff} approximates G^{-1}. The trials with the smaller command-following errors yield identified feedforward controllers G_{ff} that are better approximations of the inverse

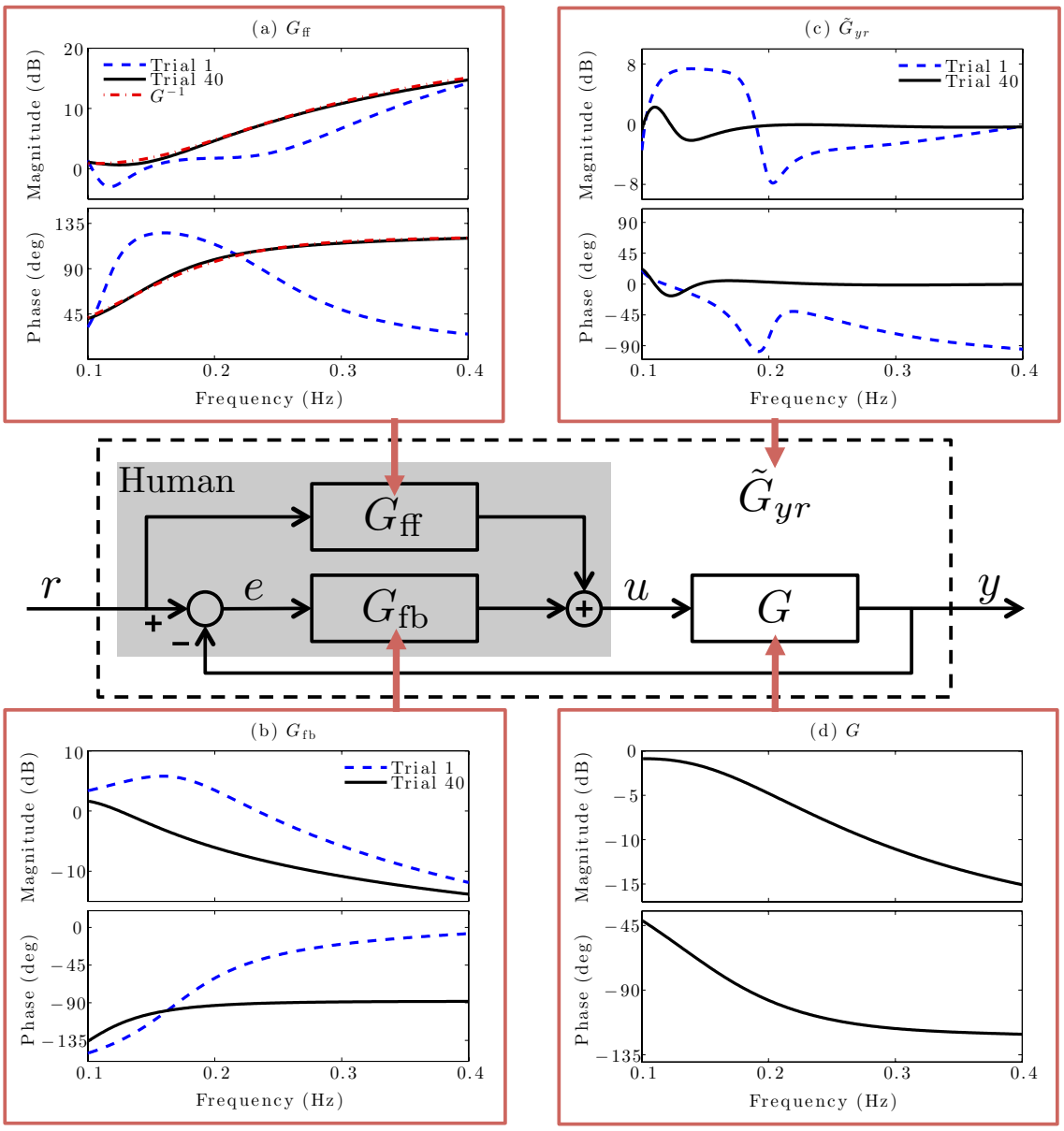

Figure 3.5: The subject's control strategy is modeled by a feedback controller G_{fb} and a feedforward controller G_{ff}, which results in the closed-loop response $\hat{y}(s) = \tilde{G}_{yr}(s)\hat{r}(s)$ from the command r to the position y. Figures (a), (b), and (c) show the Bode plots of the identified controllers G_{ff} and G_{fb}, and the closed-loop transfer function $\tilde{G}_{yr}$ for the first and last (i.e., 40th) trials of one subject. Figure (a) shows that the identified G_{ff} for the first trial does not approximate G^{-1}, whereas the identified G_{ff} for the last trial does approximate G^{-1}. Figure (b) shows that the identified G_{fb} for the first trial has higher gain (i.e., magnitude) than the identified G_{fb} for the last trial. Figure (c) shows that the closed-loop transfer function $\tilde{G}_{yr}$ is approximately 1 (i.e., 0 decibels magnitude and 0 degrees phase) for the last trial, which implies that y approximates r across the frequency range of r.

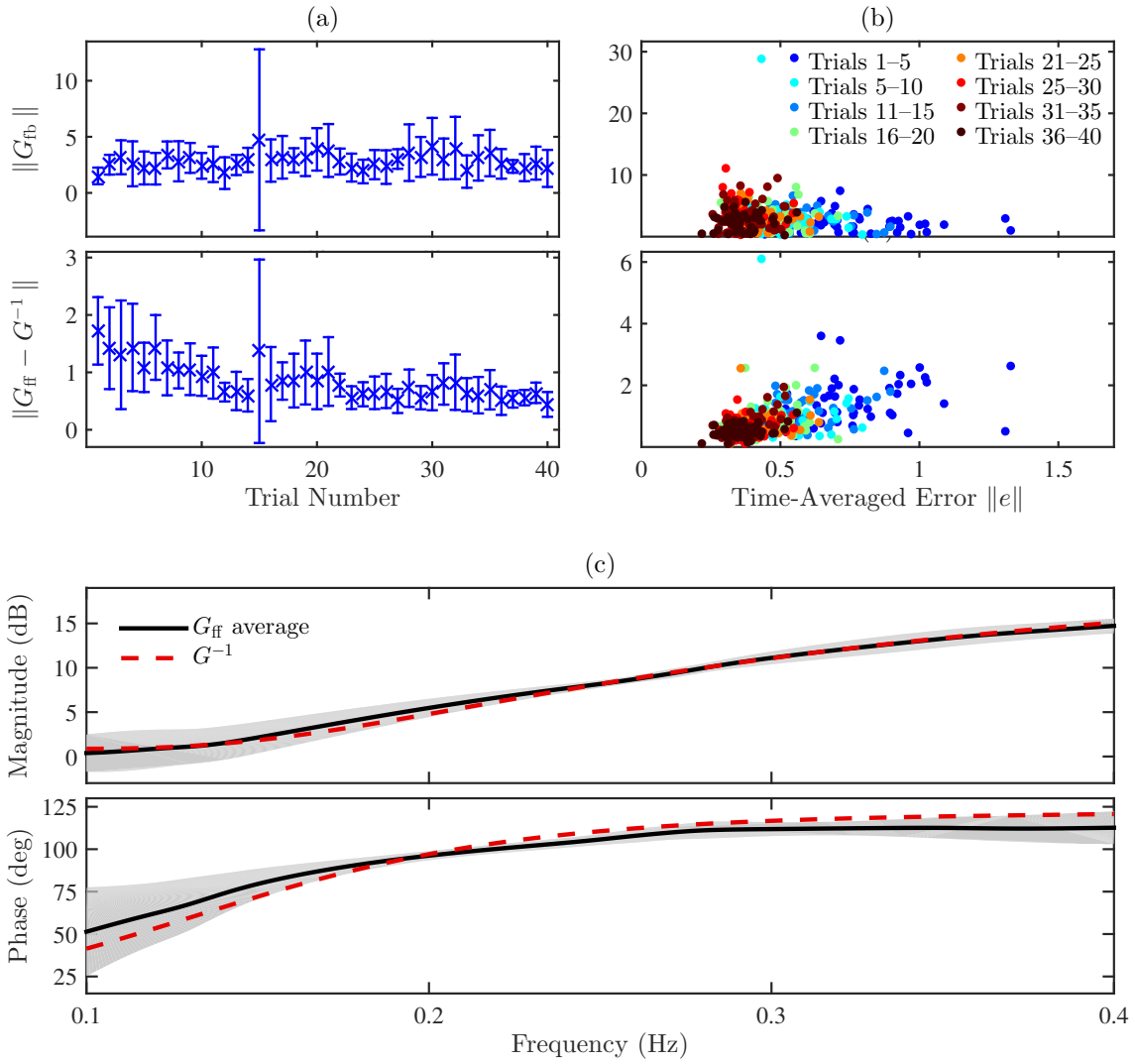

Figure 3.6: Figure (a) shows $\|G_{\text{fb}}\|$ and $\|G_{\text{ff}} - G^{-1}\|$ for the subjects' identified controllers for each of the 40 trials. The $\times$ indicates the mean of the 10 subjects and the vertical lines show one standard deviation. The difference between G_{ff} and G^{-1} decreases over the 40 trials, whereas $\|G_{\text{fb}}\|$ does not changes significantly over the trials. Figure (b) compares $\|e\|$ to how closely the identified G_{ff} approximates G^{-1}. The trials with the smaller command-following errors yield identified feedforward controllers that are better approximations of G^{-1}. Figure (c) shows the Bode plot of the average identified feedforward controller for all 10 subjects on the last trial. The shaded region shows one standard deviation above and below the average identified feedforward controller. The average feedforward controller approximates G^{-1}.

dynamics G^{-1}. Finally, Figure 3.6(c) shows the Bode plot of the average identified feedforward controller for all 10 subjects on the last trial. The average identified feedforward controller approximates G^{-1}. Thus, the data suggests that by the last

trial the subjects learned the inverse dynamics G^{-1} and used a model of those inverse dynamics in feedforward. This observation supports the internal model hypothesis.

3.7 Conclusions

In this chapter, we conducted an HITL experiment, where 10 human subjects learned to control an unknown dynamic systems over 40 trials, and the SSID algorithm in Chapter 2 is used to model feedback and feedforward controllers used by humans. Over 40 trials, the feedforward controllers used by humans tend to approximate the dynamic inversion of the plant and no clear trend in feedback controller is observed. This observation supports the IMH.

To model human control behavior in more complicated situations (e.g., with multiple inputs and outputs), a more general SSID algorithm is needed. The next chapter presents an SSID algorithm for multivariable linear time-invariant feedback and feedforward controllers.

Chapter 4 Subsystem Identification for Multi-Input Multi-Output Subsystems

In this chapter, we present a frequency-domain subsystem identification technique for identifying discrete-time multivariable feedback and feedforward subsystems that are interconnected with a known subsystem. This subsystem identification algorithm uses closed-loop input-output data, but no other system signals are assumed to be measured. In particular, neither the feedback signal nor the outputs of the unknown subsystems are assumed to be measured. We use a candidate-pool approach to identify the feedback and feedforward transfer functions, while guaranteeing asymptotic stability of the identified closed-loop transfer function. The main analytic result shows that if the data noise is sufficiently small and the candidate pool is sufficiently dense, then the parameters of the identified feedback and feedforward transfer functions are arbitrarily close to the true parameters. The methods and results of this chapter have been submitted for publication in [110].

4.1 Introduction

Subsystem identification (SSID) is the process of building empirical models of unknown dynamic subsystems, which are interconnected with known dynamic subsystems. These connections can be series, parallel, or feedback. SSID relies on measured data to identify the unknown subsystems. However, not all input and output signals to the unknown subsystems are necessarily accessible, that is, available for measurement.

This chapter is concerned with closed-loop SSID of unknown feedback and feedforward subsystems interconnected with a known subsystem as shown in Figure 4.1. The

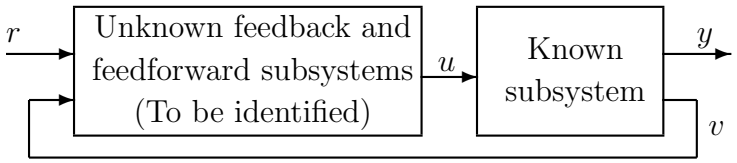

Figure 4.1: The unknown feedback and feedforward subsystems are to be identified using the measured data r and y. The internal signals u and v are inaccessible.

exogenous input r and closed-loop output y are measured, whereas internal signals u and v are not assumed to be accessible.

Note that closed-loop SSID is distinct from the well-studied problem of system identification in closed loop [62–65], specifically, the unknown subsystems have inputs and outputs that are inaccessible.

SSID has applications in biology and physics as well as human-in-the-loop systems. For example, many biological systems are modeled by the interconnection of subsystems [77], which may be unknown and have inaccessible inputs and outputs. Similarly, physical systems are often modeled by a composition of subsystems, which are based on either physical laws or empirical information. For example, in [78], a large-scale physics-based model of the global ionosphere-thermosphere is improved by using measured data to estimate thermal conductivity, which can be regarded as an unknown feedback subsystem. In this application, the output of the unknown subsystem is inaccessible.

SSID also has application to modeling human behavior. For example, there is interest in modeling human-in-the-loop behavior for applications such as aircraft [67–69, 111] and automobiles [70–72]. In addition, SSID methods can be used to model human behavior in motor control experiments, which study human learning [73–76, 91, 92].

Closed-loop SSID of feedback and feedforward models is considered in [78, 88–90]. However, these approaches may identify feedback and feedforward models that result in unstable closed-loop dynamics. To address closed-loop stability, [91, 92] presents an SSID technique that guarantees asymptotic stability of the identified closed-loop transfer function. The approach in [91,92] applies to single-input single-output (SISO) subsystems and requires that the measured closed-loop output y is the same as the feedback v.

The new contribution of this chapter is a closed-loop SSID method that: i) identifies multi-input multi-output (MIMO) feedback and feedforward subsystems; ii) allows for a measured output y that is not necessarily the same as the feedback v; and iii) guarantees asymptotic stability of the identified closed-loop transfer function. This chapter adopts techniques from [91, 92] but goes beyond the previous work by addressing MIMO subsystems and allowing for the measured output y to differ from the feedback v. Furthermore, the discrete-time SSID approach in this chapter can improve computational efficiency relative to the continuous-time approaches in [91, 92]. In this chapter, the feedforward subsystem model is parameterized as a finite impulse response (FIR) transfer function, which can improve computational efficiency as discussed in Section 4.7. To accomplish i)–iii), a candidate-pool approach is adopted to the SSID problem. Our main analytic result shows that if the data noise is sufficiently small and the candidate pool is sufficiently dense, then the parameters of the identified feedback and feedforward transfer functions are arbitrarily close to the true parameters.

4.2 Notation

Let $\mathbb{F}$ be either $\mathbb{R}$ or $\mathbb{C}$. Then, $x_{(i)}$ denotes the ith component of $x \in \mathbb{F}^n$, and $A_{(i,j)}$ denotes the (i, j) entry of $A \in \mathbb{F}^{m\times n}$. Let $\|\cdot\|$ be a norm on $\mathbb{F}^{m\times n}$, and let $\|\cdot\|_2$ be the two-norm on $\mathbb{F}^n$. Next, let A^* denote the complex conjugate transpose of $A \in \mathbb{F}^{m\times n}$,

and define $\|A\|_{\mathrm{F}} \triangleq \sqrt{\mathrm{tr} A^* A}$, which is the Frobenius norm of $A \in \mathbb{F}^{m\times n}$. Let A^{A} denote the adjugate of $A \in \mathbb{F}^{m\times n}$.

Let $\mathrm{vec}\, A$ be the vector in $\mathbb{F}^{mn}$ formed by stacking the columns of $A \in \mathbb{F}^{m\times n}$. Let vec^{-1} be the inverse vec operator, that is, $\mathrm{vec}^{-1}(\mathrm{vec}\, A) = A$. Let $A \otimes B$ denote the Kronecker product of $A \in \mathbb{F}^{m\times n}$ and $B \in \mathbb{F}^{k\times l}$.

Define the *open ball of radius* $\epsilon > 0$ *centered at* $c \in \mathbb{F}^{m\times n}$ by $\mathbb{B}_\epsilon(c) \triangleq \{x \in \mathbb{F}^{m\times n} \colon \|x - c\| < \epsilon\}$. Let $\mathbb{Z}^+$ denote the set of positive integers.

Definition 4.1. Let $\Delta \subseteq \mathbb{F}^{m\times n}$ be bounded and contain no isolated points. For all $j \in \mathbb{Z}^+$, let $\Delta_j \subseteq \Delta$ be a finite set. Then, $\{\Delta_j\}_{j=1}^\infty$ *converges to* Δ if for each $x \in \Delta$, there exists a sequence $\{x_j \colon x_j \in \Delta_j\}_{j=1}^\infty$ such that for all $\epsilon > 0$, there exists $L \in \mathbb{Z}^+$ such that for all $j > L$, $x_j \in \mathbb{B}_\epsilon(x)$.

Let $\mathbb{R}[z]$ denote the set of polynomials with coefficients in $\mathbb{R}$, and let $\mathbb{R}^{m\times n}[z]$ denote the set of $m \times n$ polynomial matrices, that is, the set of matrix functions $P \colon \mathbb{C} \to \mathbb{C}^{m\times n}$ whose entries are elements in $\mathbb{R}[z]$. The degree of the polynomial $p \in \mathbb{R}[z]$ is denoted by $\deg p$, and the degree of the polynomial matrix $P \in \mathbb{R}^{m\times n}[z]$ is denoted by $\deg P \triangleq \max_{i=1,\ldots,m;j=1,\ldots,n} \deg P_{(i,j)}$.

4.3 Problem Formulation

Let $G_y \colon \mathbb{C} \to \mathbb{C}^{n\times m}$ and $G_v \colon \mathbb{C} \to \mathbb{C}^{l\times m}$ be a real rational transfer function matrices, and consider the linear time-invariant system

$$y(z) = G_y(z)[u(z) + \gamma_u(z)] + \gamma_y(z), \tag{4.1}$$

$$v(z) = G_v(z)[u(z) + \gamma_u(z)], \tag{4.2}$$

where $y(z) \in \mathbb{C}^n, \gamma_y(z) \in \mathbb{C}^n, u(z) \in \mathbb{C}^m$, $\gamma_u(z) \in \mathbb{C}^m$, and $v(z) \in \mathbb{C}^l$ are the z-transforms of the output, output noise, control, control noise, and feedback, respectively. The control u is generated by feedback and feedforward as shown in Figure

4.2. In particular, let $G_{\mathrm{ff}}, G_{\mathrm{fb}} \colon \mathbb{C} \to \mathbb{C}^{m \times l}$ be real rational transfer function matrices,

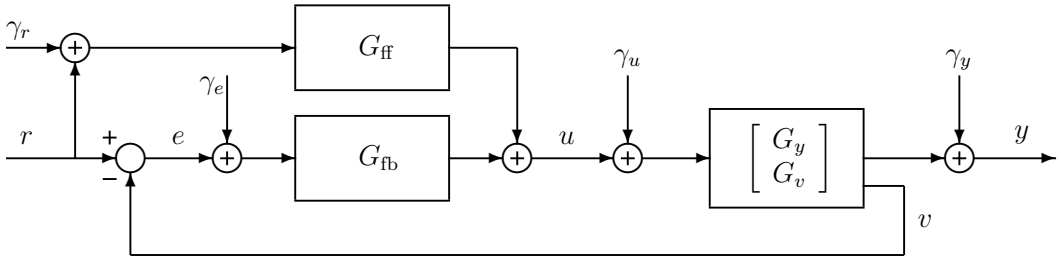

Figure 4.2: The input r and output y are measured, but all internal signals (e.g., u and v) and the noises $\gamma_r, \gamma_e, \gamma_u$, and γ_y are unmeasured.

and consider the control

$$u(z) = G_{\mathrm{ff}}(z)[r(z) + \gamma_r(z)] + G_{\mathrm{fb}}(z)[e(z) + \gamma_e(z)], \tag{4.3}$$

where $r(z) \in \mathbb{C}^l$ is the exogenous input, $\gamma_r(z) \in \mathbb{C}^l$ is the feedforward noise, $e(z) \triangleq r(z) - v(z)$ is the error, and $\gamma_e(z) \in \mathbb{C}^l$ is the error noise. We assume that G_{ff} is asymptotically stable, that is, the poles of G_{ff} are contained in the open unit disk. The closed-loop system obtained from (4.1)–(4.3) is

$$y(z) = \tilde{G}(z)r(z) + \gamma(z),$$

where

$$\tilde{G} \triangleq G_y(I_m + G_{\mathrm{fb}}G_v)^{-1}(G_{\mathrm{fb}} + G_{\mathrm{ff}}) \tag{4.4}$$

is assumed to be asymptotically stable, and the noise is

$$\gamma \triangleq G_y(I_m + G_{\mathrm{fb}}G_v)^{-1}(G_{\mathrm{ff}}\gamma_r + G_{\mathrm{fb}}\gamma_e - G_{\mathrm{fb}}G_v\gamma_u) + G_y\gamma_u + \gamma_y.$$

Let $N \in \mathbb{Z}^+$ be the number of frequency response data, and define $\mathcal{N} \triangleq \{1, 2, \ldots, N\}$.

For all $k \in \mathcal{N}$, let $\theta_k \in [0, \pi]$, where $\theta_1 < \cdots < \theta_N$. Define the *closed-loop frequency response data*

$$H(\theta_k) \triangleq \tilde{G}(e^{\jmath\theta_k}) + \Gamma(e^{\jmath\theta_k}) \in \mathbb{C}^{n\times l}, \tag{4.5}$$

where $\Gamma \colon \mathbb{C} \to \mathbb{C}^{n\times l}$ is such that, for all $i \in \{1, 2, \ldots, n\}$ and all $j \in \{1, 2, \ldots, l\}$, $\Gamma_{(i,j)} \triangleq \gamma_{(i)}/r_{(j)}$.

This chapter presents an SSID method to identify G_{ff} and G_{fb} under the assumption that G_y, G_v, and $\{H(\theta_k)\}_{k=1}^N$ are known. For each $k \in \mathcal{N}$, $H(\theta_k)$ can be calculated from y and r as $H_{(i,j)}(\theta_k) = y_{(i)}(e^{\jmath\theta_k})/r_{(j)}(e^{\jmath\theta_k})$. Thus, $\{H(\theta_k)\}_{k=1}^N$ can be obtained from the accessible signals r and y, and does not depend on the internal signals (e.g., u and v) or the noise signals $\gamma_r, \gamma_e, \gamma_u$, and γ_y, which are not assumed to be measured.

Assume that G_{ff} is FIR. Thus, the feedforward transfer function can be expressed as $G_{\mathrm{ff}}(z) = z^{-n_{\mathrm{ff}}} N_{\mathrm{ff}}(z)$, where $N_{\mathrm{ff}} \in \mathbb{R}^{m\times l}[z]$ and $n_{\mathrm{ff}} \triangleq \deg N_{\mathrm{ff}}$. Since G_{ff} is asymptotically stable, it follows that for sufficiently large order n_{ff}, G_{ff} can approximate an IIR transfer function to arbitrary accuracy evaluated along the unit circle. Thus, the assumption that G_{ff} is FIR does not significantly restrict the class of feedforward behavior. The SSID approach in this chapter can also be used with an IIR feedforward model, but using an FIR feedforward model improves computational efficiency, as discussed in Section 4.7.

Let G_y and G_v have the right-matrix-fraction descriptions $G_y = N_y D^{-1}$ and $G_v = N_v D^{-1}$, and let G_{fb} have the left-matrix-fraction description $G_{\mathrm{fb}} = D_{\mathrm{fb}}^{-1} N_{\mathrm{fb}}$, where $N_y \in \mathbb{R}^{n\times m}[z]$, $N_v \in \mathbb{R}^{l\times m}[z]$, $N_{\mathrm{fb}} \in \mathbb{R}^{m\times l}[z]$, and $D, D_{\mathrm{fb}} \in \mathbb{R}^{m\times m}[z]$. Without loss of generality, it is assumed that D and D_{fb} are monic. Thus, (4.4) can be expressed as

$$\tilde{G}(z) = N_y(z)\tilde{D}^{-1}(z)[N_{\mathrm{fb}}(z) + z^{-n_{\mathrm{ff}}} D_{\mathrm{fb}}(z) N_{\mathrm{ff}}(z)],$$

where $\tilde{D} \triangleq D_{\mathrm{fb}} D + N_{\mathrm{fb}} N_v \in \mathbb{R}^{m\times m}[z]$. Define $d \triangleq \deg D$, $d_{\mathrm{fb}} \triangleq \deg D_{\mathrm{fb}}$, $n_y \triangleq \deg N_y$,

$n_v \triangleq \deg N_v$, and $n_{\mathrm{fb}} \triangleq \deg N_{\mathrm{fb}}$. We make the following assumptions:

(A3.1) $d + d_{\mathrm{fb}} > n_v + n_{\mathrm{fb}}$.

(A3.2) $N > n_y + (m-1)(d + d_{\mathrm{fb}}) + d_{\mathrm{fb}} + n_{\mathrm{ff}}$.

(A3.3) If $\lambda \in \mathbb{C}$ and $\det \tilde{D}(\lambda) = 0$, then $|\lambda| < 1$.

Assumption (A3.1) states that $G_{\mathrm{fb}}G_{vu}$ is strictly proper. Assumption (A3.2) requires that the number N of frequency response data points is sufficiently large. Assumption (A3.3) implies that $\tilde{G}$ is asymptotically stable. Also assume that $n_{\mathrm{ff}}, d_{\mathrm{fb}}$, and n_{fb} are known.

To formulate the SSID problem, define $a \triangleq l(n_{\mathrm{fb}} + 1) + md_{\mathrm{fb}}$ and $b \triangleq m(n_{\mathrm{ff}} + 1)$, and consider the functions $\mathcal{N}_{\mathrm{ff}} \colon \mathbb{C} \times \mathbb{R}^{b \times l} \to \mathbb{C}^{m \times l}$, $\mathcal{N}_{\mathrm{fb}} \colon \mathbb{C} \times \mathbb{R}^{a \times m} \to \mathbb{C}^{m \times l}$, $\mathcal{D}_{\mathrm{fb}} \colon \mathbb{C} \times \mathbb{R}^{a \times m} \to \mathbb{C}^{m \times m}$ given by

$$
\begin{aligned}
\mathcal{N}_{\mathrm{ff}}(z, \beta) &\triangleq \left(\begin{bmatrix} z^{n_{\mathrm{ff}}} & \cdots & z & 1 \end{bmatrix} \otimes I_m \right) \beta, \\
\mathcal{N}_{\mathrm{fb}}(z, \phi) &\triangleq \phi^{\mathrm{T}} \begin{bmatrix} I_l \otimes \begin{bmatrix} z^{n_{\mathrm{fb}}} & \cdots & z & 1 \end{bmatrix}^{\mathrm{T}} \\ 0_{md_{\mathrm{fb}} \times l} \end{bmatrix}, \\
\mathcal{D}_{\mathrm{fb}}(z, \phi) &\triangleq z^{d_{\mathrm{fb}}} I_m + \phi^{\mathrm{T}} \begin{bmatrix} 0_{l(n_{\mathrm{fb}}+1) \times m} \\ I_m \otimes \begin{bmatrix} z^{d_{\mathrm{fb}}-1} & \cdots & z & 1 \end{bmatrix}^{\mathrm{T}} \end{bmatrix},
\end{aligned}
$$

where $\beta \in \mathbb{R}^{b \times l}$ contains the unknown parameters of $\mathcal{N}_{\mathrm{ff}}$, and $\phi \in \mathbb{R}^{a \times m}$ contains the unknown parameters of $\mathcal{N}_{\mathrm{fb}}$ and $\mathcal{D}_{\mathrm{fb}}$. Consider $\mathcal{G}_{\mathrm{ff}} \colon \mathbb{C} \times \mathbb{R}^{b \times l} \to \mathbb{C}^{m \times l}$ and $\mathcal{G}_{\mathrm{fb}} \colon \mathbb{C} \times \mathbb{R}^{a \times m} \to \mathbb{C}^{m \times l}$ given by

$$
\mathcal{G}_{\mathrm{ff}}(z, \beta) \triangleq z^{-n_{\mathrm{ff}}} \mathcal{N}_{\mathrm{ff}}(z, \beta), \qquad \mathcal{G}_{\mathrm{fb}}(z, \phi) \triangleq \mathcal{D}_{\mathrm{fb}}^{-1}(z, \phi) \mathcal{N}_{\mathrm{fb}}(z, \phi),
$$

which, for each $\beta \in \mathbb{R}^{b \times l}$ and $\phi \in \mathbb{R}^{a \times m}$, are real rational transfer function matrices.

Let $\beta_* \in \mathbb{R}^{b \times l}$ and $\phi_* \in \mathbb{R}^{a \times m}$ be such that, $N_{\mathrm{ff}}(z) \equiv \mathcal{N}_{\mathrm{ff}}(z, \beta_*)$, $N_{\mathrm{fb}}(z) \equiv \mathcal{N}_{\mathrm{fb}}(z, \phi_*)$, and $D_{\mathrm{fb}}(z) \equiv \mathcal{D}_{\mathrm{fb}}(z, \phi_*)$. Thus, $\mathcal{G}_{\mathrm{ff}}(z, \beta_*) \equiv G_{\mathrm{ff}}(z)$ and $\mathcal{G}_{\mathrm{fb}}(z, \phi_*) \equiv G_{\mathrm{fb}}(z)$. Consider

$\tilde{\mathcal{G}}\colon \mathbb{C} \times \mathbb{R}^{b\times l} \times \mathbb{R}^{a\times m} \to \mathbb{C}^{n\times l}$ given by

$$\tilde{\mathcal{G}}(z,\beta,\phi) \triangleq N_y(z)\tilde{\mathcal{D}}^{-1}(z,\phi)[\mathcal{N}_{\mathrm{fb}}(z,\phi) + z^{-n_{\mathrm{ff}}}\mathcal{D}_{\mathrm{fb}}(z,\phi)\mathcal{N}_{\mathrm{ff}}(z,\beta)], \tag{4.6}$$

where

$$\tilde{\mathcal{D}}(z,\phi) \triangleq \mathcal{D}_{\mathrm{fb}}(z,\phi)D(z) + \mathcal{N}_{\mathrm{fb}}(z,\phi)N_v(z).$$

Note that $\tilde{\mathcal{G}}(z,\beta,\phi)$ is the closed-loop transfer function obtained using β and ϕ. Thus, $\tilde{\mathcal{G}}(z,\beta_*,\phi_*) = \tilde{G}(z)$.

Our objective is to determine β and ϕ such that $\mathcal{G}_{\mathrm{ff}}$ and $\mathcal{G}_{\mathrm{fb}}$ approximate G_{ff} and G_{fb}, respectively. To achieve this objective, we seek to minimize

$$J(\beta,\phi) = \sum_{k=1}^{N} \left\| \tilde{\mathcal{G}}(e^{\jmath\theta_k},\beta,\phi) - H(\theta_k) \right\|_{\mathrm{F}}^2, \tag{4.7}$$

subject to the constraint that $\tilde{\mathcal{D}}(z,\phi)$ is asymptotically stable, that is,

$$\phi \in \mathcal{S} \triangleq \{\phi \in \mathbb{R}^{a\times m}\colon \text{if } \lambda \in \mathbb{C} \text{ and } \det \tilde{\mathcal{D}}(\lambda,\phi) = 0, \text{ then } |\lambda| < 1\}.$$

The cost (4.7) is a measure of the difference between the data $\{H(\theta_k)\}_{k=1}^N$ and the closed-loop transfer function obtained from the estimates $\mathcal{G}_{\mathrm{ff}}$ and $\mathcal{G}_{\mathrm{fb}}$. The cost (4.7) and constraint $\phi \in \mathcal{S}$ are nonlinear and nonconvex in (β,ϕ). If $\Gamma(e^{\jmath\theta_k}) \equiv 0$, then $J(\beta_*,\phi_*) = 0$.

4.4 Subsystem Identification Algorithm

Now, we develop an SSID algorithm to estimate $G_{\rm ff}$ and $G_{\rm fb}$. For each $k \in \mathcal{N}$, define $\sigma_k \triangleq e^{\jmath\theta_k}$, and define

$$\mathcal{A}_k(\phi) \triangleq \sigma_k^{-n_{\rm ff}} N_y(\sigma_k)\tilde{\mathcal{D}}^{-1}(\sigma_k,\phi)\mathcal{D}_{\rm fb}(\sigma_k,\phi)\nu(\sigma_k), \tag{4.8}$$

$$\mathcal{B}_k(\phi) \triangleq N_y(\sigma_k)\tilde{\mathcal{D}}^{-1}(\sigma_k,\phi)\mathcal{N}_{\rm fb}(\sigma_k,\phi) - H(\theta_k), \tag{4.9}$$

where $\nu(z) \triangleq \left[\begin{array}{cccccc} z^{n_{\rm ff}} & z^{n_{\rm ff}-1} & \cdots & z & 1 \end{array}\right] \otimes I_m$. It follows from (4.6)–(4.9) that

$$\begin{aligned} J(\beta,\phi) &= \sum_{k=1}^{N} \|\mathcal{A}_k(\phi)\beta + \mathcal{B}_k(\phi)\|_{\rm F}^2 \\ &= \sum_{k=1}^{N} \|{\rm vec}\,\mathcal{A}_k(\phi)\beta + {\rm vec}\,\mathcal{B}_k(\phi)\|_2^2 \\ &= \sum_{k=1}^{N} \|[I_l \otimes \mathcal{A}_k(\phi)]{\rm vec}\,\beta + {\rm vec}\,\mathcal{B}_k(\phi)\|_2^2, \end{aligned}$$

which can be expressed as

$$J(\beta,\phi) = [{\rm vec}\,\beta]^{\rm T}\Omega_2(\phi){\rm vec}\,\beta + \Omega_1^{\rm T}(\phi){\rm vec}\,\beta + \Omega_0(\phi), \tag{4.10}$$

where

$$\Omega_0(\phi) \triangleq \sum_{k=1}^{N} \|\mathcal{B}_k(\phi)\|_{\rm F}^2 \in \mathbb{R}, \tag{4.11}$$

$$\Omega_1(\phi) \triangleq 2{\rm Re}\sum_{k=1}^{N} {\rm vec}\,\mathcal{A}_k^*(\phi)\mathcal{B}_k(\phi) \in \mathbb{R}^{lb}, \tag{4.12}$$

$$\Omega_2(\phi) \triangleq I_l \otimes {\rm Re}\sum_{k=1}^{N} \mathcal{A}_k^*(\phi)\mathcal{A}_k(\phi) \in \mathbb{R}^{lb\times lb}. \tag{4.13}$$

For the remaining of this chapter, it is assumed that for all $\phi \in \mathcal{S}$, $\Omega_2(\phi)$ is positive

definite. The following result provides a sufficient (but not necessary) condition such that $\Omega_2(\phi)$ is positive definite.

Proposition 4.1. Consider Ω_2 given by (4.13), where (A3.1) and (A3.2) are satisfied. Assume that $\max_{z\in\mathbb{C}} \operatorname{rank} N_y(z) = m \leq n$. Then, for all $\phi \in \mathcal{S}$, $\Omega_2(\phi)$ is positive definite.

Proof. Let $\phi \in \mathcal{S}$. Then, for all $k \in \mathcal{N}$, $\tilde{\mathcal{D}}(\sigma_k, \phi)$ is nonsingular, and thus, it follows from (4.8) and (4.13) that $\Omega_2(\phi)$ is well defined and positive semidefinite. Assume for contradiction that there exists $x \in \mathbb{R}^b \backslash \{0\}$ such that $x^{\mathrm{T}}[\operatorname{Re} \sum_{k=1}^{N} \mathcal{A}_k^*(\phi)\mathcal{A}_k(\phi)]x = 0$. Let $k \in \mathcal{N}$, and it follows that $\mathcal{A}_k(\phi)x = 0$. Define

$$\Xi(z) \triangleq N_y(z)\tilde{\mathcal{D}}^{\mathrm{A}}(z,\phi)\mathcal{D}_{\mathrm{fb}}(z,\phi)\nu(z)x \in \mathbb{R}^n[z].$$

Thus, (4.8) implies that $0 = \Xi(\sigma_k)/[\sigma_k^{n_{\mathrm{ff}}} \det \tilde{\mathcal{D}}(\sigma_k, \phi)]$, which implies that $\Xi(\sigma_k) = 0$. Since $\deg \tilde{\mathcal{D}} = d + d_{\mathrm{fb}}$, it follows that $\deg \tilde{\mathcal{D}}^{\mathrm{A}} \leq (m-1)(d + d_{\mathrm{fb}})$. Since, in addition, $\deg \nu(z)x \leq n_{\mathrm{ff}}$, it follows from (A3.2) that $\deg \Xi \leq n_y + (m-1)(d+d_{\mathrm{fb}}) + d_{\mathrm{fb}} + n_{\mathrm{ff}} < N$. Since $\Xi(\sigma_1) = \cdots = \Xi(\sigma_N) = 0$ and $\deg \Xi < N$, it follows that $\Xi = 0$.

Define $\mathcal{T} \triangleq \{z \in \mathbb{C} \colon \min\{\operatorname{rank} N_y(z), \operatorname{rank} \tilde{\mathcal{D}}^{\mathrm{A}}(z,\phi), \operatorname{rank} \mathcal{D}_{\mathrm{fb}}(z,\phi)\} < m\}$. Since, for all $z \in \mathbb{C}\backslash\mathcal{T}$, $\operatorname{rank} N_y(z) = m \leq n$, it follows that N_y has full column rank, which implies that for all $z \in \mathbb{C}\backslash\mathcal{T}$, $N_y(z)$ is left invertible. Thus, for all $z \in \mathbb{C}\backslash\mathcal{T}$, $\tilde{\mathcal{D}}^{\mathrm{A}}(z,\phi)\mathcal{D}_{\mathrm{fb}}(z,\phi)\nu(z)x = 0$. Since for all $z \in \mathbb{C}\backslash\mathcal{T}$, $\tilde{\mathcal{D}}^{\mathrm{A}}(z,\phi)$ and $\mathcal{D}_{\mathrm{fb}}(z,\phi)$ are nonsingular, it follows that for all $z \in \mathbb{C}\backslash\mathcal{T}$, $\nu(z)x = 0$. Finally, the structure of ν implies that $x = 0$, which is a contradiction. Thus, $\operatorname{Re} \sum_{k=1}^{N} \mathcal{A}_k^*(\phi)\mathcal{A}_k(\phi)$ is positive definite. Therefore, it follows from (4.13) that $\Omega_2(\phi)$ is positive definite. □

The next result shows that for each $\phi \in \mathcal{S}$, $J(\beta, \phi)$ has a unique global minimizer. See Proposition 2.2 for the proof of this result.

Proposition 4.2. Consider J given by (4.10), where (A3.1) and (A3.2) are satisfied. Let $\phi \in \mathcal{S}$ and define $\beta_{\min} \triangleq -\frac{1}{2}\operatorname{vec}^{-1}[\Omega_2^{-1}(\phi)\Omega_1(\phi)] \in \mathbb{R}^{b\times l}$. Let $\beta \in$

$\mathbb{R}^{b\times l}\backslash\{\beta_{\min}\}$. Then, $J(\beta_{\min},\phi) < J(\beta,\phi)$.

Let $\Phi \subseteq \mathcal{S}$ be a set with M elements. Call Φ the *candidate pool*. Now, a candidate sequence is created using the M elements in Φ. For $i,j \in \mathcal{M} \triangleq \{1,2,\ldots,M\}$, let ϕ_i be such that $\phi_i \in \Phi$ and if $i \neq j$, then $\phi_i \neq \phi_j$. Now, for all $i \in \mathcal{M}$, define the quadratic cost function

$$\mathcal{J}_i(\beta) \triangleq J(\beta,\phi)\Big|_{\phi=\phi_i} = [\mathrm{vec}\,\beta]^{\mathrm{T}}\Omega_2(\phi_i)\mathrm{vec}\,\beta + \Omega_1^{\mathrm{T}}(\phi_i)\mathrm{vec}\,\beta + \Omega_0(\phi_i).$$

Since $\phi_1,\ldots,\phi_M \in \Phi \subseteq \mathcal{S}$, it follows that $\Omega_2(\phi_1),\ldots,\Omega_2(\phi_M)$ are positive definite. Then, for each $i \in \mathcal{M}$, define $\beta_i \triangleq -\frac{1}{2}\mathrm{vec}^{-1}[\Omega_2^{-1}(\phi_i)\Omega_1(\phi_i)] \in \mathbb{R}^{b\times l}$, and it follows from Proposition 4.2 that β_i is the unique global minimizer of $\mathcal{J}_i$. Next, let $\ell \in \mathcal{M}$ be the smallest integer such that

$$\mathcal{J}_\ell(\beta_\ell) = \min_{i\in\mathcal{M}} \mathcal{J}_i(\beta_i).$$

Thus, the identified parameters are $\beta^+ \triangleq \beta_\ell$ and $\phi^+ \triangleq \phi_\ell$, and the identified transfer functions are

$$G_{\mathrm{ff}}^+(z) \triangleq \mathcal{G}_{\mathrm{ff}}(z,\beta^+), \qquad G_{\mathrm{fb}}^+(z) \triangleq \mathcal{G}_{\mathrm{fb}}(z,\phi^+).$$

Note that $\arg\min_{i\in\mathcal{M}} \mathcal{J}_i(\beta_i)$ is not necessarily unique. In this case, $\ell \in \mathcal{M}$ is the smallest integer such that $\mathcal{J}_\ell(\beta_\ell) = \min_{i\in\mathcal{M}} \mathcal{J}_i(\beta_i)$. In practice, $\arg\min_{i\in\mathcal{M}} \mathcal{J}_i(\beta_i)$ is usually unique. Now, this SSID method is summerized.

Algorithm 4.1. Consider the closed-loop transfer function (4.4), where G_y, G_v, and $\{H(\theta_k)\}_{k=1}^N$ are known, and (A3.1)–(A3.3) are satisfied. Then, the subsystem identification algorithm is as follows:

Step 1. Generate the candidate pool $\Phi \subseteq \mathcal{S}$ and candidate sequence $\{\phi_i\}_{i=1}^M$.

Step 2. For each $i \in \mathcal{M}$, find $\beta_i = -\frac{1}{2}\mathrm{vec}^{-1}[\Omega_2^{-1}(\phi_i)\Omega_1(\phi_i)] \in \mathbb{R}^{b\times l}$, which is the unique global minimizer of $\mathcal{J}_i$.

Step 3. Find the smallest integer $\ell \in \mathcal{M}$ such that $\mathcal{J}_\ell(\beta_\ell) = \min_{i\in\mathcal{M}} \mathcal{J}_i(\beta_i)$.

Step 4. The identification results are $\beta^+ = \beta_\ell$, $\phi^+ = \phi_\ell$, $G_{\mathrm{ff}}^+(z) = \mathcal{G}_{\mathrm{ff}}(z, \beta^+)$, and $G_{\mathrm{fb}}^+(z) = \mathcal{G}_{\mathrm{fb}}(z, \phi^+)$.

4.5 Analysis of Subsystem Identification Algorithm

Assume N_{fb} and D_{fb} are left coprime. We impose the following assumption, which is stronger than (A3.2):

(A3.4) $N > n_y + (2m-1)(d + d_{\mathrm{fb}}) + n_{\mathrm{ff}} + \max\{d_{\mathrm{fb}}, n_{\mathrm{fb}}\}$.

Assumption (A3.4) is used in the next result to provide sufficient conditions on $\beta \in \mathbb{R}^{b\times l}$ and $\phi \in \mathbb{R}^{a\times m}$ such that $\tilde{\mathcal{G}}(z, \beta, \phi) \equiv \tilde{G}(z)$.

Proposition 4.3. Let $\beta \in \mathbb{R}^{b\times l}$ and $\phi \in \mathbb{R}^{a\times m}$, and assume (A3.4) is satisfied. Then, $\sum_{k=1}^N \|\tilde{\mathcal{G}}(\sigma_k, \beta, \phi) - \tilde{G}(\sigma_k)\|_{\mathrm{F}} = 0$ if and only if $\tilde{\mathcal{G}}(z, \beta, \phi) \equiv \tilde{G}(z)$.

Proof. Let $\beta \in \mathbb{R}^{b\times l}$ and $\phi \in \mathbb{R}^{m\times a}$, and define $\mathcal{O}\colon \mathbb{C} \to \mathbb{C}^{n\times l}$ by $\mathcal{O}(z) \triangleq \tilde{\mathcal{G}}(z, \beta, \phi) - \tilde{G}(z)$. Next, define

$$\mathcal{P}(z) \triangleq N_y(z)\tilde{\mathcal{D}}^{\mathrm{A}}(z, \phi)[z^{n_{\mathrm{ff}}}\mathcal{N}_{\mathrm{fb}}(z, \phi) + \mathcal{D}_{\mathrm{fb}}(z, \phi)\mathcal{N}_{\mathrm{ff}}(z, \beta)] \in \mathbb{R}^{n\times l}[z],$$

$$\mathcal{Q}(z) \triangleq N_y(z)\tilde{\mathcal{D}}^{\mathrm{A}}(z, \phi_*) \times [z^{n_{\mathrm{ff}}}\mathcal{N}_{\mathrm{fb}}(z, \phi_*) + \mathcal{D}_{\mathrm{fb}}(z, \phi_*)\mathcal{N}_{\mathrm{ff}}(z, \beta_*)] \in \mathbb{R}^{n\times l}[z],$$

$$\mathcal{H}(z) \triangleq \mathcal{P}(z)\mathrm{diag}\,\tilde{\mathcal{D}}(z, \phi_*) - \mathcal{Q}(z)\mathrm{diag}\,\tilde{\mathcal{D}}(z, \phi) \in \mathbb{R}^{n\times l}[z].$$

Note that $\mathcal{O}(z) = \mathcal{H}(z)/[z^{n_{\mathrm{ff}}} \det \tilde{\mathcal{D}}(z, \phi) \det \tilde{\mathcal{D}}(z, \phi_*)]$. Since $\sum_{k=1}^N \|\mathcal{O}(\sigma_k)\|_{\mathrm{F}} = 0$, it follows that for all $k \in \mathcal{N}$, $\mathcal{O}(\sigma_k) = 0$, which implies that $\mathcal{H}(\sigma_k) = 0$. Since

$$\deg \det \tilde{\mathcal{D}}(z, \phi) = \deg \det \tilde{\mathcal{D}}(z, \phi_*) = m(d + d_{\mathrm{fb}}),$$

$$\deg \mathcal{P}, \deg \mathcal{Q} \leq n_{\mathrm{ff}} + n_y + (m-1)(d + d_{\mathrm{fb}}) + \max\{d_{\mathrm{fb}}, n_{\mathrm{fb}}\},$$

it follows that $\deg \mathcal{H} \leq n_y + (2m-1)(d + d_{\mathrm{fb}}) + n_{\mathrm{ff}} + \max\{d_{\mathrm{fb}}, n_{\mathrm{fb}}\}$. Since for all $k \in \mathcal{N}$, $\mathcal{H}(\sigma_k) = 0$, and (A3.4) implies that $\deg \mathcal{H} < N$, it follows that $\mathcal{H} = 0$, which implies that $\mathcal{O} = 0$. Thus, $\tilde{\mathcal{G}}(z, \beta, \phi) \equiv \tilde{G}(z)$. □

The conditions in Proposition 4.3 are not sufficient to conclude that $\beta = \beta_*$ and $\phi = \phi_*$. The following example demonstrates this scenario.

Example 4.1. Let

$$G_y(z) = G_v(z) = \frac{1}{z + 0.5}, \qquad G_{\mathrm{ff}}(z) = \frac{0.9z + 0.6}{z}, \qquad G_{\mathrm{fb}}(z) = 0.1,$$

and note that $\beta_* = [\ 0.9 \quad 0.6\ ]^{\mathrm{T}}$ and $\phi_* = 0.1$. The closed-loop transfer function (4.4) is $\tilde{G} = 1$. Let $\beta = [\ 0.8 \quad 0.7\ ]^{\mathrm{T}} \neq \beta_*$ and $\phi = 0.2 \neq \phi_*$, and it follows that $\tilde{\mathcal{G}}(z, \beta, \phi) \equiv \tilde{G}(z)$. △

In Example 4.1, the SSID problem is not well posed, because (β_*, ϕ_*) cannot be uniquely determined from the noiseless frequency response data. See [62, Chapter 13] for more details in the case with feedback only. Now, an additional assumption is imposed to ensure that $\tilde{\mathcal{G}}(z, \beta, \phi) \equiv \tilde{G}(z)$ if and only if $\beta = \beta_*$ and $\phi = \phi_*$.

Let $\Psi \subseteq \mathbb{R}^{a \times m}$ be a compact set with no isolated points such that $\phi_* \in \Psi$. In practice, Ψ is used to generate the candidate pool. Assume Ψ is known, and

(A3.5) If $\beta \in \mathbb{R}^{b \times l}$, $\phi \in \Psi \cap \mathcal{S}$, and $\tilde{\mathcal{G}}(z, \beta, \phi) \equiv \tilde{G}(z)$, then $\beta = \beta_*$ and $\phi = \phi_*$.

The following notation is needed in the proofs of Theorems 4.1 and 4.2. Define $\hat{\Omega}_1 \colon \mathcal{S} \times \mathbb{C}^{n \times lN} \to \mathbb{R}^{lb}$ by

$$\hat{\Omega}_1(\phi, \eta) \triangleq \Omega_1(\phi) + 2\mathrm{Re} \sum_{k=1}^{N} \mathrm{vec} \mathcal{A}_k^*(\phi)[H(\theta_k) - \tilde{G}(\sigma_k) - \eta_k],$$

where $\eta_1, \ldots, \eta_N \in \mathbb{C}^{n\times l}$ and $\eta \triangleq [\ \eta_1 \ \cdots \ \eta_N\ ] \in \mathbb{C}^{n\times lN}$. Define the noise matrix $\eta_* \triangleq [\ \Gamma(\sigma_1) \ \cdots \ \Gamma(\sigma_N)\ ] \in \mathbb{C}^{n\times lN}$. Note that $\hat{\Omega}_1(\phi, \eta_*) = \Omega_1(\phi)$. Thus, $\hat{\Omega}_1$ is a function not only of ϕ but also the noise η. Define $\hat{J}\colon \mathbb{R}^{b\times l} \times \mathcal{S} \times \mathbb{C}^{n\times lN} \to [0, \infty)$, $\hat{\theta}\colon \mathcal{S} \times \mathbb{C}^{n\times lN} \to \mathbb{R}^{b\times l}$, and $\hat{Q}\colon \mathcal{S} \times \mathbb{C}^{n\times lN} \to [0, \infty)$ by

$$\hat{J}(\beta, \phi, \eta) \triangleq \sum_{k=1}^{N} \left\| \tilde{\mathcal{G}}(\sigma_k, \beta, \phi) - \tilde{G}(\sigma_k) - \eta_k \right\|_{\mathrm{F}}^2 \in \mathbb{R}, \tag{4.14}$$

$$\hat{\theta}(\phi, \eta) \triangleq -\frac{1}{2}\mathrm{vec}^{-1}\left[\Omega_2^{-1}(\phi)\hat{\Omega}_1(\phi, \eta)\right] \in \mathbb{R}^{b\times l}, \tag{4.15}$$

$$\hat{Q}(\phi, \eta) \triangleq \hat{J}(\hat{\theta}(\phi, \eta), \phi, \eta) \in \mathbb{R}. \tag{4.16}$$

Note that $\hat{J}(\beta, \phi, \eta_*) = J(\beta, \phi)$.

It follows from (4.6), (4.8), (4.9), and (4.14)–(4.16) that

$$\hat{\theta}(\phi_*, 0) = -\frac{1}{2}\mathrm{vec}^{-1}\left[\Omega_2^{-1}(\phi_*)\hat{\Omega}_1(\phi_*, 0)\right] = \beta_*, \tag{4.17}$$

$$\hat{Q}(\phi_*, 0) = \hat{J}(\beta_*, \phi_*, 0) = 0. \tag{4.18}$$

The following result addresses the case where ϕ_* is in the candidate pool Φ.

Theorem 4.1. Assume (A3.1)–(A3.5) are satisfied. Let $\Phi \subseteq (\Psi \cap \mathcal{S})$, and assume $\phi_* \in \Phi$. Let β^+ and ϕ^+ denote the identified parameters obtained from Algorithm 4.1 with the candidate pool Φ. Then, the following statements hold:

(i) There exists $\delta_0 > 0$ such that if $\|\eta_*\| < \delta_0$, then $\phi^+ = \phi_*$. Moreover, for all $\epsilon > 0$, there exists $\delta \in (0, \delta_0)$ such that if $\|\eta_*\| < \delta$, then $\beta^+ \in \mathbb{B}_\epsilon(\beta_*)$.

(ii) If $\eta_* = 0$, then $\beta^+ = \beta_*$ and $\phi^+ = \phi_*$.

Proof. To prove (i), let $\phi \in \Phi\backslash\{\phi_*\}$, and assume for contradiction that $\hat{Q}(\phi, 0) = 0$. It follows from (4.14) and (4.16) that

$$0 = \hat{Q}(\phi, 0) = \hat{J}(\hat{\theta}(\phi, 0), \phi, 0) = \sum_{k=1}^{N} \|\tilde{\mathcal{G}}(\sigma_k, \hat{\theta}(\phi, 0), \phi) - \tilde{G}(\sigma_k)\|_{\mathrm{F}}^2.$$

Thus, Proposition 4.3 implies that $\tilde{\mathcal{G}}(z, \hat{\theta}(\phi, 0), \phi) \equiv \tilde{G}(z)$, and it follows from (A3.5) that $\phi = \phi_*$, which is a contradiction. Therefore, $\hat{Q}(\phi, 0) > 0$. Define $U \triangleq \min_{x \in \Phi \backslash \{\phi_*\}} \hat{Q}(x, 0) > 0$. It can be shown that $\hat{Q}$ is continuous on $\mathcal{S} \times \mathbb{C}^{n \times lN}$. Thus, for each $j \in \mathcal{M}$, $\hat{Q}(\phi_j, \cdot)$ is continuous on $\mathbb{C}^{n \times lN}$, which implies that, for each $j \in \mathcal{M}$, there exists $\delta_j > 0$ such that for all $\eta \in \mathbb{B}_{\delta_j}(0)$,

$$|\hat{Q}(\phi_j, \eta) - \hat{Q}(\phi_j, 0)| < U/2.$$

Define $\delta_0 \triangleq \min_{j \in \mathcal{M}} \delta_j$, and assume that $\|\eta_*\| < \delta_0$. Since $\phi_* \in \Phi$, it follows that there exists $i \in \mathcal{M}$ such that $\phi_i = \phi_*$. Since $\hat{Q}(\phi_i, 0) = \hat{Q}(\phi_*, 0) = 0$, it follows that $\hat{Q}(\phi_i, \eta_*) = |\hat{Q}(\phi_i, \eta_*) - \hat{Q}(\phi_i, 0)| < U/2$. Let $j \in \mathcal{M} \backslash \{i\}$, and it follows that $-U/2 < \hat{Q}(\phi_j, \eta_*) - \hat{Q}(\phi_j, 0)$, which implies that $\hat{Q}(\phi_j, \eta_*) > \hat{Q}(\phi_j, 0) - U/2$. Since, in addition, $\hat{Q}(\phi_j, 0) \geq U$, it follows that $\hat{Q}(\phi_j, \eta_*) > U/2$. Thus, $\hat{Q}(\phi_i, \eta_*) < \hat{Q}(\phi_j, \eta_*)$, which implies that $\mathcal{J}_i(\beta_i) < \mathcal{J}_j(\beta_j)$ using (4.7) and (4.14)–(4.16). Therefore, it follows from Algorithm 4.1 that $\phi^+ = \phi_i = \phi_*$ and

$$\beta^+ = \beta_i = \hat{\theta}(\phi_*, \eta_*).$$

Let $\epsilon > 0$. It can be shown that $\hat{\theta}$ is continuous on $\mathcal{S} \times \mathbb{C}^{n \times lN}$. Thus, $\hat{\theta}(\phi_*, \cdot)$ is continuous on $\mathbb{C}^{n \times lN}$. Therefore, there exists $\delta \in (0, \delta_0)$ such that for all $\eta \in \mathbb{B}_\delta(0)$, $\hat{\theta}(\phi_*, \eta) \in \mathbb{B}_\epsilon(\hat{\theta}(\phi_*, 0))$. Finally, assume $\|\eta_*\| < \delta$. Since $\beta^+ = \hat{\theta}(\phi_*, \eta_*)$, it follows from (4.17) that $\beta^+ \in \mathbb{B}_\epsilon(\beta_*)$, which confirms (i).

To prove (ii), assume $\eta_* = 0$. Thus, $\|\eta_*\| = 0 < \delta_0$ and part (i) implies that $\phi^+ = \phi_*$. Since $\eta_* = 0$, it follows from (4.17) that $\beta^+ = \hat{\theta}(\phi_*, 0) = \beta_*$. □

Theorem 4.1 (i) provides sufficient conditions such that $\phi^+ = \phi_*$. This result also shows that if the norm of the noise η_* is sufficiently small, then the identified parameter β^+ is arbitrarily close to β_*. In fact, if the frequency response data is noiseless and $\phi_* \in \Phi$, then the identified parameters are equal to the true parameters.

Now, the analysis is extended to address the case where ϕ_* is not necessarily in the candidate pool Φ. Let $\rho \in (0,1)$ be such that if $\lambda \in \mathbb{C}$ and $\det \tilde{\mathcal{D}}(\lambda, \phi_*) = 0$, then $|\lambda| < \rho$, and define

$$\mathcal{S}_\rho \triangleq \{\phi \in \mathbb{R}^{a\times m} \colon \text{if } \lambda \in \mathbb{C} \text{ and } \det \tilde{\mathcal{D}}(\lambda, \phi) = 0, \text{ then } |\lambda| < \rho\}.$$

In practice, $\mathcal{S}_\rho$ is used to generate the candidate pool, and ρ can be selected sufficiently closed to 1 to ensure that $\phi_* \in \mathcal{S}_\rho$.

In the following result, consider Algorithm 4.1 with a sequence of candidate pools that converges to $\Psi \cap \mathcal{S}_\rho$, which is bounded and contains no isolated points (see Proposition 2.7). This result demonstrates that a sufficiently dense candidate pool and sufficiently small noise $\|\eta_*\|$ yield identified parameters β^+ and ϕ^+ that are arbitrarily close to β_* and ϕ_*.

Theorem 4.2. Assume (A3.1)–(A3.5) are satisfied. For all $j \in \mathbb{Z}^+$, let $\Lambda_j \subseteq (\Psi \cap \mathcal{S}_\rho)$ be a finite set such that $\{\Lambda_j\}_{j=1}^\infty$ converges to $\Psi \cap \mathcal{S}_\rho$. For each $j \in \mathbb{Z}^+$, let β_j^+ and ϕ_j^+ denote the identified parameters obtained from Algorithm 4.1 with the candidate pool $\Phi = \Lambda_j$. Then, for all $\epsilon > 0$, there exist $\delta > 0$ and $L \in \mathbb{Z}^+$ such that if $\|\eta_*\| < \delta$ and $j > L$, then $\beta_j^+ \in \mathbb{B}_\epsilon(\beta_*)$ and $\phi_j^+ \in \mathbb{B}_\epsilon(\phi_*)$.

Proof. Let $\epsilon > 0$. It can be shown that $\hat{\theta}$ is continuous on $\mathcal{S} \times \mathbb{C}^{n\times lN}$. Since, in addition, $\phi_* \in \mathcal{S}$, it follows that there exists $\delta_0 > 0$ such that for all $\phi \in \mathbb{B}_{\delta_0}(\phi_*)$ and all $\eta \in \mathbb{B}_{\delta_0}(0)$,

$$\hat{\theta}(\phi, \eta) \in \mathbb{B}_\epsilon(\hat{\theta}(\phi_*, 0)). \tag{4.19}$$

Define $\epsilon_1 \triangleq \min\{\epsilon, \delta_0\}$ and $\Lambda_{\mathrm{c}} \triangleq \overline{\Psi \cap \mathcal{S}_\rho}$. Using the process in Proposition 2.8, it can be shown that $\Lambda_{\mathrm{c}} \subseteq \mathcal{S}$ is compact. Since Λ_{c} is compact, and $\{x \in \mathbb{R}^{a\times m} \colon \|x - \phi_*\| \geq \epsilon_1\}$

is closed, it follows that

$$\Lambda_{\epsilon_1} \triangleq \Lambda_{\mathrm{c}} \backslash \mathbb{B}_{\epsilon_1}(\phi_*) = \Lambda_{\mathrm{c}} \cap \{x \in \mathbb{R}^{a \times m} \colon \|x - \phi_*\| \geq \epsilon_1\}$$

is compact.

Let $c > \delta_0$, define $C \triangleq \{x \in \mathbb{C}^{n \times lN} \colon \|x\| \leq c\}$, and note that $\hat{Q}$ is continuous on $\Lambda_{\epsilon_1} \times C$. Next, define $\Theta \colon C \to [0, \infty)$ by $\Theta(\eta) \triangleq \min_{\phi \in \Lambda_{\epsilon_1}} \hat{Q}(\phi, \eta)$, which exists because Λ_{ϵ_1} is compact and $\hat{Q}$ is continuous on $\Lambda_{\epsilon_1} \times C$ [93, Theorem 7.7].

Assume for contradiction that $\Theta(0) = 0$. Thus, there exists $x \in \Lambda_{\epsilon_1}$ such that $\hat{Q}(x, 0) = 0$, and it follows from (4.14)–(4.16) that

$$0 = \hat{J}(\hat{\theta}(x, 0), x, 0) = \sum_{k=1}^{N} \|\tilde{\mathcal{G}}(\sigma_k, \hat{\theta}(x, 0), x) - \tilde{G}(\sigma_k)\|_{\mathrm{F}}^2.$$

Thus, Proposition 4.3 implies that $\tilde{\mathcal{G}}(z, \hat{\theta}(\phi, 0), \phi) \equiv \tilde{G}(z)$, and it follows from (A3.5) that $x = \phi_* \notin \Lambda_{\epsilon_1}$, which is a contradiction. Thus, $\Theta(0) > 0$. Since $\hat{Q}$ is continuous on $\Lambda_{\epsilon_1} \times C$, and Λ_{ϵ_1} and C are compact, it follows from [94, Theorem 9.14] that Θ is continuous on C. Furthermore, since $\hat{Q}$ is continuous on $\mathcal{S} \times \mathbb{C}^{n \times lN}$, it follows that $\hat{Q}(\phi_*, \cdot)$ is continuous on C. Thus, $W \colon C \to \mathbb{R}$ defined by $W(\eta) \triangleq \Theta(\eta) - \hat{Q}(\phi_*, \eta)$ is continuous on C. Note that (4.18) implies that $W(0) = \Theta(0) - \hat{Q}(\phi_*, 0) = \Theta(0) > 0$. Therefore, it follows that there exists $\delta_1 \in (0, c)$ such that for all $\eta \in \mathbb{B}_{\delta_1}(0)$, $W(\eta) > 0$. Define $\delta \triangleq \min\{\delta_0, \delta_1\} > 0$ and assume $\|\eta_*\| < \delta$. Then, $W(\eta_*) > 0$.

Since $W(\eta_*) > 0$ and $\hat{Q}(\cdot, \eta_*)$ is continuous on Λ_{c}, it follows from the continuity of $\hat{Q}(\cdot, \eta_*)$ that there exists $\delta_2 > 0$ such that for all $\phi \in (\Lambda_{\mathrm{c}} \cap \mathbb{B}_{\delta_2}(\phi_*))$, $|\hat{Q}(\phi, \eta_*) - \hat{Q}(\phi_*, \eta_*)| < W(\eta_*)$. Thus, for all $\phi \in (\Lambda_{\mathrm{c}} \cap \mathbb{B}_{\delta_2}(\phi_*))$, $\hat{Q}(\phi, \eta_*) - \hat{Q}(\phi_*, \eta_*) \leq |\hat{Q}(\phi, \eta_*) - \hat{Q}(\phi_*, \eta_*)| < W(\eta_*) = \Theta(\eta_*) - \hat{Q}(\phi_*, \eta_*)$, which implies that

$$\hat{Q}(\phi, \eta_*) < \Theta(\eta_*). \tag{4.20}$$

Since $\{\Lambda_j\}_{j=1}^{\infty}$ converges to $(\Psi \cap \mathcal{S}_\rho) \subseteq \Lambda_{\mathrm{c}}$, it follows from Definition 4.1 that there exists a sequence $\{\phi_j \colon \phi_j \in \Lambda_j\}_{j=1}^{\infty}$ and $L \in \mathbb{Z}^+$ such that for all $j > L$, $\phi_j \in \mathbb{B}_{\min\{\epsilon_1,\delta_2\}}(\phi_*)$. Thus, it follows from (4.20) that for all $j > L$, $\hat{Q}(\phi_j, \eta_*) < \Theta(\eta_*)$.

Let $j \in \mathbb{Z}^+$ be such that $j > L$. It follows from Algorithm 4.1, (4.14)–(4.16), and (4.20) that $\hat{Q}(\phi_j^+, \eta_*) \leq \hat{Q}(\phi_j, \eta_*) < \Theta(\eta_*)$. Assume for contradiction that $\phi_j^+ \notin \mathbb{B}_{\epsilon_1}(\phi_*)$, which implies that $\phi_j^+ \in \Lambda_{\epsilon_1}$. Thus, $\Theta(\eta_*) = \min_{\phi \in \Lambda_{\epsilon_1}} \hat{Q}(\phi, \eta_*) \leq \hat{Q}(\phi_j^+, \eta_*) < \Theta(\eta_*)$, which is a contradiction. Therefore, $\phi_j^+ \in \mathbb{B}_{\epsilon_1}(\phi_*) \subseteq \mathbb{B}_{\epsilon}(\phi_*)$. Since $\phi_j^+ \in \mathbb{B}_{\epsilon_1}(\phi_*) \subseteq \mathbb{B}_{\delta_0}(\phi_*)$, it follows from (4.17) and (4.19) that $\beta_j^+ = \hat{\theta}(\phi_j^+, \eta_*) \in \mathbb{B}_{\epsilon}(\hat{\theta}(\phi_*, 0)) = \mathbb{B}_{\epsilon}(\beta_*)$. □

4.6 Numerical Examples

We present numerical examples, where $m = l = n = 2$. For all examples, let $D(z) = \mathrm{diag}\,(z + 0.1, z - 0.2)$, $N_y(z) = N_v(z) = \mathrm{diag}\,(1, -1)$, $D_{\mathrm{fb}}(z) = I_2$, and

$$N_{\mathrm{fb}}(z) = \begin{bmatrix} 0.3 & 1 \\ 0.2 & 0.4 \end{bmatrix}, \qquad N_{\mathrm{ff}}(z) = \begin{bmatrix} z - 0.3 & z + 0.4 \\ 0.5z & 1 \end{bmatrix}.$$

Note that

$$\beta_* = \begin{bmatrix} 1 & 0.5 & -0.3 & 0 \\ 1 & 0 & 0.4 & 1 \end{bmatrix}^{\mathrm{T}}, \qquad \phi_* = \begin{bmatrix} 0.3 & 1 \\ 0.2 & 0.4 \end{bmatrix}^{\mathrm{T}}.$$

Let $N = 20$, and for $k \in \mathcal{N}$, let $\theta_k = 0.02\pi k$. This example satisfies (A3.1)–(A3.4), and for any compact set $\Psi \subseteq \mathbb{R}^{a \times m}$ containing ϕ_*, (A3.5) is satisfied.

Example 4.2. Consider the case with $\phi_* \in \Phi$ and noiseless data. Define the candidate pool

$$\Lambda_0 \triangleq \{\phi \in \mathbb{R}^{2\times 2} \colon \text{ for } i, j \in \{1, 2\}, \phi_{(i,j)} \in \{-0.5 + 0.1k\}_{k=0}^{20}\} \cap \mathcal{S},$$

and note that $\phi_* \in \Lambda_0$. Algorithm 4.1 is used with the candidate pool $\Phi = \Lambda_0$ to obtain $\beta^+ = \beta_*$ and $\phi^+ = \phi_*$, which agrees with (ii) of Theorem 4.1. $\triangle$

Example 4.3. Consider the case with $\phi_* \in \Phi$ and noisy data. For $i = 1, \ldots, 15$, let $\Gamma_i(z) \in \mathbb{C}^{2\times 2}$ be the noise, and define the noise-to-signal ratio

$$R_i \triangleq \frac{1}{N} \sum_{k=1}^{N} \frac{\|\Gamma_i(\sigma_k)\|_{\mathrm{F}}}{\|\tilde{G}(\sigma_k)\|_{\mathrm{F}}}.$$

For $i = 1, \ldots, 15$, the frequency response data is $H_i(\theta_k) \triangleq \tilde{G}(\sigma_k) + \Gamma_i(\sigma_k)$. In this example, $\Gamma_1, \ldots, \Gamma_{15}$ are randomly generated such that $R_1 > R_2 > \cdots > R_{15}$. For example, $R_1 = 2.39$, $R_2 = 1.29$, $R_4 = 0.28$, $R_7 = 3.76 \times 10^{-2}$, and $R_{15} = 1.42 \times 10^{-4}$. For $i = 1, \ldots, 15$, Algorithm 4.1 is used with the candidate pool $\Phi = \Lambda_0$ and data $\{H_i(\theta_k)\}_{k=1}^N$ to obtain the identified parameters β_i^+ and ϕ_i^+. Figure 4.3 shows that for $i \geq 7$, $\phi_i^+ = \phi_*$, and for sufficiently large i, $\|\beta_i^+ - \beta_*\|_{\mathrm{F}}$ is arbitrarily small, which agrees with (i) of Theorem 4.1. $\triangle$

Example 4.4. Consider the case with $\phi_* \notin \Phi$ and noisy data. For $j = 1, \ldots, 18$, define the candidate pool

$$\Lambda_j \triangleq \{\phi \in \mathbb{R}^{2\times 2} \colon \text{ for } i, h \in \{1, 2\}, \phi_{(i,h)} \in \{-0.5 + 2k/(1+j)\}_{k=0}^{1+j}\} \cap \mathcal{S}_\rho,$$

where $\rho = 0.99$, and note that for $j = 1, \ldots, 18$, $\phi_* \notin \Lambda_j$. For $i = 2, 4, 15$, and $j = 1, \ldots, 18$, Algorithm 4.1 is used with the candidate pool $\Phi = \Lambda_j$ and data $\{H_i(\theta_k)\}_{k=1}^N$ to obtain the identified parameters $\beta_{j,i}^+$ and $\phi_{j,i}^+$. Figure 4.4 shows that for sufficient large j and i, $\|\beta_{j,i}^+ - \beta_*\|_{\mathrm{F}}$ and $\|\phi_{j,i}^+ - \phi_*\|_{\mathrm{F}}$ are arbitrarily small, which agrees with Theorem 4.2. $\triangle$

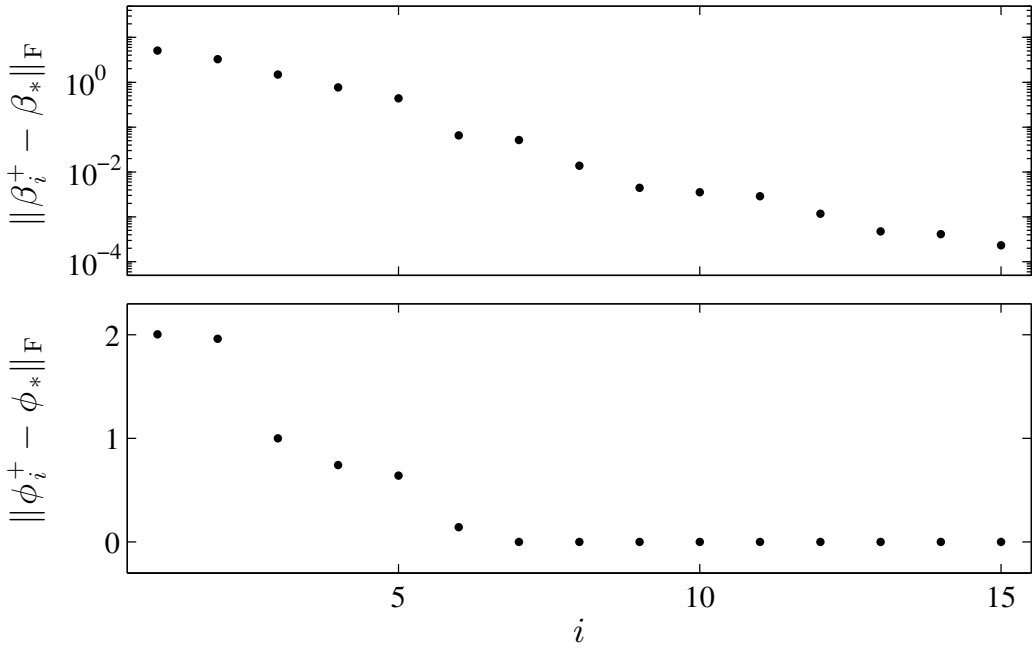

Figure 4.3: *Noisy data and* $\phi_* \in \Phi$. For $i = 1, \ldots, 15$, Algorithm 4.1 is used with the candidate pool Λ_0 and data $\{H_i(\theta_k)\}_{k=1}^N$ to obtain β_i^+ and ϕ_i^+. For $i \geq 7$, $\phi_i^+ = \phi_*$, and for sufficiently large i, $\|\beta_i^+ - \beta_*\|_{\mathrm{F}}$ is arbitrarily small.

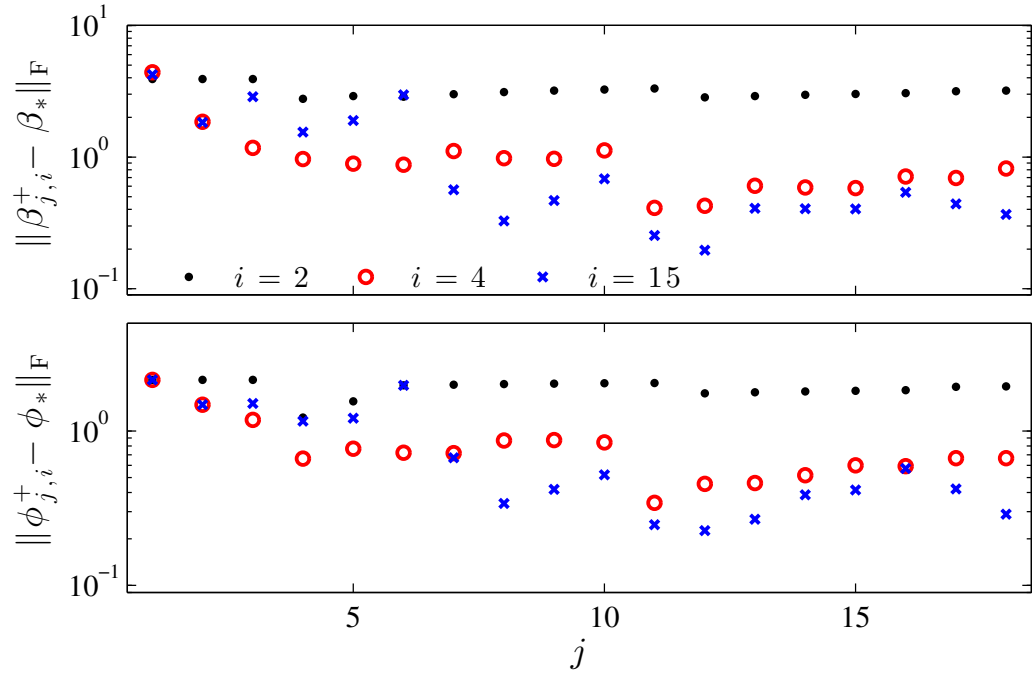

Figure 4.4: *Noisy data and* $\phi_* \notin \Phi$. For $i = 2, 4, 15$, and $j = 1, \ldots, 18$, Algorithm 4.1 is used with the candidate pool Λ_j and data $\{H_i(\theta_k)\}_{k=1}^N$ to obtain $\beta_{j,i}^+$ and $\phi_{j,i}^+$. For sufficient large j and i, $\|\beta_{j,i}^+ - \beta_*\|_{\mathrm{F}}$ and $\|\phi_{j,i}^+ - \phi_*\|_{\mathrm{F}}$ are arbitrarily small.

4.7 Computational Complexity

The computational complexity of Algorithm 4.1 is dominated by Step 2, where a quadratic minimization problem is solved by M times. The modified Gram Schmidt method [112, Chapter 14] is used to perform this quadratic minimization. It follows from [112, Chapter 14] that the computation complexity of Algorithm 4.1 is $C \triangleq M[4Nnm^2l^3(n_{\rm ff}+1)^2 + 2Nnml^2(n_{\rm ff}+1)]$ flops.

Next, we compare the computational complexity of Algorithm 4.1 with that of Algorithm 2.1. The Algorithm 2.1 also uses a candidate pool approach; however, $\mathcal{G}_{\rm ff}$ is parameterized as an IIR transfer function, and the method only applies to subsystems that are SISO (i.e., $v = y$ and $l = m = n = 1$). For SISO subsystems, the computational complexity of Algorithm 4.1 is $C = M[4N(n_{\rm ff}+1)^2+2N(n_{\rm ff}+1)]$ flops. Next, consider Algorithm 2.1, where $\hat{N}$ denotes the number of frequency response data points, $M_{\rm fb}$ denotes the number of elements in the feedback candidate pool, and $M_{\rm ff}$ denotes the number of elements in the feedforward candidate pool. Let $\hat{n}_{\rm ff}$ denote the degree of numerator of $\mathcal{G}_{\rm ff}$. It follows from [112, Chapter 14] that the computation complexity of Algorithm 2.1 is $\hat{C} = M_{\rm ff}M_{\rm fb}[4\hat{N}(\hat{n}_{\rm ff}+1)^2 + 2\hat{N}(\hat{n}_{\rm ff}+1)]$ flops.

To compare the computational complexities of these algorithms, it is assumed that these algorithms use the same frequency response data and feedback candidate pool, which implies that $N = \hat{N}$ and $M = M_{\rm fb}$. Thus, the computational complexity ratio is

$$\mathcal{R} \triangleq \frac{C}{\hat{C}} = \frac{2(n_{\rm ff}+1)^2 + (n_{\rm ff}+1)}{M_{\rm ff}[2(\hat{n}_{\rm ff}+1)^2 + (\hat{n}_{\rm ff}+1)]}.$$

In general, $\hat{n}_{\rm ff} \leq n_{\rm ff}$ and $M_{\rm ff} \gg 1$, which result $\mathcal{R} < 1$.

Example 4.5. Let

$$G_y(z) = G_v(z) = \frac{0.4}{z-0.9}, \qquad G_{\rm ff}(z) = \frac{0.2(z-0.77)}{(z-0.83)(z-0.89)}, \qquad G_{\rm fb}(z) = \frac{0.32}{z-0.81}.$$

Let $N = 31$, and for $k \in \mathcal{N}$, let $\theta_k = 0.008\pi(k-1)$. Consider the candidate pool

$$\Lambda_0 \triangleq \{\phi \in \mathbb{R}^2 \colon \phi_{(1)} \in \{-2 + 0.05k\}_{k=0}^{40}, \phi_{(2)} \in \{-2 + 0.05k\}_{k=0}^{80}\} \cap \mathcal{S},$$

which contains 297 elements.

First, we use Algorithm 4.1 with the candidate pool Λ_0. For $n_{\mathrm{ff}} = 1, 2, \ldots, 17$, we identify feedforward and feedback controllers, where $\mathcal{G}_{\mathrm{ff}}$ is FIR even though G_{ff} is IIR.

Next, consider Algorithm 2.1, where $\mathcal{G}_{\mathrm{ff}}$ is parameterized as IIR with $\hat{n}_{\mathrm{ff}} = 1$. Consider feedforward candidate pool

$$F = \{[\ x_1 + x_2 \quad x_1 x_2\ ]^{\mathrm{T}} \in \mathbb{R}^2 \colon x_1, x_2 \in \{-0.05k\}_{k=0}^{19}\},$$

which contains $M_{\mathrm{ff}} = 210$ elements. We use Algorithm 2.1 with the candidate pool $F \times \Lambda_0$ to identify feedback and feedforward controllers.

Figure 4.5 shows the identification errors

$$\mathcal{E}_{\mathrm{fb}} \triangleq \int_{\theta_1}^{\theta_N} \left|G_{\mathrm{fb}}^{+}(e^{\jmath\theta}) - G_{\mathrm{fb}}(e^{\jmath\theta})\right| \mathrm{d}\theta, \qquad \mathcal{E}_{\mathrm{ff}} \triangleq \int_{\theta_1}^{\theta_N} \left|G_{\mathrm{ff}}^{+}(e^{\jmath\theta}) - G_{\mathrm{ff}}(e^{\jmath\theta})\right| \mathrm{d}\theta$$

for each algorithm. In this example, for $n_{\mathrm{ff}} = 14, \ldots, 17$, Algorithm 4.1 yields errors $\mathcal{E}_{\mathrm{fb}}$ and $\mathcal{E}_{\mathrm{ff}}$ smaller than those obtained from Algorithm 2.1. Figure 4.5 also shows that for $n_{\mathrm{ff}} = 1, 2, \ldots, 17$, $\mathcal{R} < 0.32$. $\triangle$

4.8 Conclusions

In this chapter, we presented a discrete-time SSID algorithm for MIMO systems with feedback and feedforward architecture. This discrete-time SSID method ensures asymptotic stability of the identified closed-loop transfer function. The analytic results are in Theorems 4.1–4.2, which describe the properties of the discrete-time SSID algorithm. In particular, Theorem 4.2 shows that the coefficients of the identified feed-

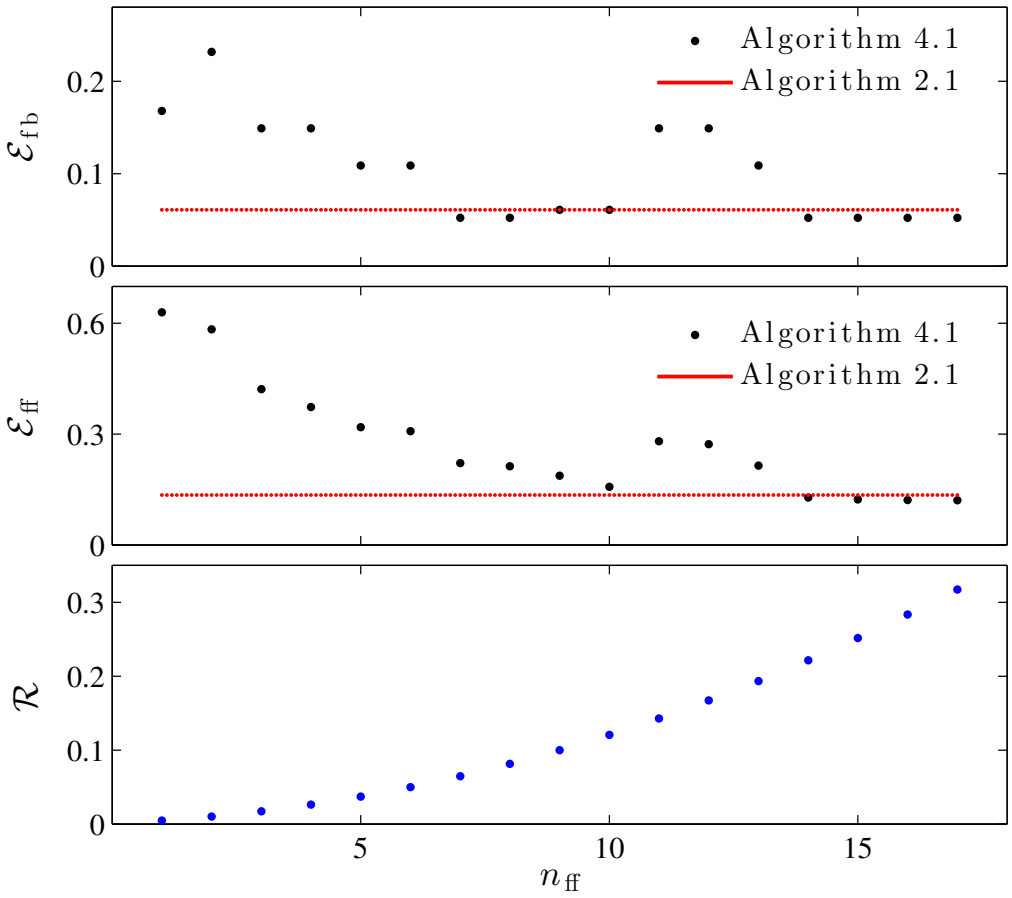

Figure 4.5: *Computation complexity.* For $n_{\mathrm{ff}} = 14, \ldots, 17$, Algorithm 4.1 yields errors $\mathcal{E}_{\mathrm{fb}}$ and $\mathcal{E}_{\mathrm{ff}}$ smaller than those obtained from Algorithm 2.1. For $n_{\mathrm{ff}} = 1, 2, \ldots, 17$, $\mathcal{R} < 0.32$.

back and feedforward transfer functions are arbitrarily close to the true coefficients if the candidate pool is sufficiently dense and the data noise is sufficiently small. Also, the computational complexity of the SSID algorithm is discussed.

In the next chapter, the SSID algorithm is used to model human control behavior when human subjects learn to control an unknown nonminimum-phase system, which is interesting because the dynamic inversion of nonminimum-phase system is unstable.

Chapter 5 The Impact of System Zeros on Human Learning

In this chapter, we present results from a human-in-the-loop (HITL) experiment in which human subjects learn to control unknown dynamic systems over 40 trials. We examine the impact of system zeros on human learning by comparing results for humans interacting with 3 different systems, which have the same poles but different zeros. For each trial, the subsystem identification (SSID) algorithm in Chapter 4 is used to model each subject's feedforward and feedback control behavior. By comparing the experimental results and identified control strategies used by humans, we examine the impact of system zeros. Preliminary results related to this chapter have been published in [113].

5.1 Introduction

Humans learn to control a wide range of complex dynamic systems, including bicycles, kites, and hula hoops. The objective of research on human motor control is to determine how the central nervous system directs motion. The internal model hypothesis (IMH) proposes that the brain constructs models of the body's interactions with the physical world and that those models are used for control [6, 7, 97]. Suggested uses of internal models include prediction, state estimation, inverse model, and forward model [10, 98–104].

One approach to explore the IMH is to compare the results of human control experiments with mathematical models of proposed human control architectures [8, 38–50, 52, 105]. However, vastly different control strategies can yield similar dynamic

behavior. Thus, a model that reproduces qualitative features of an experiment does not necessarily provide an accurate representation of the human's control strategy.

In contrast to the approaches in [8, 38–50, 52, 105], we use SSID to obtain feedforward and feedback controllers that are the best fit to data obtained from a human control experiment. Other studies that use system identification approaches to model human responses include [74, 75, 85, 86, 106–108]. Specifically, [85] identifies models of a human's precision grip force and [86] identifies models of a human's oculomotor system. However, the HITL systems investigated in [85, 86] are modeled without feedback. In [106–108], identification methods are used to model the behavior of human pilots; however, these models include error feedback only and thus, do not incorporate feedforward control. In [74, 75], feedforward and feedback controllers are estimated for humans performing ramp-tracking tasks. However, these feedforward and feedback models rely on an assumed control strategy, specifically, the feedforward models are assumed to include the inverse system dynamics.

In contrast to [74, 75, 85, 86, 106–108], we use an SSID method to model a human's response with both feedforward and feedback control without assuming *a priori* a specific feedforward or feedback control strategy.

In Chapter 3, we presented results from an HITL experiment where human subjects learn to control a linear time-invariant (LTI) dynamic system, which is minimum phase, that is, has asymptotically stable inverse dynamics. The results of Chapter 3 suggest that, for a minimum-phase system, humans tend to learn to approximate the inverse dynamics in feedforward. In this case, the inverse dynamics are asymptotically stable and can thus be used in feedforward. However, not all LTI systems have asymptotically stable inverse dynamics. An LTI system with unstable inverse dynamics is referred to as nonminimum phase. Since the inverse dynamics of a nonminimum-phase system are unstable, we ask the questions: Can humans learn to control a nonminimum-phase system? What control strategies do humans use with

nonminimum-phase systems? Are nonminimum-phase systems harder to control than minimum-phase systems, and if so why?

5.2 Experimental Methods

Subjects participating in this experiment use a single-degree-of-freedom joystick to affect the motion of an object displayed on a computer screen as shown in Figure 5.1. The controlled object's position y and the joystick position u are functions of time t

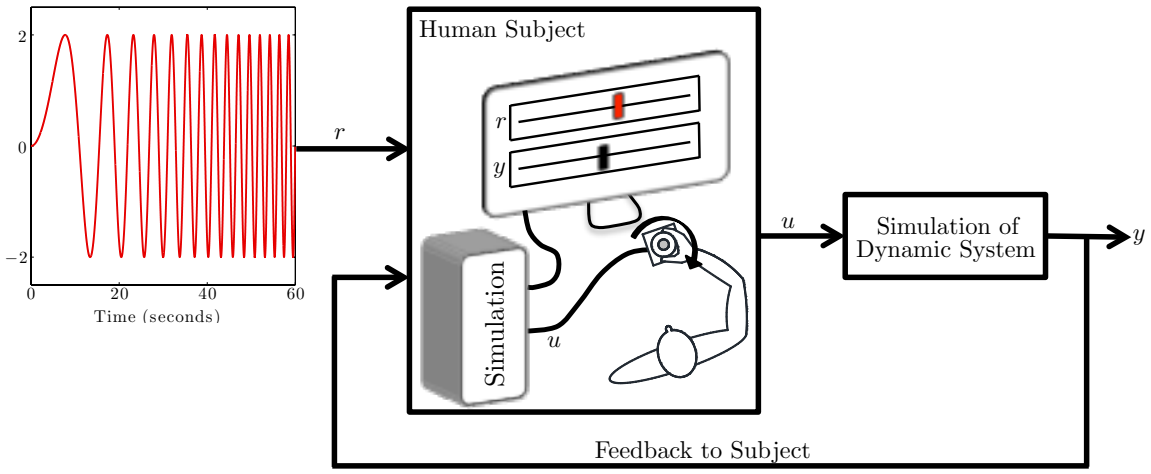

Figure 5.1: Subjects use a joystick to affect the motion of an object on a computer screen. The object's position y represents the output of a dynamic system and the joystick position u represents the input to the dynamic system. A reference object is also displayed on the screen, and its position r is an 60s chirp signal.

and are related to each other by a dynamic system. A reference object, whose position r is independent of the joystick position u, also moves on the computer screen. The subject's objective is to manipulate the joystick in a manner that makes the controlled object and the reference object have the same position at each instant of time. Specifically, the objective is to generate a control u that minimizes the magnitude of the command-following error $e = r - y$. Prior to performing the experiment, a subject has no knowledge of the reference object's motion r or the dynamic system relating u and y.

Thirty-three people voluntarily participated in this study. At the time of the exper-

iment, the subjects had no known neurological or motor control disorders and were 18–35 years of age. Each subject performed 40 trials of the experiment in a period of 7 days. A trial is an 60-second time period during which a subject operates the joystick. Each subject's trials were divided into 4 sessions, and each session consisted of 10 trials, which were completed within a period of 20 minutes. No subject participated in more than one session in a 12-hour period. For each session, a subject is placed in an isolated area free from distraction and sits in a chair facing a computer screen. A subject's dominant hand is used to manipulate a single-degree-of-freedom joystick.

This experiment satisfies the U.S. Department of Health and Human Services Code of Federal Regulation for human subject research (45 CFR 46) and was approved by the University of Kentucky Institutional Review Board (IRB number 14-0526-P4S).

The reference object's position r is an 60-second chirp signal with frequency content between 0 and 0.5 Hz. Specifically, for all $t \in [0, 60]$, the reference is

$$r(t) = 2 \sin \frac{\pi}{120} t^2.$$

The magnitude of reference r is 2, which is within the ± 8 range of motion displayed on the computer screen.

The controlled object's position y satisfies the differential equation

$$m\ddot{y}(t) + c\dot{y}(t) + ky(t) = f(t), \tag{5.1}$$

where m, c, and k are real numbers and the exogenous force f is determined from the joystick input u according to

$$f(t) = a\dot{u}(t) + bu(t), \tag{5.2}$$

where all initial conditions are zero.

The differential equations (5.1) and (5.2) can be used to model a variety of second-order dynamic systems, including simple electrical circuits or a single-link robotic arm. In this experiment, (5.1) and (5.2) models the spring-mass-damper system shown in Figure 5.2, where y represents the position of the mass, and f, which is generated from the joystick input u, represents the force applied to the mass. In this case, m is the

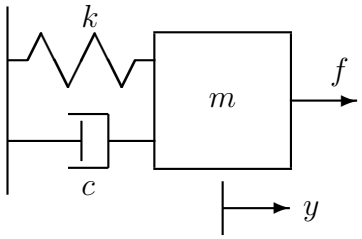

Figure 5.2: The single-degree-of-freedom mass-spring-damper system.

mass, k is the spring stiffness, and c is the damping constant. Thus, the relationship between u and y can be written in the Laplace domain as $\hat{y}(s) = G(s)\hat{u}(s)$, where

$$G(s) = \frac{as + b}{ms^2 + cs + k} \tag{5.3}$$

is the transfer function from u to y, and $\hat{u}(s)$ and $\hat{y}(s)$ are the Laplace transforms of u and y.

5.3 System Zeros

In general, an LTI system can be expressed in the Laplace domain as $\hat{y}_{\mathcal{G}}(s) = \mathcal{G}(s)\hat{u}_{\mathcal{G}}(s)$, where $\hat{y}_{\mathcal{G}}$ is the Laplace transform of a scalar output, $\hat{u}_{\mathcal{G}}$ is the Laplace transform of a scalar input, and $\mathcal{G}$ is a real rational transfer function, which can be written as

$$\mathcal{G}(s) = \frac{\mathcal{N}(s)}{\mathcal{D}(s)},$$

where $\mathcal{N}$ and $\mathcal{D}$ are polynomials in s. For this discussion, we assume that $\mathcal{N}$ and $\mathcal{D}$ have no common roots. The roots of $\mathcal{N}$ are the *zeros* of $\mathcal{G}$, while the roots of $\mathcal{D}$ are the *poles* of $\mathcal{G}$.

The poles of $\mathcal{G}$ are determined from the physics (e.g., the physical parameters) of the dynamic system. For example, the poles of G are determined from the mass m, damping c, and spring stiffness k. The poles determine whether $\mathcal{G}$ is asymptotically stable or unstable. In addition, the poles determine the natural frequencies and growth or decay rate of the impulse response of $\mathcal{G}$ (i.e., the response if $\hat{u}_{\mathcal{G}} = 1$, which is the Laplace transform of the Dirac delta function). The transfer function $\mathcal{G}$ is *asymptotically stable* if every pole is in the open-left-half plane (OLHP). In this case, the impulse response of $\mathcal{G}$ decays exponentially to 0. Conversely, $\mathcal{G}$ is *unstable* if at least one pole is in the open-right-half plane (ORHP). In this case, the impulse response of $\mathcal{G}$ grows exponentially and diverges to infinity. Since the physical parameters m, c, and k are positive, it follows that G is asymptotically stable.

In contrast to poles, the zeros of $\mathcal{G}$ are determined not only from the physics of the dynamic system but also from the location and type of sensors and actuators. For example, the zeros of G are determined from a and b, which are the parameters that govern how the actuation force f is determined from the joystick input u. Zeros play an important role in control theory and control systems design [114].

A zero of $\mathcal{G}$ is *minimum phase* if it is in the OLHP, whereas a zero of $\mathcal{G}$ is *nonminimum phase* if it is in the ORLP. For example, the zero of G is $-b/a$, which is minimum phase if $b/a > 0$ and nonminimum phase if $b/a < 0$. The transfer function $\mathcal{G}$ is *minimum phase* if all zeros are minimum phase. In contrast, $\mathcal{G}$ is *nonminimum phase* if at least one zero is nonminimum phase.

Many physical systems are modeled by transfer functions containing only minimum-phase zeros. For example, a vibration absorber attached to a vibrational system is minimum phase. In this case, a vibration absorber is connected to a primary system

to reduce the vibration of the primary system. Assume that the primary system is for example the single-degree-of-freedom mass-spring-damper system shown in Figure 5.2. Then, the transfer function from the external force f to the position y of the mass in the primary system is minimum phase [115]. However, nonminimum-phase zeros also arise in physical systems. For example, driving a car backwards is a dynamic system containing nonminimum-phase zeros. When we drive a car backwards (e.g., parallel parking), the transfer function from the steering angle to the lateral position of the center of the front wheels is nonminimum phase [114].

To examine the effect of system zeros on human learning, we divided the 33 subjects into 3 groups, where each group has 11 subjects. The subjects interact with the dynamic system (5.1) and (5.2), where $m = 1, c = 3.6, k = 4$, and $b = 4.4$, but where a is different for each group. For one group, $a = 2$, which means that the transfer function G is given by

$$G_{\mathrm{m}}(s) \triangleq \frac{2(s + 2.2)}{s^2 + 3.6s + 4}, \tag{5.4}$$

which has a minimum-phase zero at -2.2. For another group, $a = -2$, which means that G is given by

$$G_{\mathrm{n}}(s) \triangleq \frac{-2(s - 2.2)}{s^2 + 3.6s + 4}, \tag{5.5}$$

which has a nonminimum-phase zero at $+2.2$. For the third group, $a = -5.5$, which means that G is given by

$$G_{\mathrm{sn}}(s) \triangleq \frac{-5.5(s - 0.8)}{s^2 + 3.6s + 4}, \tag{5.6}$$

which has a slower (i.e., closer to the imaginary axis) nonminimum-phase zero at $+0.8$. Note that $G_{\mathrm{m}}, G_{\mathrm{n}}$, and G_{sn} have the same poles, which are $-1.8 \pm 0.87\jmath$. Thus,

all 3 transfer functions are asymptotically stable. Moreover, all 3 transfer functions have the same zero-frequency gain, that is, $G_{\mathrm{m}}(0) = G_{\mathrm{n}}(0) = G_{\mathrm{sn}}(0) = 1.1$. Thus, these transfer functions differ only by the location of the zero.

Figure 5.3 shows the Bode plots for G_{m}, G_{n}, and G_{sn}. Notice that the magnitude

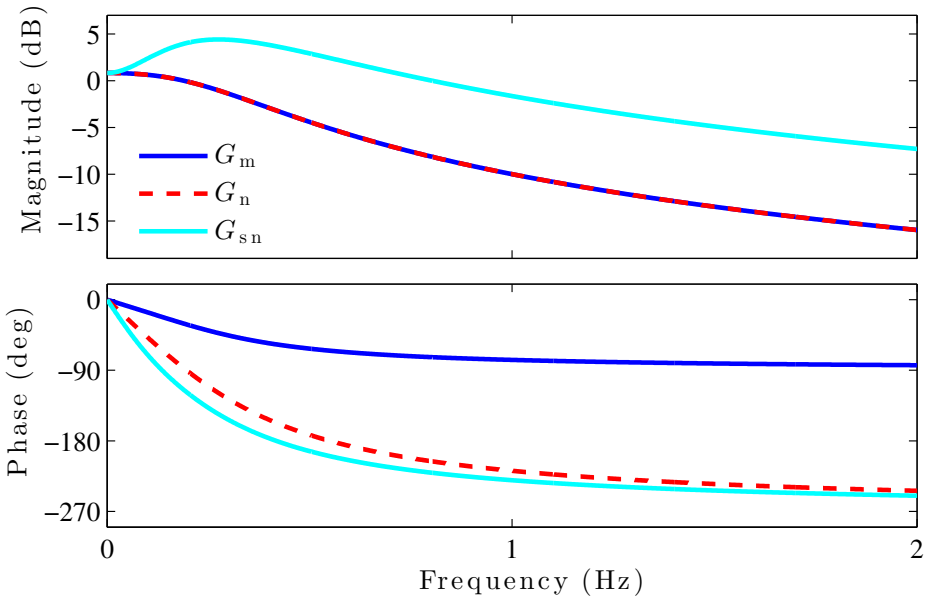

Figure 5.3: Bode plots of G_{m}, G_{m}, and G_{sn}.

plots for G_{m} and G_{n} coincide, whereas the phase plot for G_{n} has 180° more asymptotic phase lag. This phase lag is an important feature of nonminimum-phase zeros—a feature that tends to limit robustness and achievable performance in automatic control system technology [114, 116]. Although G_{n} and G_{sn} both have 270° of asymptotic phase lag, the phase of G_{sn} decreases more rapidly than that of G_{n} as shown in Figure 5.3. In addition, the magnitude of G_{sn} is always larger than that of G_{m} and G_{n}.

A nonminimum-phase zero has the property that it can "block" a specific unbounded input. For example, Figure 5.4 shows that the response y of G_{m} and G_{n} to the unbounded input $u(t) = e^{2.2t}$. The response of G_{m} is unbounded, whereas the response of G_{n} is bounded and, in fact, converges to 0. Notice that the expo-

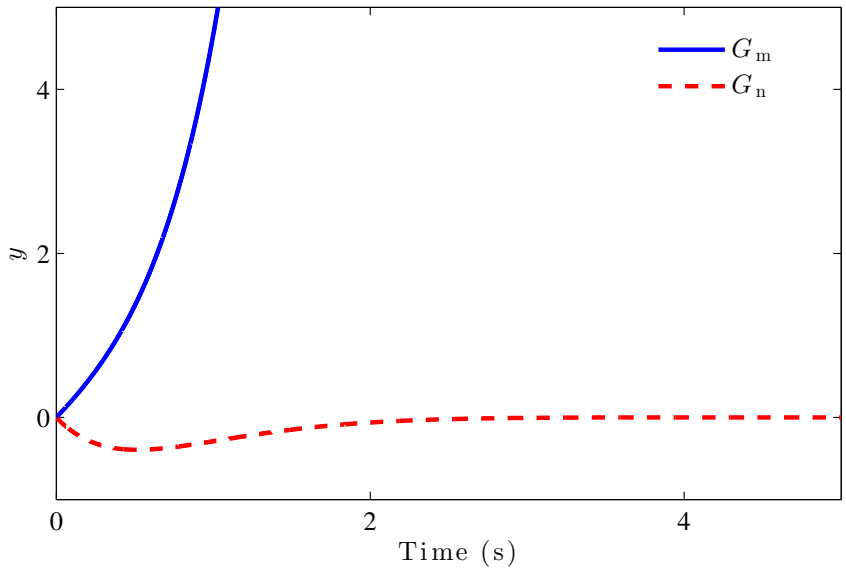

Figure 5.4: For a bounded input $u(t) = e^{2.2t}$, the output of G_{m} is unbounded, but the output of G_{n} is bounded and converges to 0.

nential growth rate of $u(t) = e^{2.2t}$ is 2.2, which corresponds to the location of the nonminimum-phase zero of G_{n}. This matching of growth rate and zero location is why the response y of G_{n} decays to 0, even though the input $u(t) = e^{2.2t}$ is unbounded. For every dynamic system with a nonminimum-phase zero, there exists an unbounded input that leads to a bounded response that converges to 0 [114]. In contrast, minimum-phase zeros can "block" only bounded inputs.

Since the zero of G_{m} is minimum phase, the inverse dynamics G_{m}^{-1} are asymptotically stable; however, the zero of G_{n} is nonminimum phase, which implies that the inverse dynamics G_{n}^{-1} are unstable. The unstable inverse dynamics associated with G_{n} may be an impediment to humans approximating G_{n}^{-1} in feedforward for control.

Figure 5.5 shows the step response of $G_{\mathrm{m}}, G_{\mathrm{n}}$, and G_{sn}, that is, the response y with input $u(t) \equiv 1$. For G_{n} and G_{sn}, the response y departs from 0 in the nonasymptotic direction. This phenomenon is called initial undershoot [114]. The step response of an asymptotically stable, strictly proper (i.e., the degree of numerator is smaller than

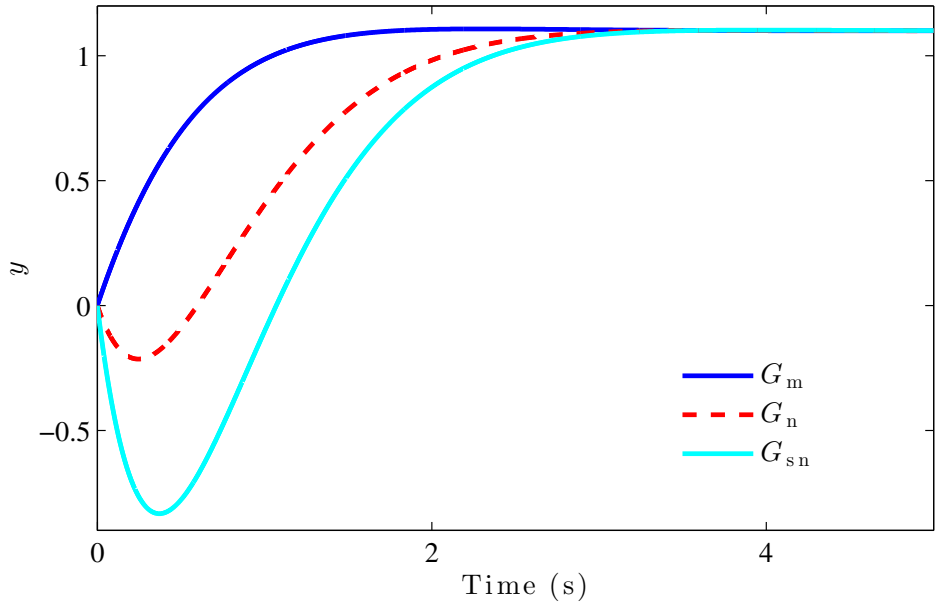

Figure 5.5: Step responses of G_{m}, G_{m}, and G_{sn}.

that of the denominator) transfer function exhibits initial undershoot if and only if the transfer function has an odd number of positive zeros [117–119]. Initial undershoot may be an impediment to a human's ability to control a nonminimum-phase system. In particular, initial undershoot may make it difficult for a human to learn to generate a control u in the "correct" direction.

5.4 Experimental Results in Time Domain

Each trial of the experiment lasts for $T = 60$s. For each trial in the experiment, we record data r, u, and y with the sampling time $T_{\mathrm{s}} = 0.02$s and obtain the sequences $r(iT_{\mathrm{s}})$, $u(iT_{\mathrm{s}})$, $y(iT_{\mathrm{s}})$, and $e(iT_{\mathrm{s}})$, where $i = 0, 1, 2, \ldots, 3000$.

For certain trials, the output $\{y(iT_{\mathrm{s}})\}_{i=0}^{3000}$ exceeds the ± 8 display boundary on the computer screen. A trial where, for any $i = 0, 1, 2, \ldots, 3000$, $y(iT_{\mathrm{s}})$ exceed ± 8 is termed a divergent trial. For the remainder of this chapter, divergent trials are omitted from the reported results.

For each trial of the experiment, we define the time-averaged error

$$\|e\| \triangleq \frac{1}{3001}\sum_{i=0}^{3000}|e(iT_{\rm s})|.$$

Figure 5.6 shows the reference r, output y, and command-following error e for the first and last trials of the subject from each group who has the median time-averaged error among the 11 subjects in the group. We observe that, for all 3 groups, the command-following error on the last trial is improved relative to the error on the first trial. We also note that the command-following error for the subject in the group with $G_{\rm m}$ is smaller than that in the group with $G_{\rm n}$, which is smaller than that in the group with $G_{\rm sn}$.

Figure 5.7 shows that, for each group, the mean time-averaged error improved over 40 trials. Figure 5.7 also shows that the mean $\|e\|$ with $G_{\rm m}$ is smaller than that with $G_{\rm n}$, and the mean $\|e\|$ with $G_{\rm n}$ is smaller than that with $G_{\rm sn}$.

For each group, the number of divergent trials over the 40 trails is shown in Figure 5.8. We observe that there are more divergent trials at the beginning than the end of the 40 trials, which implies that the subjects learn to control the systems such that the output y is within the ± 8 display boundary. The number of divergent trials for the groups with $G_{\rm m}$, $G_{\rm n}$, and $G_{\rm sn}$ are 1, 10 , and 61, respectively. One possible interpretation for the difference in the number of divergent trials is related to the high-gain limitations of the 3 systems. For the group with $G_{\rm n}$, if a subject tries to reduce the error e by using high-gain feedback, then the high-gain feedback is more likely to destabilize the closed-loop system than it is with $G_{\rm m}$. Similarly, high-gain feedback is more likely to destabilize the closed-loop system with $G_{\rm sn}$ than it is with $G_{\rm n}$.

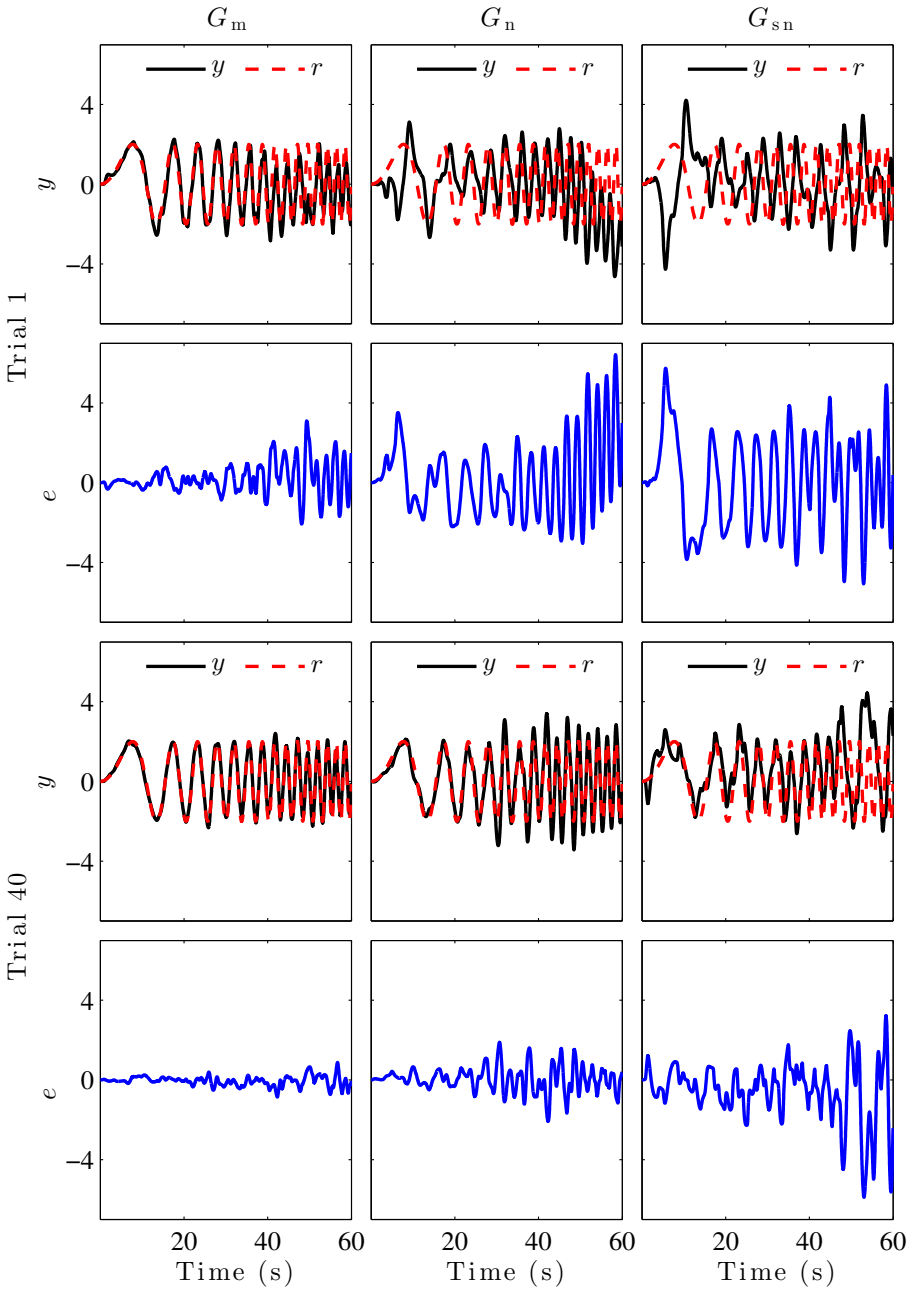

Figure 5.6: The reference r, output y, and command-following error e for the first and last trials of the subject from each group who has the median time-averaged error among the 11 subjects in the group. The command-following error e for the subject in the group with G_{m} is smaller than that in the group with G_{n}, which is smaller than that in the group with G_{sn}.

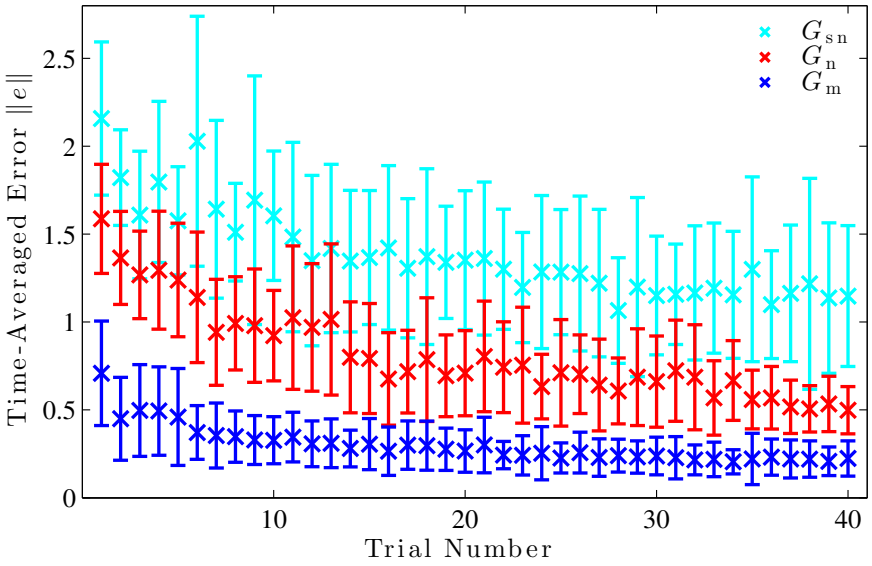

Figure 5.7: For each group, the time-averaged error $\|e\|$ of the 11 subjects for each of the 40 trials. The $\times$ indicates the mean of the 11 subjects and the vertical lines show one standard deviation. The mean $\|e\|$ improves over trials. The mean $\|e\|$ with G_{m} is smaller than that with G_{n}, and the mean $\|e\|$ with G_{n} is smaller than that with G_{sn}.

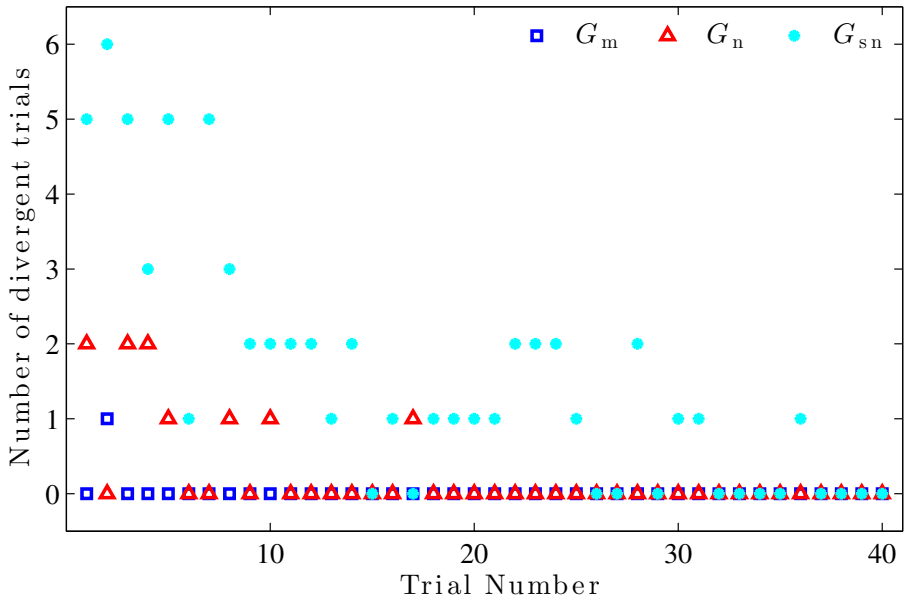

Figure 5.8: The total number of divergent trials for the groups with G_{m}, G_{n}, and G_{sn} are 1, 10, and 61, respectively.

5.5 Discussion of Potential Control Strategies

The linear time-invariant control architecture shown in Figure 5.9 is used to model each subject's control strategy. See [6] for a physiological interpretation of this archi-

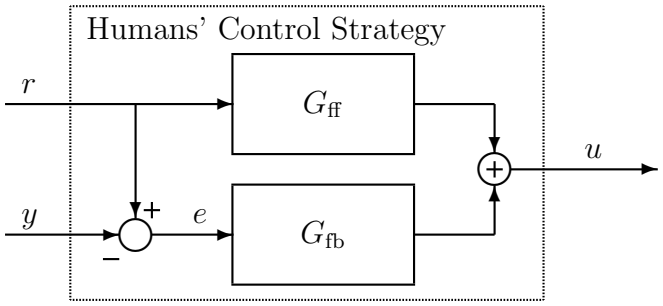

Figure 5.9: Each subject's control strategy is modeled using a feedback controller G_{fb} and a feedforward controller G_{ff}.

tecture. A subject's control strategy is modeled by

$$\hat{u}(s) = G_{\text{fb}}(s)\hat{e}(s) + G_{\text{ff}}(s)\hat{r}(s),$$

where $\hat{e}(s)$ and $\hat{r}(s)$ are the Laplace transforms of e and r, and the transfer functions G_{fb} and G_{ff} are the feedback and feedforward controllers. Feedback is the reactive control determined from the observed error e, whereas feedforward is the anticipatory control determined solely from the reference r. The closed-loop response is $\hat{e}(s) = \tilde{G}_{er}(s)\hat{r}(s)$, where

$$\tilde{G}_{er}(s) \triangleq \frac{1 - G_{\text{ff}}(s)G(s)}{1 + G_{\text{fb}}(s)G(s)} \tag{5.7}$$

is the closed-loop transfer function from r to e. The frequency response of $\tilde{G}_{er}$ is the complex-valued function $\tilde{G}_{er}(\jmath\omega)$, where ω is the frequency.

To ensure that the error e is bounded, the controllers G_{ff} and G_{fb} must be such that the closed-loop transfer function $\tilde{G}_{er}$ is asymptotically stable. To make the error e small, G_{ff} and G_{fb} must make the magnitude of $\tilde{G}_{er}(\jmath\omega)$ small at frequencies coinciding with the 0-to-0.5 Hz frequency content of the reference r.

First, we consider control strategies that could be used to achieve good command following for the dynamic system G_{m}. One control strategy is to use high gain in feedback. It follows from (5.7) that $|\tilde{G}_{er}(\jmath\omega)|$ is small if $|G_{\mathrm{fb}}(\jmath\omega)|$ is large. Therefore, as long as $\tilde{G}_{er}$ is asymptotically stable, the magnitude of e is decreased by increasing $|G_{\mathrm{fb}}(\jmath\omega)|$ at the frequencies of r. Figure 5.10(a) shows that using high gain in feedback can make the magnitude of e small. High-gain feedback makes the magnitude of e small by making the closed-loop transfer function from r to y

$$\tilde{G}_{yr}(s) \triangleq 1 - \tilde{G}_{er}(s) = \frac{G(s)[G_{\mathrm{ff}}(s) + G_{\mathrm{fb}}(s)]}{1 + G(s)G_{\mathrm{fb}}(s)}$$

close to 1 over the 0-to-0.5 Hz frequency range. Note that humans cannot use arbitrarily high gain in feedback due to delay in a human's reaction as well as the physical limitations of a human's speed and range of motion.

Another control strategy is to use the inverse dynamics G_{m}^{-1} in feedforward. If $G_{\mathrm{ff}} \approx G_{\mathrm{m}}^{-1}$, then it follows from (5.7) that $\tilde{G}_{er} \approx 0$, which implies that the command-following error is small, that is, $e \approx 0$. In this case, the human must learn to approximate the inverse dynamics G_{m}^{-1} in feedforward. Figure 5.10(b) shows that using the approximate inverse dynamics in feedforward can make the magnitude of e small.

We now consider control strategies that could be used to achieve good command following for the dynamic system G_{n}. Similar to the case with G_{m}, high gain in feedback and dynamic inversion in feedforward can make e small. However, the feedback and feedforward controllers required to achieve good command following are more mathematically complex than those with G_{m}.

To design a proportional feedback controller $G_{\mathrm{fb}} \in \mathbb{R}$ that yields relatively small command-following error to the chirp command r with no feedforward (i.e., $G_{\mathrm{ff}} = 0$),

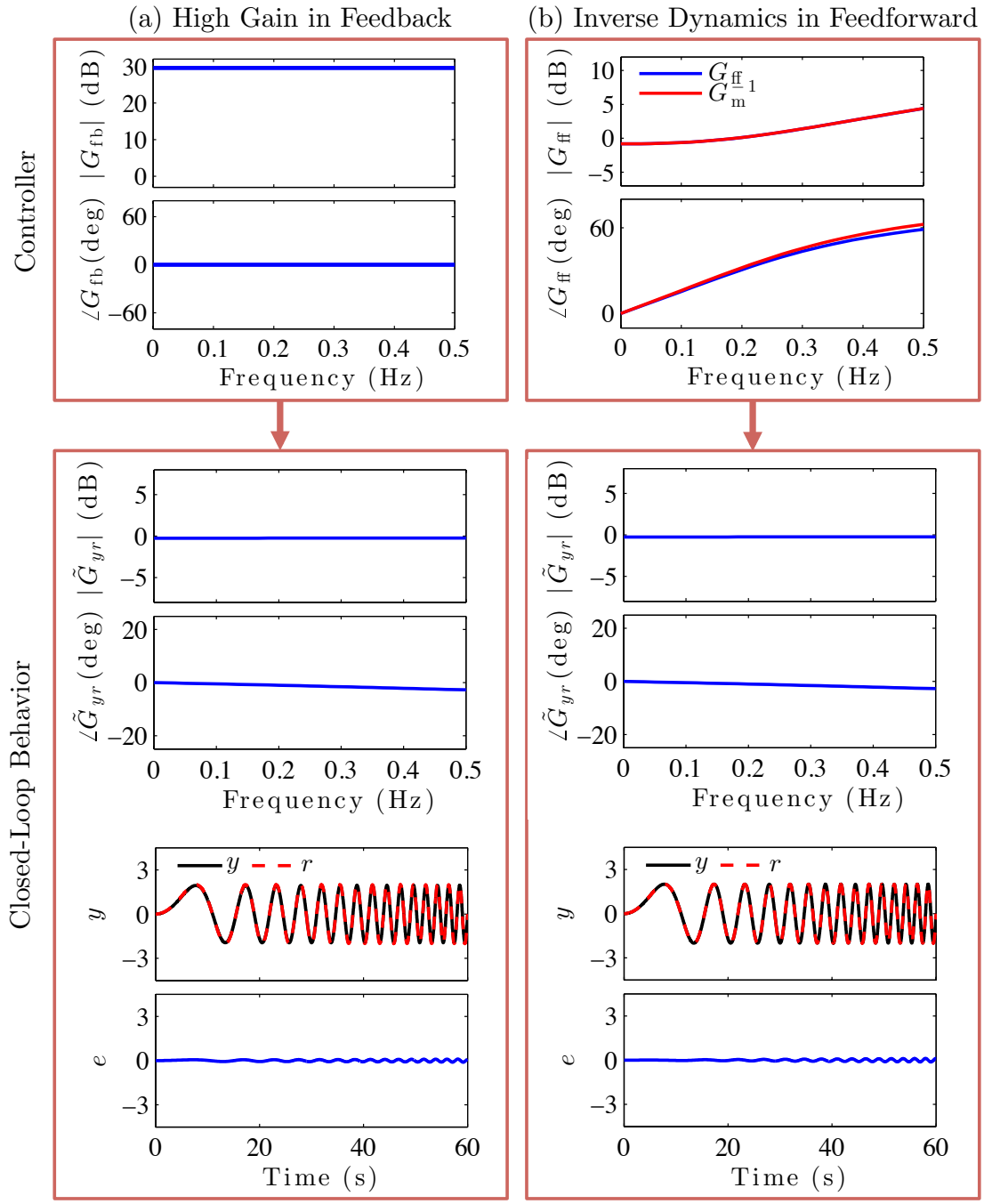

Figure 5.10: Two control strategies for G_{m} that make the magnitude of the error e small are high gain in feedback and approximate inverse dynamics in feedforward. Figure (a) shows the high-gain control strategy with the proportional feedback controller $G_{\mathrm{fb}} = 30$ and with no feedforward control (i.e., $G_{\mathrm{ff}} = 0$). Figure (b) shows the control strategy of approximating the inverse dynamics in feedforward. The feedforward controller is $G_{\mathrm{ff}}(s) = 50G_{\mathrm{m}}^{-1}(s)/(s + 50)$, which is a proper approximation of G_{n}^{-1} across the 0-to-0.5 Hz frequency range. There is no feedback controller (i.e., $G_{\mathrm{fb}} = 0$). In both cases, the magnitude of the error e is small.

consider the cost function

$$\mathcal{C}_{\mathrm{fb}}(G_{\mathrm{fb}}) = \int_0^{\pi} |\tilde{G}_{er}(\jmath\omega)|^2 \mathrm{d}\omega = \int_0^{\pi} \left| \frac{1}{1 + G_{\mathrm{fb}} G_{\mathrm{n}}(\jmath\omega)} \right|^2 \mathrm{d}\omega.$$

Minimizing $\mathcal{C}_{\mathrm{fb}}$ subject to the constraint that $\tilde{G}_{er}$ is asymptotically stable yields the proportional feedback $G_{\mathrm{fb}} = -0.0535$. Figure 5.11(a) shows the closed-loop transfer function $\tilde{G}_{yr}$ and closed-loop behavior with this proportional feedback controller. The magnitude of e shown in Figure 5.11(a) is larger than that shown in Figure 5.10(a) for proportional feedback with G_{m}.

To design a second-order feedforward controller G_{ff} that yields relatively small command-following error to the chirp command r with no feedback (i.e., $G_{\mathrm{fb}} = 0$), consider the cost function

$$\mathcal{C}_{\mathrm{ff}}(G_{\mathrm{ff}}) = \int_0^{\pi} |\tilde{G}_{er}(\jmath\omega)|^2 \mathrm{d}\omega = \int_0^{\pi} |G_{\mathrm{ff}}(\jmath\omega) G_{\mathrm{n}}(\jmath\omega) - 1|^2 \, \mathrm{d}\omega.$$

Minimizing $\mathcal{C}_{\mathrm{ff}}$ subject to the constraint that $\tilde{G}_{er}$ is asymptotically stable and the magnitude of poles of G_{ff} is less than or equal to 50 rad/s, yields the second-order feedforward controller $G_{\mathrm{ff}}(s) = \frac{742.8s^2+1025.9s+1597.4}{s^2+2s+2500}$. Note that poles of G_{ff} with magnitude larger than 50 rad/s have negligible effect on G_{ff} over the 0-to-0.5 Hz frequency range. Figure 5.11(b) shows the closed-loop transfer function $\tilde{G}_{yr}$ and closed-loop behavior with this second-order feedforward controller. The magnitude of e shown in Figure 5.11(b) is larger than that shown in Figure 5.10(b) for second-order feedforward with G_{m}.

We now explore control strategies for G_{n} to make e small by using higher-order controllers. Figure 5.12(a) shows that using high gain in feedback can make the magnitude of e small. Note that the feedback controller in Figure 5.12(a) is a forth-order controller, which is more mathematically complicated than the proportional

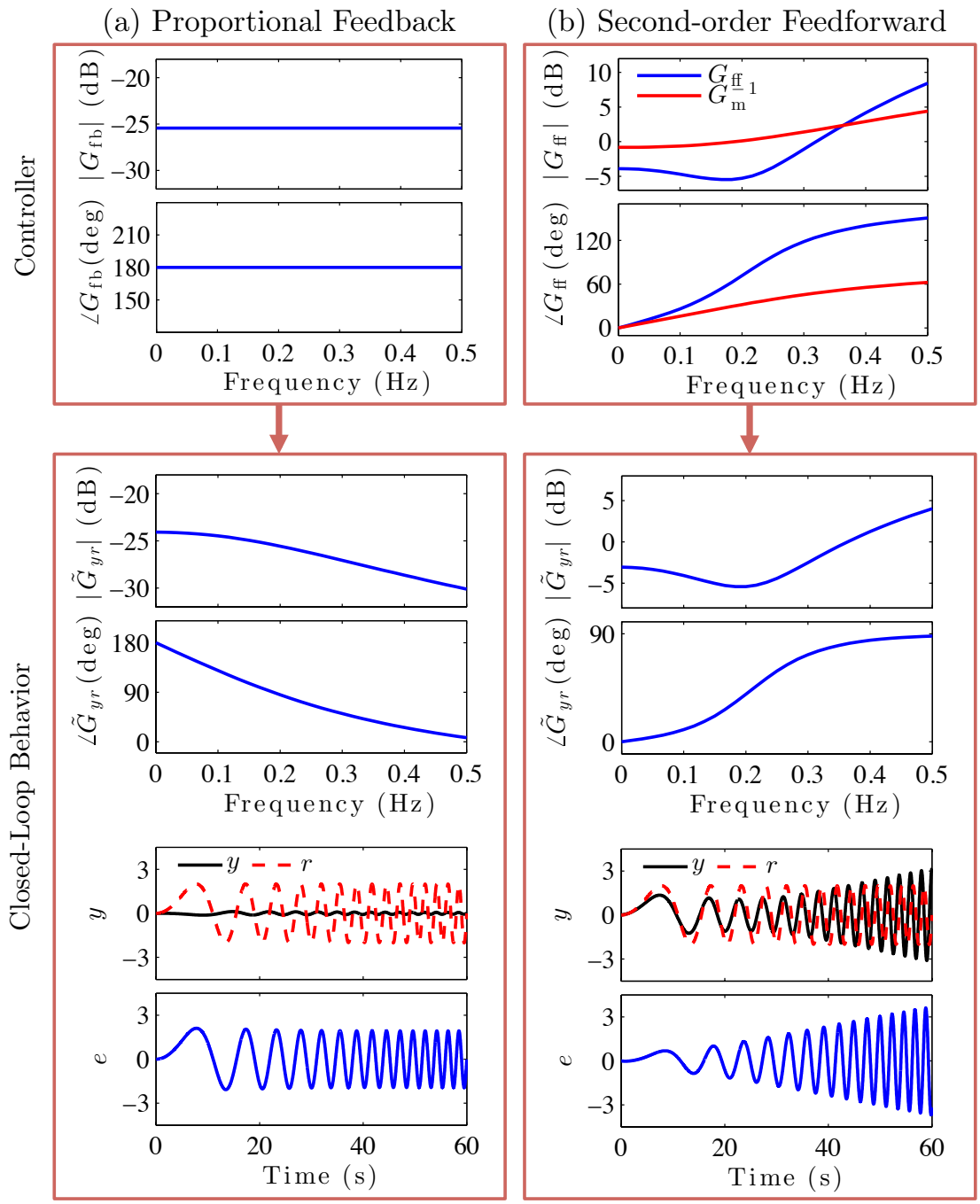

Figure 5.11: Two control strategies for G_n. Figure (a) shows the proportional feedback controller $G_{fb} = -0.0535$ with no feedforward controller (i.e., $G_{ff} = 0$). Figure (b) shows the second-order feedforward controller $G_{ff}(s) = \frac{742.8s^2+1025.9s+1597.4}{s^2+2s+2500}$ with no feedback controller (i.e., $G_{fb} = 0$). In both cases, the magnitude of the error e is larger than that shown in Figure 5.10 for G_m with high-gain feedback or dynamic-inversion feedforward.

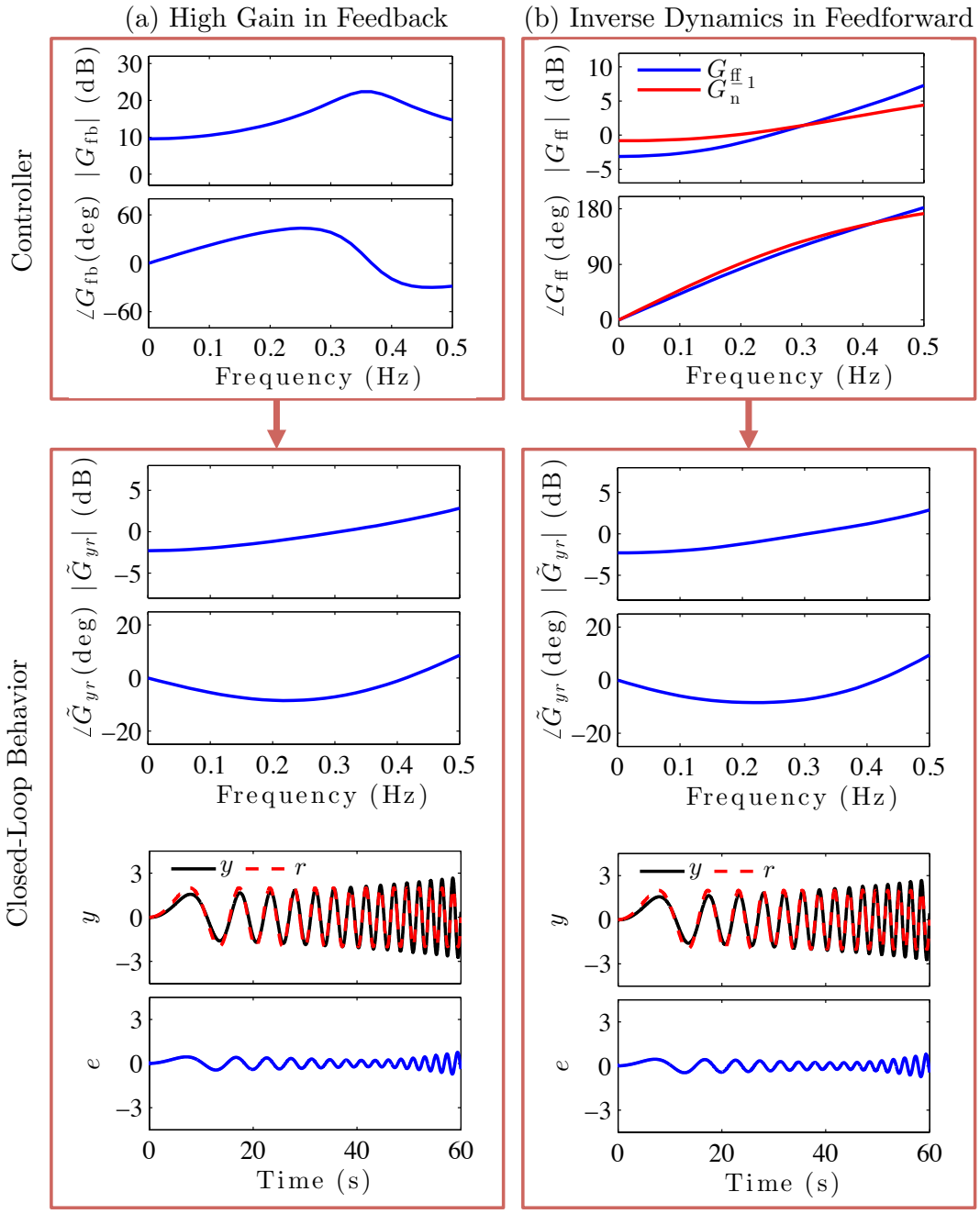

Figure 5.12: Two control strategies for G_{n} that make the magnitude of the error e small are high gain in feedback and approximate inverse dynamics in feedforward. Figure (a) shows the high-gain control strategy with the feedback controller $G_{\mathrm{fb}}(s) = \frac{1.99\times10^8(s+2.03)(s^2+4.47s+15.42)}{(s^2+0.73s+5.2)(s^2+607.1s+2.98\times10^8)}$ and with no feedforward controller (i.e., $G_{\mathrm{ff}} = 0$). Figure (b) shows the control strategy of approximating the inverse dynamics in feedforward. The feedforward controller is $G_{\mathrm{ff}}(s) = \frac{4.69\times10^4(s^2+2.91s+2.88)(s^2+3.37s+13.21)}{(s+40)^4}$, which is a proper approximation of G_{n}^{-1} across the 0-to-0.5 Hz frequency range. There is no feedback controller (i.e., $G_{\mathrm{fb}} = 0$). In both cases, the magnitude of the error e is small.

feedback controller in Figure 5.10(a). Nevertheless, the error in Figure 5.12(a) is still larger than that in Figure 5.10(a). Even higher-order feedback controllers could be designed to yield closed-loop behavior with G_{n} similar to that observed in Figure 5.10(a) with G_{m}.

Figure 5.12(b) shows a forth-order feedforward controller, which is more mathematically complicated than the second-order controller in Figure 5.11(b). The magnitude of error e shown in Figure 5.12(b) is smaller than that in Figure 5.11(b). However, the magnitude of e in Figure 5.12(b) is still larger than that in Figure 5.10(b).

5.6 Modeling Human Control Behavior

We review the SSID algorithm in Chapter 4 in a simplified form and use it to identify the feedback and feedforward controllers used by humans in the experiment.

5.6.1 Summary of Subsystem Identification Algorithm

For each trial of the experiment, we calculate the discrete Fourier transform of $\{r(iT_{\mathrm{s}})\}_{i=0}^{3000}$ and $\{y(iT_{\mathrm{s}})\}_{i=0}^{3000}$ at the frequencies $\omega_k = \frac{\pi}{30}(k-1)$ rad/s, where $k = 1, 2, \ldots, N = 31$. For $k = 1, 2, \ldots, N$, let $r_{\mathrm{dft}}(\omega_k)$ and $y_{\mathrm{dft}}(\omega_k)$ be the discrete Fourier transforms of the time-domain signals $\{r(iT_{\mathrm{s}})\}_{i=0}^{3000}$ and $\{y(iT_{\mathrm{s}})\}_{i=0}^{3000}$, and define the closed-loop frequency response data $H(\omega_k) \triangleq y_{\mathrm{dft}}(\omega_k)/r_{\mathrm{dft}}(\omega_k)$.

For the remainder of this chapter, let $G(z)$ denote the discrete-time transfer function obtained by discretizing $G(s)$ using a zero-order hold on the input with sampling time T_{s}. The open-loop dynamics are expressed with the z-transform as $\hat{y}(z) = G(z)\hat{u}(z)$, where $\hat{y}(z)$ and $\hat{u}(z)$ are the z-transforms of the output and control input. For each group in this experiment, G is the discrete-time transfer function obtained from a zero-order-hold discretization of G_{m}, G_{n}, or G_{sn} as appropriate.

Let $G_{\mathrm{ff}}, G_{\mathrm{fb}} \colon \mathbb{C} \to \mathbb{C}$ denote discrete-time real rational transfer functions. For each

trial, a subject's control strategy is modeled using the LTI control structure

$$\hat{u}(z) = G_{\text{fb}}(z)\hat{e}(z) + G_{\text{ff}}(z)\hat{r}(z), \tag{5.8}$$

where $\hat{e}$ and $\hat{r}$ are $z-$transforms of the error and the command. The discrete-time closed-loop transfer function is

$$\tilde{G}_{yr}(z) \triangleq \frac{G(z)[G_{\text{ff}}(z) + G_{\text{fb}}(z)]}{1 + G(z)G_{\text{fb}}(z)}.$$

Our objective is to determine G_{ff} and G_{fb} such that the modeled frequency response $\{\tilde{G}_{yr}(\gamma_k)\}_{k=1}^N$ approximates the data $\{H(\omega_k)\}_{k=1}^N$, where $\gamma_k \triangleq e^{\jmath\omega_k T_{\text{s}}}$. To achieve this objective, we seek to find G_{ff} and G_{fb} that minimize the cost

$$\begin{aligned} J(G_{\text{ff}}, G_{\text{fb}}) &= \sum_{k=1}^{N} \left| \tilde{G}_{yr}(\gamma_k) - H(\omega_k) \right|^2 \\ &= \sum_{k=1}^{N} \left| \frac{G(\gamma_k)\,[G_{\text{ff}}(\gamma_k) + G_{\text{fb}}(\gamma_k)]}{1 + G(\gamma_k)G_{\text{fb}}(\gamma_k)} - H(\omega_k) \right|^2, \end{aligned} \tag{5.9}$$

subject to the constraint that $\tilde{G}_{yr}$ is asymptotically stable. We assume that G_{ff} is finite impulse response (FIR) and G_{fb} is infinite impulse response (IIR).

We parameterize the feedback and feedforward controllers by their numerator and denominator coefficients and cast the discrete-time SSID problem in terms of these coefficients. Let n_{ff} and n_{fb} be nonnegative integers that denote the degrees of the numerator polynomials of G_{ff} and G_{fb}. Similarly, let d_{ff} and d_{fb} be nonnegative integers that denote the degrees of the denominator polynomials of G_{ff} and G_{fb}. Define $d \triangleq d_{\text{fb}} + n_{\text{fb}} + 1$, and consider the functions $\mathcal{N}_{\text{ff}} \colon \mathbb{C} \times \mathbb{R}^{n_{\text{ff}}+1} \to \mathbb{C}$, $\mathcal{N}_{\text{fb}} \colon \mathbb{C} \times \mathbb{R}^{d} \to \mathbb{C}$, and $\mathcal{D}_{\text{fb}} \colon \mathbb{C} \times \mathbb{R}^{d} \to \mathbb{C}$ given by

$$\mathcal{N}_{\text{ff}}(z, \beta) \triangleq \nu_{\text{ff}}(z)\beta, \quad \mathcal{N}_{\text{fb}}(z, \phi) \triangleq \nu_{\text{fb}}(z)\phi, \quad \mathcal{D}_{\text{fb}}(z, \phi) \triangleq z^{d_{\text{fb}}} + \mu_{\text{fb}}(z)\phi,$$

where $\nu_{\mathrm{ff}} : \mathbb{C} \to \mathbb{C}^{1\times(n_{\mathrm{ff}}+1)}$ and $\nu_{\mathrm{fb}}, \mu_{\mathrm{fb}} : \mathbb{C} \to \mathbb{C}^{1\times d}$ are given by

$$\begin{aligned}
\nu_{\mathrm{ff}}(z) &\triangleq \begin{bmatrix} z^{n_{\mathrm{ff}}} & z^{n_{\mathrm{ff}}-1} & \cdots & z & 1 \end{bmatrix}, \\
\nu_{\mathrm{fb}}(z) &\triangleq \begin{bmatrix} z^{n_{\mathrm{fb}}} & z^{n_{\mathrm{fb}}-1} & \cdots & z & 1 & 0_{1\times d_{\mathrm{fb}}} \end{bmatrix}, \\
\mu_{\mathrm{fb}}(z) &\triangleq \begin{bmatrix} 0_{1\times(n_{\mathrm{fb}}+1)} & z^{d_{\mathrm{fb}}-1} & z^{d_{\mathrm{fb}}-2} & \cdots & z & 1 \end{bmatrix}.
\end{aligned}$$

We consider the functions $\mathcal{G}_{\mathrm{ff}} \colon \mathbb{C} \times \mathbb{R}^{n_{\mathrm{ff}}+1} \times \mathbb{R}^d \to \mathbb{C}$ and $\mathcal{G}_{\mathrm{fb}} \colon \mathbb{C} \times \mathbb{R}^d \to \mathbb{C}$ given by

$$\mathcal{G}_{\mathrm{ff}}(z,\beta) \triangleq \frac{\mathcal{N}_{\mathrm{ff}}(z,\beta)}{z^{d_{\mathrm{ff}}}}, \qquad \mathcal{G}_{\mathrm{fb}}(z,\phi) \triangleq \frac{\mathcal{N}_{\mathrm{fb}}(z,\phi)}{\mathcal{D}_{\mathrm{fb}}(z,\phi)},$$

where β contains the numerator coefficients of $\mathcal{G}_{\mathrm{ff}}$, and ϕ contains the numerator and denominator coefficients of $\mathcal{G}_{\mathrm{fb}}$.

The real rational transfer function G can be expressed as $G(z) = N_{\mathrm{d}}(z)/D_{\mathrm{d}}(z)$, where N_{d} and D_{d} are coprime polynomials. Next, consider the cost function $\mathcal{J} \colon \mathbb{R}^{n_{\mathrm{ff}}+1} \times \mathbb{R}^d \to [0,\infty)$ given by

$$\mathcal{J}(\beta,\phi) \triangleq J(\mathcal{G}_{\mathrm{ff}}(z,\beta), \mathcal{G}_{\mathrm{fb}}(z,\phi)) = \beta^{\mathrm{T}}\Omega_2(\phi)\beta + \Omega_1^{\mathrm{T}}(\phi)\beta + \Omega_0(\phi),$$

where

$$\begin{aligned}
\Omega_0(\phi) &\triangleq \sum_{k=1}^{N} \left| \frac{\tilde{\mathcal{N}}_2(\gamma_k,\phi)}{\tilde{\mathcal{D}}(\gamma_k,\phi)} - H(\omega_k) \right|^2, \\
\Omega_1(\phi) &\triangleq 2\mathrm{Re} \sum_{k=1}^{N} \left[\frac{\tilde{\mathcal{N}}_2(\gamma_k,\phi)}{\tilde{\mathcal{D}}(\gamma_k,\phi)} - H(\omega_k) \right] \frac{\tilde{\mathcal{N}}_1^{\mathrm{T}}(\gamma_k^{-1},\phi)}{\tilde{\mathcal{D}}(\gamma_k^{-1},\phi)}, \\
\Omega_2(\phi) &\triangleq \mathrm{Re} \sum_{k=1}^{N} \frac{\tilde{\mathcal{N}}_1^{\mathrm{T}}(\gamma_k^{-1},\phi)\tilde{\mathcal{N}}_1(\gamma_k,\phi)}{\left|\tilde{\mathcal{D}}(\gamma_k,\phi)\right|^2},
\end{aligned}$$

and

$$\tilde{\mathcal{N}}_2(z,\phi) \triangleq N_{\mathrm{d}}(z)z^{d_{\mathrm{ff}}}\mathcal{N}_{\mathrm{fb}}(z,\phi),$$
$$\tilde{\mathcal{N}}_1(z,\phi) \triangleq N_{\mathrm{d}}(z)\mathcal{D}_{\mathrm{fb}}(z,\phi)\nu_{\mathrm{ff}}(z),$$
$$\tilde{\mathcal{D}}(z,\phi) \triangleq [D_{\mathrm{d}}(z)\mathcal{D}_{\mathrm{fb}}(z,\phi) + N_{\mathrm{d}}(z)\mathcal{N}_{\mathrm{fb}}(z,\phi)]z^{d_{\mathrm{ff}}}.$$

For each $\phi \in \mathbb{R}^d$, $\Omega_0(\phi) \in \mathbb{R}$, $\Omega_1(\phi) \in \mathbb{R}^{n_{\mathrm{ff}}+1}$, and $\Omega_2(\phi) \in \mathbb{R}^{(n_{\mathrm{ff}}+1)\times(n_{\mathrm{ff}}+1)}$ is positive semidefinite.

We restrict our attention to $\phi \in \mathbb{R}^d$ contained in

$$\mathcal{S} \triangleq \{\phi \in \mathbb{R}^d\colon \text{ if } p \in \mathbb{C} \text{ and } \tilde{\mathcal{D}}(p,\phi) = 0, \text{ then } |p| < 1\},$$

which is the set of parameters that yield asymptotically stable closed-loop transfer functions. Let M be a positive integer, and let $\Phi \subset \mathcal{S}$ be a set with M elements. We call Φ the *candidate pool*. Next, we create a candidate sequence using the M elements in the candidate pool Φ. Specifically, for $i, j = 1, 2, \ldots, M$, let $\phi_i, \phi_j \in \Phi$ such that if $i \neq j$, then $\phi_i \neq \phi_j$. The sequence $\{\phi_i\}_{i=1}^M$ is not unique; however, the order of the sequence is selected arbitrarily.

Define $\mathcal{M} \triangleq \{1, 2, \ldots, M\}$, and for all $i \in \mathcal{M}$, define the quadratic cost function

$$\mathcal{J}_i(\beta) \triangleq \mathcal{J}(\beta, \phi_i) = \beta^{\mathrm{T}}\Omega_2(\phi_i)\beta + \Omega_1^{\mathrm{T}}(\phi_i)\beta + \Omega_0(\phi_i).$$

It follows from Proposition 4.1 that If the number N of frequency response data is sufficiently large, then $\Omega_2(\phi_1), \ldots, \Omega_2(\phi_M)$ are positive definite and thus nonsingular. In this case, for each $i = 1, \ldots, N$, define

$$\beta_i \triangleq -\frac{1}{2}\Omega_2^{-1}(\phi_i)\Omega_1(\phi_i),$$

which is the unique global minimizer of $\mathcal{J}_i$. Specifically, for each $i \in \mathcal{M}$ and for all $\beta \in \mathbb{R}^{n_{\mathrm{ff}}+1} \backslash \{\beta_i\}$,

$$\mathcal{J}_i(\beta_i) < \mathcal{J}_i(\beta).$$

Let $\ell \in \mathcal{M}$ be the smallest integer such that $\mathcal{J}_\ell(\beta_\ell) = \min_{i \in \mathcal{M}} \mathcal{J}_i(\beta_i)$. Thus, the identified parameters are β_ℓ and ϕ_ℓ and the identified transfer functions are

$$G_{\mathrm{ff}}(z) \triangleq \frac{\mathcal{N}_{\mathrm{ff}}(z, \beta_\ell)}{z^{d_{\mathrm{ff}}}}, \qquad G_{\mathrm{fb}}(z) \triangleq \frac{\mathcal{N}_{\mathrm{fb}}(z, \phi_\ell)}{\mathcal{D}_{\mathrm{fb}}(z, \phi_\ell)}. \tag{5.10}$$

The linear feedback-and-feedforward control (5.8) with are estimates of the unknown subsystem. We now summarize this SSID method.

Algorithm 5.1. Consider the known discrete-time transfer function G and the known closed-loop frequency response data $\{H(\omega_k)\}_{k=1}^N$. Then, the subsystem identification algorithm is as follows:

Step 1. Generate the candidate pool $\Phi \subset \mathcal{S}$ and candidate sequence $\{\phi_i\}_{i=1}^M$.

Step 2. For each $i \in \mathcal{M}$, find $\beta_i \triangleq -\frac{1}{2}\Omega_2^{-1}(\phi_i)\Omega_1(\phi_i)$, which is the unique global minimizer of $\mathcal{J}_i$.

Step 3. Find the smallest $\ell \in \mathcal{M}$ such that $\mathcal{J}_\ell(\beta_\ell) = \min_{i \in \mathcal{M}} \mathcal{J}_i(\beta_i)$.

Step 4. The identified parameters are β_ℓ and ϕ_ℓ.

Step 5. The identified feedforward and feedback discrete-time transfer functions are G_{ff} and G_{fb} given by (5.10).

5.6.2 Application of SSID Algorithm to Experimental Data

We use the SSID algorithm to identify feedback and feedforward control strategies used by humans subjects for the groups with G_{m} and G_{n}. Note that for the group

with G_{sn}, the average of the time-averaged error $\|e\|$ among all subjects on the last trial is approximately 1.2 (as shown in Figure 5.7), which is close to the time-averaged error $\|e\|$ with no control (i.e., $u = 0$).

The controller orders d_{fb} and d_{ff} are chosen sufficiently large to capture different control approaches that lead to good command-following performance. For example, we select the controller orders to allow for high gain in feedback as well as approximate dynamic inversion in feedforward. For the groups with G_{m} and G_{n}, the feedback is modeled as a second-order exactly proper controller (i.e., $n_{\mathrm{fb}} = d_{\mathrm{fb}} = 2$). To allow for feedforward dynamic inversion as a possible control strategy, we select d_{ff} large enough to allow G_{ff} to approximate G^{-1} with approximately 0.1% error over the 0-to-0.5 Hz range. Thus, d_{ff} is 2 and 6 for G_{m} and G_{n}. Higher-order controllers can be used; however, this can lead to poor conditioning for the SSID problem.

The candidate pool Φ is designed to capture a wide range of behavior over the 0-to-0.5 Hz frequency range. We construct the candidate pool Φ subject to the following conditions:

C1) If $\phi \in \Phi$, $\lambda \in \mathbb{C}$, and $\mathcal{D}_{\mathrm{fb}}(e^{\lambda T_{\mathrm{s}}}, \phi) = 0$, then $|\lambda| \leq 31.5$.

C2) If $\phi \in \Phi$, $\lambda \in \mathbb{C}$, and $\mathcal{N}_{\mathrm{fb}}(e^{\lambda T_{\mathrm{s}}}, \phi) = 0$, then $|\lambda| \leq 31.5$.

C3) If $\phi \in \Phi$, then $\max_{\omega \in [0,\pi]} \left|\mathcal{G}_{\mathrm{fb}}(e^{\jmath\omega T_{\mathrm{s}}}, \phi)\right| \leq 30.5$.

C4) If $\phi \in \Phi$, $\lambda \in \mathbb{C}$, and $\tilde{\mathcal{D}}(e^{\lambda T_{\mathrm{s}}}, \phi) = 0$, then $\operatorname{Re}\lambda < -0.1$.

Conditions C1)–C2) constrain Φ to include only elements that have a significant impact on controller dynamics over the 0-to-0.5 Hz frequency range. Specifically, C1)–C2) state that for each $\phi \in \Phi$, the poles and zeros of the feedback controller have absolute value between 0 and 31.5 rad/s. This condition arises because the data $\{H(\omega_k)\}_{k=1}^{N}$ is at frequencies $\omega_1, \ldots, \omega_N \in [0, \pi]$ rad/s, which corresponds to the the frequency range of the chirp signal r. Thus, we seek to identify G_{ff} and G_{fb} on the interval $[0, \pi]$ rad/s. The upper limit 31.5 rad/s on the magnitude of the poles and

zeros is one decade above the π rad/s limit on the chirp frequency (i.e., $10\pi \approx 31.5$). Moreover, a pole or zero with magnitude greater than 31.5 rad/s has negligible effect on the Bode plot over the frequency range $[0, \pi]$ rad/s. Thus, we restrict the candidate pool to elements that correspond to poles and zeros with absolute value between 0 and 31.5 rad/s.

Conditions C3) states that for each $\phi \in \Phi$, the peak magnitude of the feedback controller $\mathcal{G}_{\text{fb}}(z, \phi)$ over the frequency range $[0, \pi]$ rad/s is no more than 30.5 (or approximately 30 dB). We impose an upper limit on the magnitude of the feedback controller because a human cannot use arbitrarily high gain in feedback. The 30 dB upper limit is determined from another experiment with 10 subjects, where each subject was asked to follow a single-frequency sinusoid using only error feedback (i.e., feedforward of the command signal was not available). In this experiment, the peak magnitude of the feedback controller used by the subjects is approximately 30 dB, suggesting that 30 dB is the peak gain that a human can use in feedback.

Conditions C4) states that for each $\phi \in \Phi$, the magnitudes of the roots of $\tilde{\mathcal{D}}(z, \phi)$ are bounded away from the unit circle, specifically, less than $e^{-0.1T_{\text{s}}}$. This condition guarantees that $\Phi \subset \mathcal{S}$ (i.e., for all $\phi \in \Phi$, the roots of $\tilde{\mathcal{D}}(z, \phi)$ are in the unit circle of the complex plane). A pole with -0.1 indicates a settling time of approximately 40 s. Thus, C4) restricts the candidate pool to elements that result in closed-loop transfer functions with settling times less than 40 s. Note that the behavior observed in this experiment exhibits settling times significantly less than 40 s.

For the group with G_{m}, the candidate pool contains approximately 8.3 billion elements. For the group with G_{n}, the candidate pool contains approximately 4.5 billion elements. More details of the candidate pool are present in Appendix C.

The SSID algorithm is implemented using parallel computation on a supercomputer. Algorithm 5.1 is coded in C++ for parallel computation and implemented on the Lipscomb High Performance Computing Cluster at the University of Kentucky. For

each trial of the group with G_{m}, it takes approximately 4.6 hours to run Algorithm 5.1 on 1 compute node of the Lipscomb cluster; each node has a 16 Intel E5-2670 @ 2.6 GHz cores. Thus, performing the SSID algorithm for all 440 trials requires approximately 2,000 compute node hours. For each trial of the group with G_{n}, it takes approximately 2.3 hours to run Algorithm 5.1 on 1 compute node of the Lipscomb cluster. Thus, performing the SSID algorithm for all 440 trials requires approximately 1,000 compute node hours.

5.7 Subsystem Identification Results

We present the SSID results for the groups with G_{m} and G_{n} excluding divergent trials. Figure 5.13 shows the Bode plots of the identified feedforward controller G_{ff}, feedback controller G_{fb}, and closed-loop transfer function $\tilde{G}_{yr}$ for Trial 1 and Trial 40 of the subject from each group who has the median time-domain error. For G_{m} and G_{n}, the closed-loop transfer function $\tilde{G}_{yr}$ is near 1 (i.e., 0 decibels magnitude and 0 degrees phase) for the last trial, which implies that y approximates r across the frequency range of r as shown in Figure 5.13(c). Also, for G_{m} and G_{n}, the identified G_{ff} for the first trial does not approximate inverse dynamics, whereas the identified G_{ff} for the last trials does approximate inverse dynamics for both systems G_{m} and G_{n} as shown in Figure 5.13(a).

Define $\|G_{\mathrm{fb}}\|$ and $\|G_{\mathrm{ff}}G - 1\|$, which are the frequency-averaged magnitudes of G_{fb} and $G_{\mathrm{ff}}G - 1$, and are given by

$$\|G_{\mathrm{fb}}\| = \frac{1}{\pi}\int_0^{\pi} |G_{\mathrm{fb}}(e^{\jmath\omega T_{\mathrm{s}}})|\,\mathrm{d}\omega,$$
$$\|G_{\mathrm{ff}}G - 1\| = \frac{1}{\pi}\int_0^{\pi} |G_{\mathrm{ff}}(e^{\jmath\omega T_{\mathrm{s}}})G(e^{\jmath\omega T_{\mathrm{s}}}) - 1|\,\mathrm{d}\omega,$$

where G can be either G_{m} or G_{n}. Figure 5.14 shows that the frequency-averaged magnitude of the identified feedback controller G_{fb} does not change significantly over

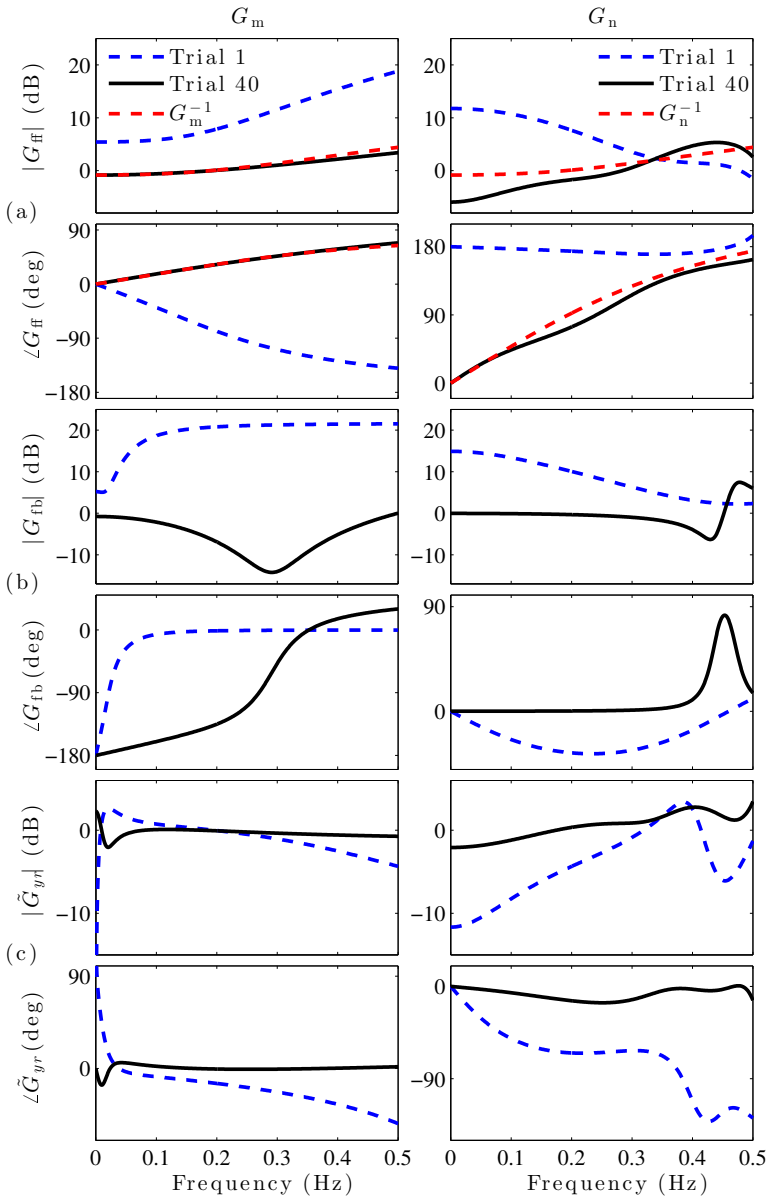

Figure 5.13: The subject's control strategy is modeled by a feedback controller G_{fb} and a feedforward controller G_{ff}, which results in the closed-loop response $\hat{y}(s) = \tilde{G}_{yr}(s)\hat{r}(s)$ from the command r to the output y. For groups with G_{m} and G_{n}, Figures (a), (b), and (c) show the Bode plots of the identified controllers G_{ff} and G_{fb}, and the closed-loop transfer function $\tilde{G}_{yr}$ for the same trials (Trials 1 and 40) shown in Figure 5.6. Figure (a) shows that the identified G_{ff} for Trial 1 does not approximate G^{-1}, whereas the identified G_{ff} for Trial 40 does approximate G^{-1}. Figure (b) shows that the identified G_{fb} for Trial 1 has higher gain (i.e., magnitude) than that for Trial 40. Figure (c) shows that the closed-loop transfer function $\tilde{G}_{yr}$ is approximately 1 (i.e., 0 decibels magnitude and 0 degrees phase) for Trial 40, which implies that y approximates r in the 0-to-0.5 Hz frequency range.

the 40 trials. Figure 5.14 also shows that the difference between the identified feed-

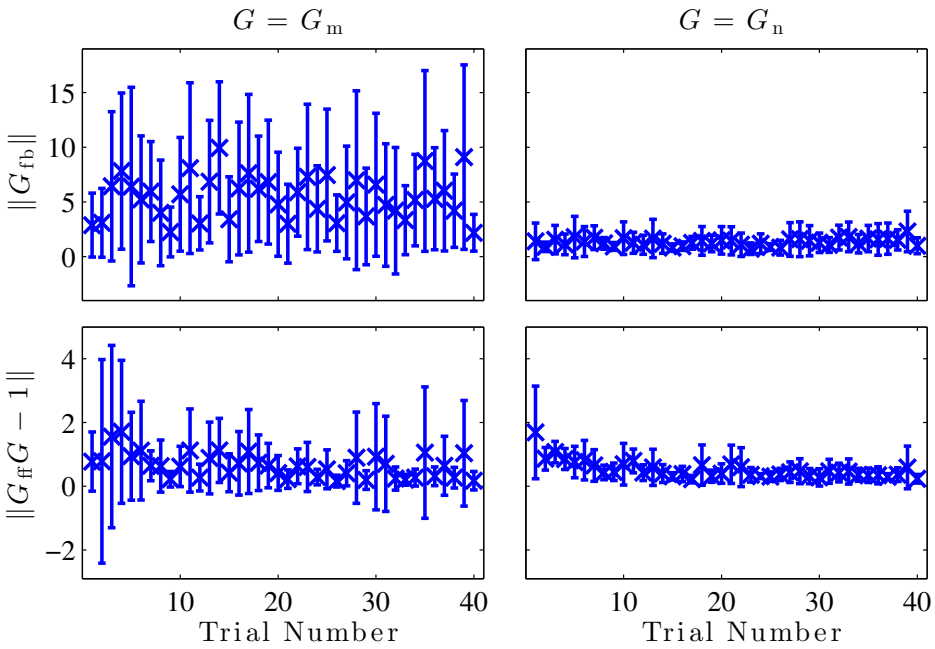

Figure 5.14: The metrics $\|G_{\mathrm{fb}}\|$ and $\|G_{\mathrm{ff}}G - 1\|$ for the subjects' identified controllers for each of the 40 trials. The $\times$ indicates the mean of the subjects and the vertical lines show one standard deviation. The difference between G_{ff} and G^{-1} decreases over the 40 trials, whereas $\|G_{\mathrm{fb}}\|$ does not changes significantly over the trials.

forward controller G_{ff} and the inverse dynamics decreases over the 40 trials for both groups.

Figure 5.15 compares the command-following error on all trials to how closely the identified G_{ff} approximates inverse dynamics. The trials with the smaller command-following errors yield identified feedforward controllers G_{ff} that are better approximations of the inverse dynamics.

Figure 5.16 shows the Bode plot of the average identified feedforward controller for all 11 subjects of each group on the last trial. For both groups, the average identified feedforward controller approximates inverse dynamics. Thus, the identification results suggest that by the last trial the subjects learned the inverse dynamics and used a model of those inverse dynamics in feedforward. This observation supports the internal model hypothesis.

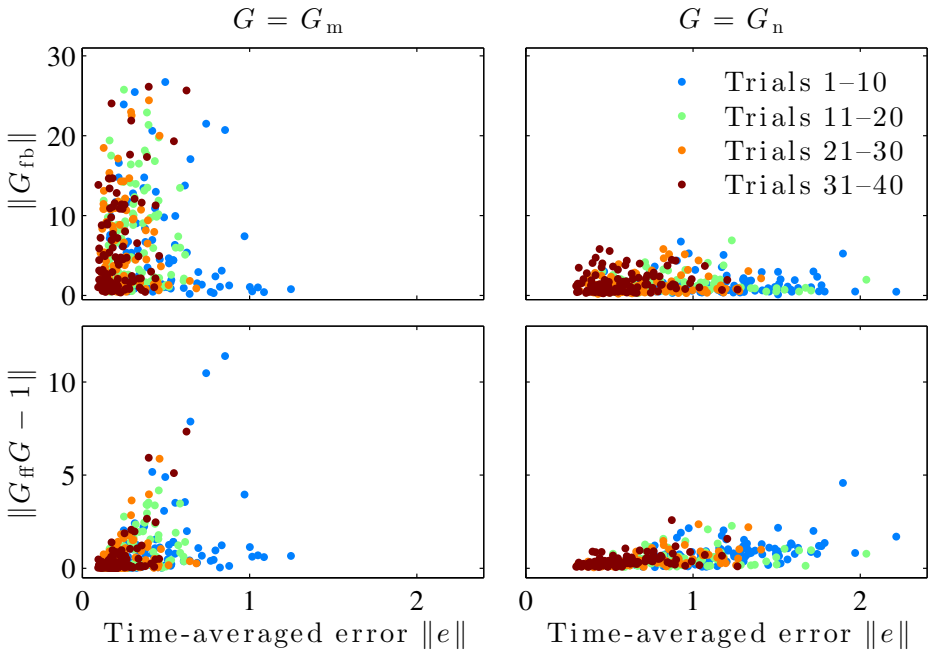

Figure 5.15: The time-averaged error $\|e\|$ compared to how closely the identified G_{ff} approximates G^{-1}. The trials with the smaller command-following errors yield identified feedforward controllers that are better approximations of G^{-1}.

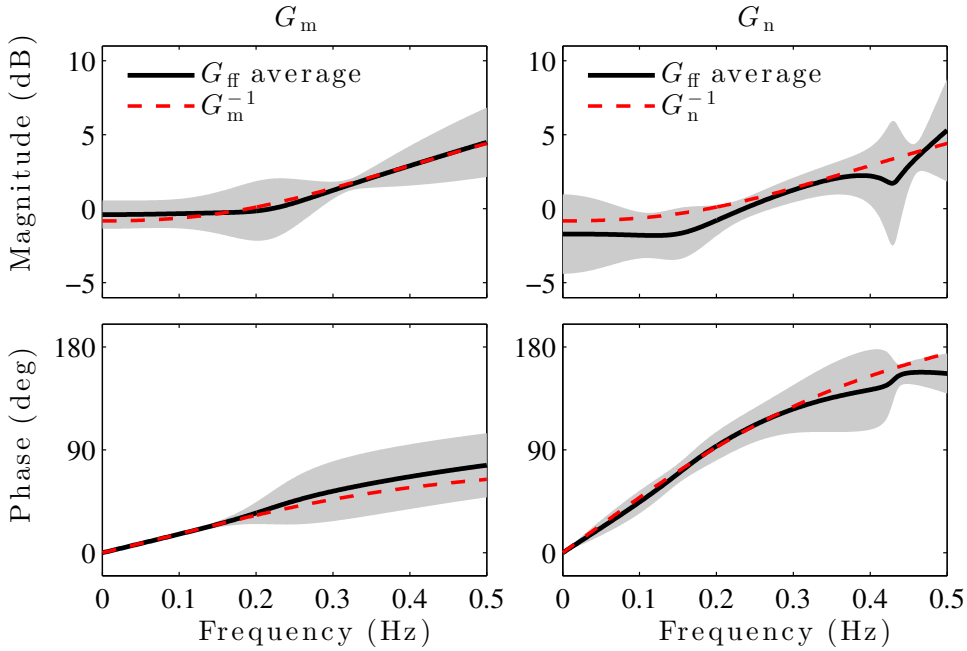

Figure 5.16: The Bode plot of the average identified feedforward controller for all 11 subjects on the last trial. The shaded region shows one standard deviation above and below the average identified feedforward controller. For both groups, the average identified feedforward controller approximates inverse dynamics.

5.8 Discussion of the Impact of System Zeros

We now discuss the impact of system zeros on human learning. In particular, we explore reasons why the time-averaged error $\|e\|$ for G_{m} is smaller than that for G_{n}, and the time-averaged error $\|e\|$ for G_{n} is smaller than that for G_{sn}. In other words, we explore reasons why nonminimum-phase zeros make a system difficult to control.

Although the SSID results in Section 5.7 suggest that the subjects learned to approximate the inverse dynamics G_{m}^{-1} and G_{n}^{-1} in feedforward, subjects may not learn to approximate G_{n}^{-1} as well as G_{m}^{-1}.

Figure 5.17 shows $\|G_{\mathrm{ff}}G-1\|$ and $\|G_{\mathrm{fb}}\|$ on the last trial for each subject in each groups with G_{m} and G_{n}. For the group with G_{m}, the identified feedforward controllers

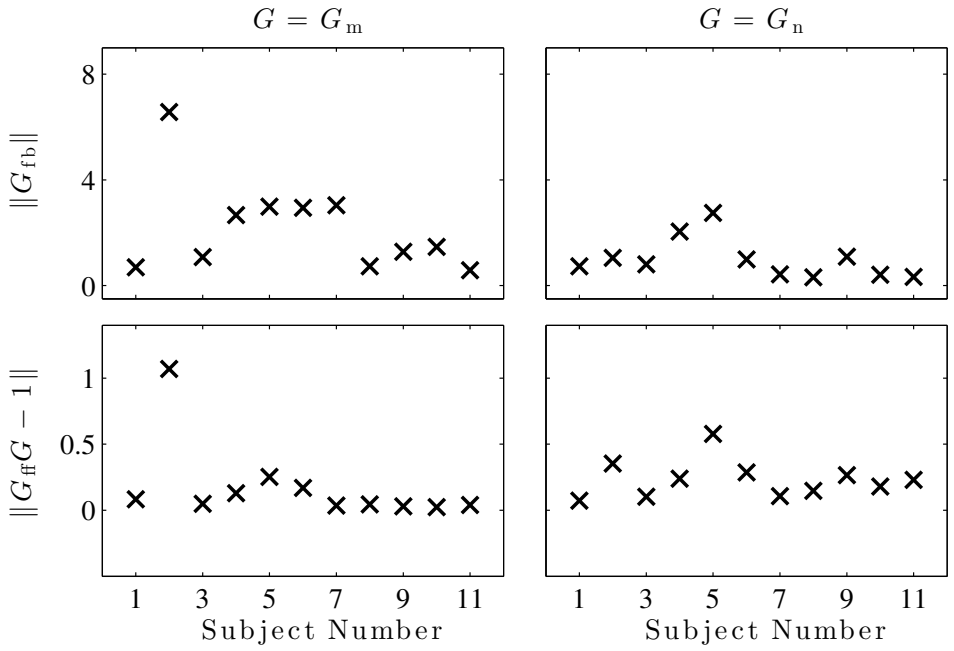

Figure 5.17: The metrics $\|G_{\mathrm{ff}}G-1\|$ and $\|G_{\mathrm{fb}}\|$ for the last trial for each in the groups with G_{m} and G_{n}. For the group with G_{n}, the identified G_{ff} for all 11 subjects is close to G_{n}^{-1}. For the group with G_{m}, the identified G_{ff} for 10 subjects is close to G_{m}^{-1}, and the remaining subject (i.e., number 2) has appears to rely on higher gain in feedback.

for 10 subjects appear approximate of G_{m}^{-1}, while the identified feedback controller for the one remaining subject (i.e., number 2) has higher gain (i.e., $\|G_{\mathrm{fb}}\| = 6.6$).

On the last trial, the average of $\|G_{\text{ff}}G_{\text{m}} - 1\|$ for all 11 subjects is 0.17, which is smaller than the average of $\|G_{\text{ff}}G_{\text{n}} - 1\|$, which is 0.23. However, on the last trial, the standard deviation of $\|G_{\text{ff}}G_{\text{m}} - 1\|$ is 0.29, which is larger than the standard deviation of $\|G_{\text{ff}}G_{\text{n}} - 1\|$, which is 0.14. If we exclude the largest and smallest values of $\|G_{\text{ff}}G - 1\|$, then the average and standard deviation on the last trial with G_{m} are 0.093 and 0.072, which are smaller than those with G_{n}, which are 0.21 and 0.080.

Figure 5.18 shows the Bode plots of the average identified $G_{\text{ff}}G_{\text{m}}$ and $G_{\text{ff}}G_{\text{n}}$ for the subjects on the last trial excluding the smallest and largest values of $\|G_{\text{ff}}G - 1\|$. The

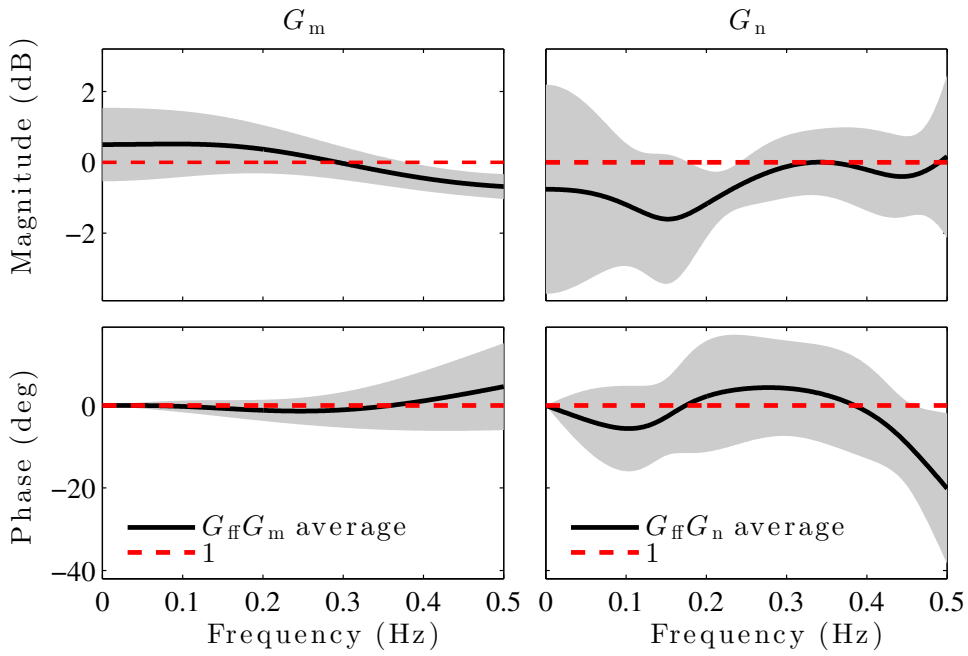

Figure 5.18: The Bode plot of the average identified $G_{\text{ff}}G_{\text{m}}$ and $G_{\text{ff}}G_{\text{n}}$ for all 11 subjects on the last trial excluding the largest and smallest values of $\|G_{\text{ff}}G_{\text{m}} - 1\|$ and $\|G_{\text{ff}}G_{\text{m}} - 1\|$. The shaded region shows one standard deviation above and below the average identified value. The average identified $G_{\text{ff}}G_{\text{m}}$ and $G_{\text{ff}}G_{\text{n}}$ both approximate 1. However, the average identified $G_{\text{ff}}G_{\text{m}}$ is closer to 1 than the average identified $G_{\text{ff}}G_{\text{n}}$.

average identified $G_{\text{ff}}G_{\text{m}}$ and $G_{\text{ff}}G_{\text{n}}$ both approximate 1. However, the average identified $G_{\text{ff}}G_{\text{m}}$ is closer to 1 than the average identified $G_{\text{ff}}G_{\text{n}}$. Recall that we require a more mathematically complicated feedforward controller (i.e., higher-order transfer function) for G_{n} than for G_{m} to achieve comparably small e as shown in Figures

5.10(b), 5.11(b), and 5.12(b). The need for a more mathematically complicated feedforward for G_{n} than for G_{m} may be a reason why the mean $\|e\|$ with G_{m} is smaller than that with G_{n}.

Recall that we need a more mathematically complicated feedback controller for G_{n} than for G_{m} to achieve comparably small e as shown in Figures 5.10(a), 5.11(a), and 5.12(a). The need for a more mathematically complicated feedback for G_{n} than for G_{m} may be another reason why the mean $\|e\|$ with G_{m} is smaller than that with G_{n}, because both feedback and feedforward are needed in the process of constructing the internal model [120].

The nonminimum-phase zero in G_{n} makes it harder for subjects to use high-gain control in feedback. The SSID results in Figures 5.14 and 5.15 show that the magnitude of the identified feedback controllers for the group with G_{m} is higher than that with G_{n}.

Figure 5.19 shows the control u generated by human subjects with the median time-averaged error $\|e\|$ among all subjects for Trials 10, 20, 30, and 40 for each of the 3 groups. We observe that for G_{m}, the control u is smooth like the chirp command r. In contrast, for G_{n}, the control u is less smooth on Trial 10 but tends to become smoother on Trails 20, 30, and 40. For G_{sn}, the control u looks like a sequence of step functions, which is different from the smooth chirp command.

The observation that human subjects generate step-function control may be related to the initial undershoot phenomenon. Recall that G_{n} has initial undershoot, whereas G_{m} does not. Figure 5.19 shows that for G_{n}, the control has some step-function behavior, whereas for G_{m}, it does not. Furthermore, the initial undershoot peak for G_{sn} is larger than that for G_{n} (see Figure 5.5). Figure 5.19 shows that the control for G_{sn} has more step-function behavior than for G_{n}. Thus, we observe the most step-function behavior with G_{sn}, which also has the most initial undershoot.

It is possible that initial undershoot is an impediment to humans learning a control

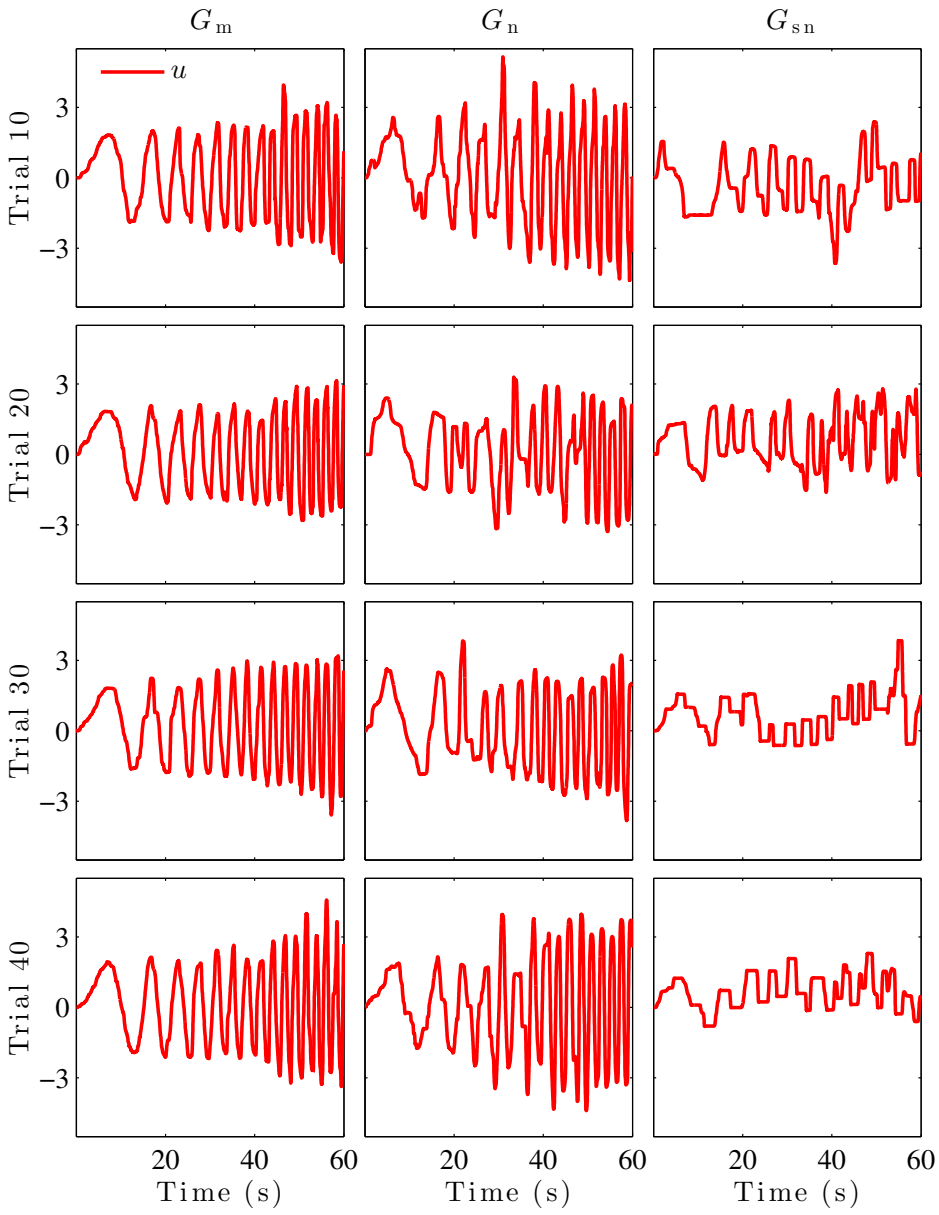

Figure 5.19: The control u generated by human subjects with the median time-averaged error $\|e\|$ among all subjects for Trials 10, 20, 30, and 40. For the group with G_{m}, the control u is smooth. For the group with G_{n}, the control u is less smoother than for G_{n}, but tends to become smoother over the trails. For the group with G_{sn}, the control u contains behavior similar to a step function.

that makes the magnitude of e small. In particular, large initial undershoot may make it more difficult for humans to learn that a smooth control can make the magnitude of e small.

Another indicator of the impact of initial undershoot is the control at the start time (i.e., $t = 0$) of each trial. Since G_{m} does not have initial undershoot, it follows that y initially moves in the same direction as r (i.e., $\dot{y}(0) > 0$) if u initially moves in the same direction as r (i.e., $\dot{u}(0) > 0$). Since G_{n} and G_{sn} each have initial undershoot, it follows that y initially moves in the same direction as r if u initially moves in the opposite direction of r (i.e., $\dot{u}(0) < 0$). For each trial, let i_0 be the smallest positive integer such that $|u(i_0 T_{\mathrm{s}})| > 0.05$. The threshold 0.05 is determined from another experiment, where a human holds the joystick but attempts no movement. Specifically, 0.05 is the maximum magnitude of the control signal in that experiment. Thus, control signals smaller than the threshold are regarded as potentially involuntary motion arising from the fact that humans can not hold the joystick perfectly still.

We define the *right control at the start time* as a control such that $u((i_0+1)T_{\mathrm{s}})$ is in the same direction as $r((i_0+1)T_{\mathrm{s}})$ for G_{m}, or in the opposite direction as $r((i_0+1)T_{\mathrm{s}})$ for G_{n} and G_{sn}.

For G_{m}, subjects generate the right control at the start time for 431 trials out of 440 trials (98%). For G_{n}, subjects generate right control at the start time for 16 trials out of 440 trials (3.6%). For G_{sn}, subjects generate right control at the start time for 115 trials out of 440 trials (26%). Initial undershoot is one explanation for the differences in numbers of trials with G_{m}, G_{n}, and G_{sn} for which subjects generate the right control at the start time. Since G_{m} does not have initial undershoot, subjects generate the right control at the start time for 98% of trials. However, 96% of the trials with G_{n} do not have the right control at the start time. This suggests that most subjects on most trials ignore the initial undershoot, that is, allow y to move initially in the opposite direction of r. In contrast, only 74% of the trials with G_{sn}

do not have the right control at the start time. This suggests that subjects ignore initial undershoot less often with G_{sn} than with G_{n}. This could be explained by the difference in the peak value of the initial undershoot as shown in Figure 5.5.

5.9 Conclusions

In this chapter, we presented results from a HITL experiment in which human subjects learn to control 3 different unknown dynamic systems over 40 trials. One of the dynamic systems has a minimum-phase zero, one has a nonminimum-phase zero, and the other one has a slower nonminimum-phase zero. For all 3 dynamic systems, the command-following error tends to decrease over 40 trials. The mean time-averaged error for the system with a minimum-phase zero is smaller than that for the system with a nonminimum-phase zero, which is smaller than that for the system with a slower nonminimum-phase zero. Thus, the system with a nonminimum-phase zero is harder to control than the system with a minimum-phase zero, and the slower nonminimum-phase zero makes the system even harder to control.

We used the SSID algorithm in Chapter 4 to model the feedback and feedforward controllers used by humans to interact with the minimum-phase system and the nonminimum-phase system. For both systems, the identified feedforward controllers approximate the inverse of the dynamic system. This observation supports the IMH. We also discussed reasons why nonminimum-phase zeros may make the systems hard for humans to control.

Chapter 6 Conclusions and Future Work

This dissertation investigated humans motor control and human learning using subsystem identification (SSID). We developed novel SSID techniques for single-input single-output (SISO) and multi-input multi-output (MIMO), linear time-invariant dynamic systems. These SSID methods identify unknown feedback and feedforward subsystems, which are interconnected with a known subsystem, and use only input and output data from the closed-loop system. These SSID methods also guarantee closed-loop stability.

We conducted human-in-the-loop (HITL) experiments, and applied the SSID methods to the experimental data to model humans' control behavior. The identification results suggest that humans can construct a model of an unknown dynamic system and use the inverse dynamics in feedforward for control. These identification results support the internal model hypothesis (IMH). Furthermore, we explored the impact of system zeros on human motor control and humans learning.

In Chapter 2, we presented a frequency-domain SSID algorithm for identifying unknown feedback and feedforward subsystems interconnected with a known subsystem. This SSID method ensures asymptotic stability of the identified closed-loop transfer function, and has application to modeling human control behavior (both feedback and feedforward). The main analytic results of Chapter 2 are Theorems 2.1–2.4, which describe the properties of the SSID algorithm. In particular, Theorem 2.4 shows that the coefficients of the identified feedback and feedforward transfer functions are arbitrarily close to the true coefficients if the candidate pool is sufficiently dense and the

data noise is sufficiently small.

In Chapter 3, we presented results from an HITL experiment where 10 subjects learn to control an unknown dynamic systems over 40 trials. The SSID algorithm in Chapter 2 was used to model the feedback and feedforward control strategies used by the subjects. Over 40 trials, the feedforward controllers used by the subjects tend to approximate the inverse of the dynamic system. This observation supports the IMH. We observed no clear trend in feedback.

In Chapter 4, a discrete-time SSID algorithm was presented for MIMO systems with feedback and feedforward subsystems. The algorithm uses frequency-domain data, and ensures asymptotic stability of the identified closed-loop transfer function. The main analytic results of Chapter 4 are Theorems 4.1–4.2, which describe the properties of the MIMO SSID algorithm. In particular, Theorem 4.2 shows that the coefficients of the identified feedback and feedforward transfer functions are arbitrarily close to the true coefficients if the candidate pool is sufficiently dense and the data noise is sufficiently small. Also, we discussed the computational complexity of the SSID algorithm.

In Chapter 5, we presented results from an HITL experiment where 33 subjects learn to control 3 unknown dynamic systems over 40 trials. The SSID algorithm in Chapter 4 was used to model the feedback and feedforward control strategies used by the subjects. One of the dynamic systems has a minimum-phase zero, one has a nonminimum-phase zero, and one has a slower (i.e., closer to the imaginary axis) nonminimum-phase zero. For all 3 dynamic systems, the command-following error tends to decrease over 40 trials. The mean time-averaged error for the system with a minimum-phase zero is smaller than that for the system with a nonminimum-phase zero, which is smaller than that for the system with a slower nonminimum-phase zero. Thus, the system with a nonminimum-phase zero is harder to control than the system with a minimum-phase zero, and the slower nonminimum-phase zero makes

the system even harder to control.

We used the SSID algorithm in Chapter 4 to model the feedback and feedforward controllers used by humans to interact with the minimum-phase system and the nonminimum-phase system. For both systems, the identified feedforward controllers approximate the inverse of the dynamic system. This observation supports the IMH. We also discussed reasons why nonminimum-phase zeros may make the systems hard for humans to control.

The process of human learning, that is, the mechanism that helps humans learn to construct internal models, is still unknown. The impact of other characteristics (e.g., system order, relative degree, stability, and nonlinearity) of dynamic systems and the impact of the command signals on human motor control and human learning can be explored in the future.

Appendices

A Proofs of Propositions 2.7 and 2.8

The following notation is needed for the proofs of Propositions 2.7 and 2.8. Let $x_1, \ldots, x_n \in \mathbb{C}$, and let $x =< x_1 \quad \ldots \quad x_n >$ be an unordered n-tuple of numbers in $\mathbb{C}$. See [121, Appendix V] for more details. Let $\mathbb{C}^n_{\mathrm{sym}}$ denote the symmetric n^{th} power of $\mathbb{C}$ as defined in [121, Appendix V]. Let $x =< x_1 \quad \ldots \quad x_n >\in \mathbb{C}^n_{\mathrm{sym}}$ and $y =< y_1 \quad \ldots \quad y_n >\in \mathbb{C}^n_{\mathrm{sym}}$, and define $\xi_n(x,y) \triangleq \min_o \max_{j=1,\ldots,n} |x_j - y_{o(j)}|$, where o is any permutation of $1, \ldots, n$ and $o(j)$ denotes the image of j through the permutation o. It follows from [121, Lemma 3D in Appendix V] that ξ_n is a metric on $\mathbb{C}^n_{\mathrm{sym}}$.

The following lemma is needed for the proofs of Propositions 2.7 and 2.8.

Lemma 1. Consider $h_n \colon \mathbb{C}^n_{\mathrm{sym}} \to \mathbb{C}^n$ given by

$$h_n(x) \triangleq \begin{bmatrix} -\sum_{j=1}^n x_j \\ (x_1x_2 + \cdots + x_1x_n) + (x_2x_3 + \cdots + x_2x_n) + \cdots + x_{n-1}x_n \\ \vdots \\ (-1)^k \sum_{1 \le i_1 < i_2 < \cdots < i_k \le n} \prod_{j=i_1}^{i_k} x_j \\ \vdots \\ (-1)^n \prod_{j=1}^n x_j \end{bmatrix}, \qquad (1)$$

where $x =< x_1 \quad \cdots \quad x_n >\in \mathbb{C}^n_{\mathrm{sym}}$. Consider the polynomial $P(s) = s^n + \tau_1 s^{n-1} + \cdots + \tau_{n-1}s + \tau_n$, where $\tau_1, \ldots, \tau_n \in \mathbb{C}$. Let $\lambda_1, \lambda_2, \ldots, \lambda_n \in \mathbb{C}$ denote the n roots of P, and define $\tau \triangleq [\ \tau_1 \quad \cdots \quad \tau_n\ ]^{\mathrm{T}} \in \mathbb{C}^n$ and $\lambda \triangleq< \lambda_1 \quad \cdots \quad \lambda_n >\in \mathbb{C}^n_{\mathrm{sym}}$. Then,

$h_n(\lambda) = \tau$, and h_n and h_n^{-1} are continuous.

Proof. It follows from [122, Fact 4.8.2] that $h_n(\lambda) = \tau$. Moreover, it follows from [121, Theorem 4A in Appendix V] that h_n and h_n^{-1} are continuous. □

The following notation is needed for the proofs of Propositions 2.7 and 2.8. Let $\kappa \triangleq d_{\mathrm{p}} + d_{\mathrm{fb}}$. Let $h_{d_{\mathrm{ff}}} \colon \mathbb{C}_{\mathrm{sym}}^{d_{\mathrm{ff}}} \to \mathbb{C}^{d_{\mathrm{ff}}}$ and $h_\kappa \colon \mathbb{C}_{\mathrm{sym}}^{\kappa} \to \mathbb{C}^{\kappa}$ be functions given by (1), where n is replaced by d_{ff} and κ, respectively. Let $a \triangleq \left[\begin{array}{cccc} a_1 & a_2 & \cdots & a_{d_{\mathrm{p}}} \end{array}\right]^{\mathrm{T}} \in \mathbb{R}^{d_{\mathrm{p}}}$ and $b \triangleq \left[\begin{array}{cccc} b_0 & b_1 & \cdots & b_{n_{\mathrm{p}}} \end{array}\right]^{\mathrm{T}} \in \mathbb{R}^{n_{\mathrm{p}}+1}$ be such that $N_{\mathrm{p}}(s) = \Gamma_{n_{\mathrm{p}}}^{\mathrm{T}}(s) b$ and $D_{\mathrm{p}}(s) = s^{d_{\mathrm{p}}} + \Gamma_{d_{\mathrm{p}}-1}^{\mathrm{T}}(s) a$. Consider the continuous function $g \colon \mathbb{R}^{d-d_{\mathrm{ff}}} \to \mathbb{R}^{\kappa}$ given by

$$g(z) \triangleq Az + B, \tag{2}$$

where $B \triangleq \left[\begin{array}{cc} a^{\mathrm{T}} & 0_{1 \times d_{\mathrm{fb}}} \end{array}\right]^{\mathrm{T}} \in \mathbb{R}^{\kappa}$ and

$$A \triangleq \left[\begin{array}{cccc:cccc} 0_{(\kappa - n_{\mathrm{p}} - n_{\mathrm{fb}} - 1) \times (n_{\mathrm{fb}}+1)} & & & & 1 & 0 & \cdots & 0 \\ \hdashline b_0 & 0 & \cdots & 0 & a_1 & 1 & \ddots & \vdots \\ b_1 & b_0 & \ddots & \vdots & a_2 & a_1 & \ddots & 0 \\ \vdots & b_1 & \ddots & 0 & \vdots & a_2 & \ddots & 1 \\ b_{n_{\mathrm{p}}} & \vdots & \ddots & b_0 & a_{d_{\mathrm{p}}} & \vdots & \ddots & a_1 \\ 0 & b_{n_{\mathrm{p}}} & & b_1 & 0 & a_{d_{\mathrm{p}}} & & a_2 \\ \vdots & & \ddots & \vdots & \vdots & & \ddots & \vdots \\ 0 & 0 & & b_{n_{\mathrm{p}}} & 0 & 0 & & a_{d_{\mathrm{p}}} \end{array}\right] \in \mathbb{R}^{\kappa \times (d - d_{\mathrm{ff}})}.$$

Proof of Proposition 2.7. Since Ψ is compact, it follows that Ψ is bounded, which implies that $(\Psi \cap \mathcal{S}_\rho) \subseteq \Psi$ is bounded.

Let $\phi \in (\Psi \cap \mathcal{S}_\rho)$, and we show that ϕ is not an isolated point. Let $\phi = \left[\begin{array}{cc} x^{\mathrm{T}} & z^{\mathrm{T}} \end{array}\right]^{\mathrm{T}}$, where $x \in \mathbb{R}^{d_{\mathrm{ff}}}$ and $z \in \mathbb{R}^{d-d_{\mathrm{ff}}}$. Since $\phi \in \Psi$ and Ψ is perfect, it follows that there exists a sequence $\{\phi_i\}_{i=1}^{\infty} \subseteq \Psi$ that converges to ϕ. For each $i \in \mathbb{Z}^+$, let $\phi_i = \left[\begin{array}{cc} x_i^{\mathrm{T}} & z_i^{\mathrm{T}} \end{array}\right]^{\mathrm{T}}$,

where $x_i \in \mathbb{R}^{d_{\mathrm{ff}}}$ and $z_i \in \mathbb{R}^{d-d_{\mathrm{ff}}}$. Thus, $\{x_i\}_{i=1}^{\infty}$ converges to x and $\{z_i\}_{i=1}^{\infty}$ converges to z.

Let $\mu_1, \ldots, \mu_{d_{\mathrm{ff}}} \in \mathbb{C}$ denote the d_{ff} roots of $\mathcal{D}_{\mathrm{ff}}(s,\phi)$, and define $p \triangleq < \mu_1 \quad \ldots \quad \mu_{d_{\mathrm{ff}}} >$. For each $i \in \mathbb{Z}^+$, let $\mu_{i,1}, \ldots, \mu_{i,d_{\mathrm{ff}}} \in \mathbb{C}$ denote the d_{ff} roots of $\mathcal{D}_{\mathrm{ff}}(s,\phi_i)$, and define $p_i \triangleq < \mu_{i,1} \quad \ldots \quad \mu_{i,d_{\mathrm{ff}}} >$. Lemma 1 implies that $x = h_{d_{\mathrm{ff}}}(p)$ and $x_i = h_{d_{\mathrm{ff}}}(p_i)$. Since $\lim_{i\to\infty} x_i = x$ and Lemma 1 implies that $h_{d_{\mathrm{ff}}}^{-1}$ is continuous, it follows that $\lim_{i\to\infty} p_i = \lim_{i\to\infty} h_{d_{\mathrm{ff}}}^{-1}(x_i) = h_{d_{\mathrm{ff}}}^{-1}(x) = p$. Since $\phi \in \mathcal{S}_\rho$, it follows that for all $j = 1, \ldots, d_1$, $\mathrm{Re}\, \mu_j < \rho$. Define $\epsilon_1 \triangleq \min_{j=1,\ldots,d_{\mathrm{ff}}} \rho - \mathrm{Re}\, \mu_j$. Since $\lim_{i\to\infty} p_i = p$ and $\xi_{d_{\mathrm{ff}}}$ is a metric on $\mathbb{C}_{\mathrm{sym}}^{d_{\mathrm{ff}}}$, it follows that there exists $L_1 \in \mathbb{Z}^+$ such that for all $i \geq L_1$, $\xi_{d_{\mathrm{ff}}}(p_i, p) < \epsilon_1$. Thus, for each $i \geq L_1$, there exists a permutation o_i of $1, \ldots, d_{\mathrm{ff}}$ such that for all $j = 1, \ldots, d_{\mathrm{ff}}$, $|\mu_{i,j} - \mu_{o_i(j)}| < \epsilon_1$. Therefore, for all $i \geq L_1$ and all $j = 1, \ldots, d_{\mathrm{ff}}$,

$$\mathrm{Re}\, \mu_{i,j} - \mathrm{Re}\, \mu_{o_i(j)} \leq |\mathrm{Re}\, \mu_{i,j} - \mathrm{Re}\, \mu_{o_i(j)}| \leq |\mu_{i,j} - \mu_{o_i(j)}| < \epsilon_1 \leq \rho - \mathrm{Re}\, \mu_{o_i(j)},$$

which implies that $\mathrm{Re}\, \mu_{i,j} < \rho$.

Next, since (A2.2) implies that $\kappa > n_{\mathrm{p}} + n_{\mathrm{fb}}$, it follows that $D_{\mathrm{p}}(s)\mathcal{D}_{\mathrm{fb}}(s,\phi) + N_{\mathrm{p}}(s)\mathcal{N}_{\mathrm{fb}}(s,\phi)$ is a monic degree κ polynomial, which can be written as $s^\kappa + \Gamma_{\kappa-1}^{\mathrm{T}}(s)\gamma$, where $\gamma \in \mathbb{R}^\kappa$. Let $\nu_1, \ldots, \nu_\kappa \in \mathbb{C}$ denote the κ roots of $D_{\mathrm{p}}(s)\mathcal{D}_{\mathrm{fb}}(s,\phi) + N_{\mathrm{p}}(s)\mathcal{N}_{\mathrm{fb}}(s,\phi)$. For each $i \in \mathbb{Z}^+$, let $\nu_{i,1}, \ldots, \nu_{i,\kappa}$ denote the κ roots of $D_{\mathrm{p}}(s)\mathcal{D}_{\mathrm{fb}}(s,\phi_i) + N_{\mathrm{p}}(s)\mathcal{N}_{\mathrm{fb}}(s,\phi_i)$, which can be written as $s^\kappa + \Gamma_{\kappa-1}^{\mathrm{T}}(s)\gamma_i$, where $\gamma_i \in \mathbb{R}^\kappa$. Using (2), it follows that $\gamma = g(z)$ and $\gamma_i = g(z_i)$. Define $q \triangleq < \nu_1 \quad \ldots \quad \nu_\kappa >$ and $q_i \triangleq < \nu_{i,1} \quad \ldots \quad \nu_{i,\kappa} >$, and Lemma 1 implies that $\gamma = g(z) = h_\kappa(q)$ and $\gamma_i = g(z_i) = h_\kappa(q_i)$. Since $\lim_{i\to\infty} z_i = z$ and g is continuous on $\mathbb{R}^{d-d_{\mathrm{ff}}}$, it follows that $\lim_{i\to\infty} \gamma_i = \lim_{i\to\infty} g(z_i) = g(z) = \gamma$. Since $\lim_{i\to\infty} \gamma_i = \gamma$ and Lemma 1 implies that h_κ^{-1} is continuous, it follows that $\lim_{i\to\infty} q_i = \lim_{i\to\infty} h_\kappa^{-1}(\gamma_i) = h_\kappa^{-1}(\gamma) = q$. Since $\phi \in \mathcal{S}_\rho$, it follows that for all $l = 1, \ldots, \kappa$, $\mathrm{Re}\, \nu_l < \rho$. Define $\epsilon_2 \triangleq \min_{l=1,\ldots,\kappa} \rho - \mathrm{Re}\, \nu_l$. Since $\lim_{i\to\infty} q_i = q$ and

ξ_κ is a metric on $\mathbb{C}^\kappa_{\rm sym}$, it follows that there exists $L_2 \in \mathbb{Z}^+$ such that for all $i \geq L_2$, $\xi_\kappa(q_i, q) < \epsilon_2$. Thus, for each $i \geq L_2$, there exists a permutation o_i of $1, \ldots, \kappa$ such that for all $l = 1, \ldots, \kappa$, $|\nu_{i,l} - \nu_{o_i(l)}| < \epsilon_2$. Therefore, for all $i \geq L_2$ and all $l = 1, \ldots, \kappa$,

$$\text{Re } \nu_{i,l} - \text{Re } \nu_{o_i(l)} \leq |\text{Re } \nu_{i,l} - \text{Re } \nu_{o_i(l)}| \leq |\nu_{i,l} - \nu_{o_i(l)}| < \epsilon_2 \leq \rho - \text{Re } \nu_{o_i(l)},$$

which implies that $\text{Re } \nu_{i,l} < \rho$.

Define $L \triangleq \max\{L_1, L_2\}$. Let $i \geq L$, and (2.5) implies that $\mu_{i,1}, \ldots, \mu_{i,d_{\rm ff}}$ and $\nu_{i,1}, \ldots, \nu_{i,\kappa}$ are the $d_{\rm ff}+d_{\rm p}+d_{\rm fb}$ roots of $\tilde{\mathcal{D}}(s, \phi_i)$. For all $j = 1, \ldots, d_{\rm ff}$ and $l = 1, \ldots, \kappa$, $\text{Re } \mu_{i,j} < \rho$ and $\text{Re } \nu_{i,l} < \rho$, which implies that $\tilde{\mathcal{D}}(s + \rho, \phi_i)$ is Hurwitz. Thus, $\phi_i \in \mathcal{S}_\rho$, which implies that $\phi_i \in (\Psi \cap \mathcal{S}_\rho)$. Therefore, $\{\phi_i\}_{i=L}^\infty \subseteq (\Psi \cap \mathcal{S}_\rho)$ converges to $\phi \in (\Psi \cap \mathcal{S}_\rho)$, which implies that ϕ is not an isolated point. □

Proof of Proposition 2.8. Since Ψ is compact, it follows that $\overline{\Psi \cap \mathcal{S}_\rho} \subseteq (\overline{\Psi} \cap \overline{\mathcal{S}}_\rho) = \Psi \cap \overline{\mathcal{S}_\rho}$, which implies that $\overline{\Psi \cap \mathcal{S}_\rho}$ is compact.

We now show that $\overline{\Psi \cap \mathcal{S}_\rho} \subseteq \mathcal{S}$. Define $E_4 \triangleq \left[\begin{array}{cc} E_2^{\rm T} & E_3^{\rm T} \end{array}\right]^{\rm T} \in \mathbb{R}^{(d-d_{\rm ff})\times d}$, $\mathcal{F} \triangleq \{\lambda \in \mathbb{C}\colon \text{Re } \lambda \leq \rho < 0\}$, and

$$S_0 \triangleq \{\phi \in \mathbb{R}^d\colon \text{ if } \lambda \in \mathbb{C} \text{ and } \tilde{\mathcal{D}}(\lambda, \phi) = 0, \text{ then } \lambda \in \mathcal{F}\},$$

$$S_1 \triangleq \{x \in \mathbb{R}^{d_{\rm ff}}\colon x = E_1\phi, \text{ where } \phi \in \mathbb{R}^d \text{ and if } \lambda \in \mathbb{C} \text{ and } \mathcal{D}_{\rm ff}(\lambda, \phi) = 0, \text{ then } \lambda \in \mathcal{F}\},$$

$$S_2 \triangleq \{z \in \mathbb{R}^{d-d_{\rm ff}}\colon z = E_4\phi, \text{ where } \phi \in \mathbb{R}^d \text{ and if } \lambda \in \mathbb{C} \text{ and}$$

$$D_{\rm p}(\lambda)\mathcal{D}_{\rm fb}(\lambda, \phi) + N_{\rm p}(\lambda)\mathcal{N}_{\rm fb}(\lambda, \phi) = 0, \text{ then } \lambda \in \mathcal{F}\}.$$

Let $x \in S_1$, $z \in S_2$, and $\phi = \left[\begin{array}{cc} x^{\rm T} & z^{\rm T} \end{array}\right]^{\rm T} \in S_0$.

First, we show that S_1 is closed in $\mathbb{R}^{d_{\rm ff}}$. Let $\mu_1, \ldots, \mu_{d_{\rm ff}}$ denote the $d_{\rm ff}$ roots of $\mathcal{D}_{\rm ff}(s, \phi)$, and define $p \triangleq <\mu_1, \ \cdots, \ \mu_{d_{\rm ff}}>$. Since $x \in S_1$, it follows that $\mu_1, \ldots, \mu_{d_{\rm ff}} \in \mathcal{F}$ and $\mu \in \mathcal{F}^{d_{\rm ff}}_{\rm sym}$. Lemma 1 implies that $x = h_{d_{\rm ff}}(p) \in h_{d_{\rm ff}}(\mathcal{F}^{d_{\rm ff}}_{\rm sym})$, which implies that $x \in (\mathbb{R}^{d_{\rm ff}} \cap h_{d_{\rm ff}}(\mathcal{F}^{d_{\rm ff}}_{\rm sym}))$. Thus, $S_1 \subseteq (\mathbb{R}^{d_{\rm ff}} \cap h_{d_{\rm ff}}(\mathcal{F}^{d_{\rm ff}}_{\rm sym}))$. Next, let $\hat{x} \in (\mathbb{R}^{d_{\rm ff}} \cap h_{d_{\rm ff}}(\mathcal{F}^{d_{\rm ff}}_{\rm sym}))$,

and let $\hat{\mu}_1, \ldots, \hat{\mu}_{d_{\rm ff}}$ denote the $d_{\rm ff}$ roots of $\mathcal{D}_{\rm ff}(s, [\ \hat{x}^{\rm T} \quad z^{\rm T}\ ]^{\rm T})$. Thus, $\hat{x} \in \mathbb{R}^{d_{\rm ff}}$ and $h_{d_{\rm ff}}^{-1}(\hat{x}) \in \mathcal{F}_{\rm sym}^{d_{\rm ff}}$, which implies that $\hat{\mu}_1, \ldots, \hat{\mu}_{d_{\rm ff}} \in \mathcal{F}$. Thus, $\hat{x} \in S_1$, which implies that $(\mathbb{R}^{d_{\rm ff}} \cap h_{d_{\rm ff}}(\mathcal{F}_{\rm sym}^{d_{\rm ff}})) \subseteq S_1$. Therefore, $S_1 = \mathbb{R}^{d_{\rm ff}} \cap h_{d_{\rm ff}}(\mathcal{F}_{\rm sym}^{d_{\rm ff}})$. Since $\mathcal{F}$ is closed in $\mathbb{C}$, it follows that $\mathcal{F}_{\rm sym}^{d_{\rm ff}}$ is closed in $\mathbb{C}_{\rm sym}^{d_{\rm ff}}$. Since Lemma 1 implies that $h_{d_{\rm ff}}^{-1}$ is continuous, it follows that $h_{d_{\rm ff}}(\mathcal{F}_{\rm sym}^{d_{\rm ff}})$ is closed in $\mathbb{C}^{d_{\rm ff}}$. Thus, $S_1 = \mathbb{R}^{d_{\rm ff}} \cap h_{d_{\rm ff}}(\mathcal{F}_{\rm sym}^{d_{\rm ff}})$ is closed in $\mathbb{R}^{d_{\rm ff}}$.

Next, we show that S_2 is closed in $\mathbb{R}^{d-d_{\rm ff}}$. Since (A2.2) implies that $\kappa > n_{\rm p} + n_{\rm fb}$, it follows that $D_{\rm p}(s)\mathcal{D}_{\rm fb}(s,\phi) + N_{\rm p}(s)\mathcal{N}_{\rm fb}(s,\phi)$ is a monic degree κ polynomial, which can be written as $s^\kappa + \Gamma_{\kappa-1}^{\rm T}(s)\gamma$, where $\gamma \in \mathbb{R}^\kappa$. Using (2), it follows that $\gamma = g(z)$. Let $\nu_1, \ldots, \nu_\kappa$ denote the κ roots of $s^\kappa + \Gamma_{\kappa-1}^{\rm T}(s)\gamma$, and define $q \triangleq < \nu_1, \ \cdots, \ \nu_\kappa >$. Since $z \in S_2$, it follows that $\nu_1, \ldots, \nu_\kappa \in \mathcal{F}$ and $q \in \mathcal{F}_{\rm sym}^\kappa$. Lemma 1 implies that $\gamma = h_\kappa(q) \in h_\kappa(\mathcal{F}_{\rm sym}^\kappa)$, which implies that $z = g^{-1}(\gamma) \in g^{-1}(\mathbb{R}^\kappa \cap h_\kappa(\mathcal{F}_{\rm sym}^\kappa))$. Thus, $S_2 \subseteq g^{-1}(\mathbb{R}^\kappa \cap h_\kappa(\mathcal{F}_{\rm sym}^\kappa))$. Next, let $\hat{z} \in g^{-1}(\mathbb{R}^\kappa \cap h_\kappa(\mathcal{F}_{\rm sym}^\kappa)) \subseteq \mathbb{R}^{d-d_{\rm ff}}$. Thus, $g(\hat{z}) \in (\mathbb{R}^\kappa \cap h_\kappa(\mathcal{F}_{\rm sym}^\kappa))$. Let $\hat{\nu}_1, \ldots, \hat{\nu}_\kappa$ denote the κ roots of $s^\kappa + \Gamma_{\kappa-1}^{\rm T}(s)g(\hat{z})$. It follows from Lemma 1 that $< \hat{\nu}_1, \ \cdots, \ \hat{\nu}_\kappa > = h_\kappa^{-1}(g(\hat{z})) \in \mathcal{F}_{\rm sym}^\kappa$, which implies that $\hat{\nu}_1, \ldots, \hat{\nu}_\kappa \in \mathcal{F}$. Thus, $\hat{z} \in S_2$, which implies that $g^{-1}(\mathbb{R}^\kappa \cap h_\kappa(\mathcal{F}_{\rm sym}^\kappa)) \subseteq S_2$. Therefore, $S_2 = g^{-1}(\mathbb{R}^\kappa \cap h_\kappa(\mathcal{F}_{\rm sym}^\kappa))$. Since $\mathcal{F}$ is closed in $\mathbb{C}$, it follows that $\mathcal{F}_{\rm sym}^\kappa$ is closed in $\mathbb{C}_{\rm sym}^\kappa$. Since Lemma 1 implies that h_κ^{-1} is continuous, it follows that $h_\kappa(\mathcal{F}_{\rm sym}^\kappa)$ is closed in $\mathbb{C}^\kappa$. Thus, $\mathbb{R}^\kappa \cap h_\kappa(\mathcal{F}_{\rm sym}^\kappa)$ is closed in $\mathbb{R}^\kappa$. Since, in addition, g is continuous, it follows that $S_2 = g^{-1}(\mathbb{R}^\kappa \cap h_\kappa(\mathcal{F}_{\rm sym}^\kappa))$ is closed in $\mathbb{R}^{d-d_{\rm ff}}$.

Since S_1 is closed in $\mathbb{R}^{d_{\rm ff}}$, S_2 is closed in $\mathbb{R}^{d-d_{\rm ff}}$, and (2.5) implies that $S_0 = S_1 \times S_2$, it follows that S_0 is closed in $\mathbb{R}^d$. Since, in addition, $\mathcal{S}_\rho \subseteq S_0$, it follows that $\overline{\mathcal{S}}_\rho \subseteq S_0$. Thus, $\overline{\Psi \cap \mathcal{S}_\rho} \subseteq (\Psi \cap \overline{\mathcal{S}}_\rho) \subseteq \overline{\mathcal{S}}_\rho \subseteq S_0 \subseteq \mathcal{S}$. $\square$

B Details of Candidate Pool used in Chapter 3

Now, C1) and C2) are used to construct a set of potential pole locations for the feedforward and feedback controllers. Since $d_{\text{ff}} = d_{\text{fb}} = 2$, it follows that $\mathcal{D}_{\text{ff}}$ and $\mathcal{D}_{\text{fb}}$ are monic second-order polynomials. If the roots of $\mathcal{D}_{\text{ff}}$ or $\mathcal{D}_{\text{fb}}$ are real, then C1) and C2) implies that the roots are on the interval $[-25, 25]$. Thus, consider the set of potential real pole locations for the feedforward and feedback controller given by

$$P_{\text{r}} \triangleq \{-25 + 0.5i\}_{i=0}^{44} \cup \{-2.6 + 0.1i\}_{i=0}^{52} \cup \{3.0 + 0.5i\}_{i=0}^{44}.$$

Note that $P_{\text{r}} \in [-25, 25]$, and that the elements of P_{r} are more densely spaced near the origin. If the roots of $\mathcal{D}_{\text{ff}}$ or $\mathcal{D}_{\text{fb}}$ are complex, then C1) and C2) implies that these roots are given by the roots of $s^2 + 2\zeta\omega_{\text{n}}s + \omega_{\text{n}}^2$, where the natural frequency is $\omega_{\text{n}} \in [0, 25]$ and the damping ratio is $\zeta \in (-1, 1)$. Thus, the set of potential natural frequencies for the poles of feedforward and feedback controller is given by

$$P_{\omega_{\text{n}}} \triangleq \{0.05i\}_{i=0}^{52} \cup \{2.7 + 0.1i\}_{i=0}^{63} \cup \{9.5 + 0.5i\}_{i=0}^{31},$$

and the set of potential damping ratios is given by

$$P_{\zeta} \triangleq \{-0.9 + 0.1i\}_{i=0}^{4} \cup \{-0.45 + 0.05i\}_{i=0}^{5} \cup \{-0.18 + 0.02i\}_{i=0}^{18} \cup \{0.2 + 0.05i\}_{i=0}^{5} \cup \{0.5 + 0.1i\}_{i=0}^{4}.$$

Note that $P_{\zeta} \in (-1, 1)$ and $P_{\omega_{\text{n}}} \in [0, 25]$. Moreover, note that the elements of P_{ζ} and $P_{\omega_{\text{n}}}$ are more densely spaced near the origin.

Now, the sets P_{r}, $P_{\omega_{\text{n}}}$, and P_{ζ} are used to construct the set of potential denominator coefficients for the feedback and feedforward controller. Specifically, the set of

potential denominator coefficients for the controllers is given by

$$P \triangleq \left\{ \begin{bmatrix} -p_1 - p_2 \\ p_1 p_2 \end{bmatrix} : p_1, p_2 \in P_{\mathrm{r}} \right\} \cup \left\{ \begin{bmatrix} 2\zeta\omega_{\mathrm{n}} \\ \omega_{\mathrm{n}}^2 \end{bmatrix} : \zeta \in P_\zeta, \omega_{\mathrm{n}} \in P_{\omega_{\mathrm{n}}} \right\}.$$

Now, C3) is used to construct a set of potential numerator coefficients for the feedback controller. Since $n_{\mathrm{fb}} = 1$, it follows that $\mathcal{N}_{\mathrm{fb}}$ is a first-order polynomial. Thus, the root of $\mathcal{N}_{\mathrm{fb}}$ is on the interval $[-25, 25]$. Specifically, the set of potential zeros for the feedback controller is P_{r}. Thus, the set of potential numerator coefficients for the feedback controller is given by

$$Z \triangleq \left\{ \begin{bmatrix} k \\ -kz \end{bmatrix} : z \in P_{\mathrm{r}}, k \in \mathbb{R} \right\}.$$

Now, C4) is used to construct a set of potential peak magnitudes for the feedback controller. Specifically, consider the set

$$K \triangleq \{0.1k\}_{k=0}^{9} \cup \{1.1^k\}_{k=0}^{35} \cup \{30.5\},$$

and note the $K \in [0, 30.5]$. Define $\Gamma \colon \mathbb{C} \to \mathbb{C}^2$ by $\Gamma(s) = \begin{bmatrix} s \\ 1 \end{bmatrix}$, and define the function $\kappa \colon Z \times P \to [0, \infty)$ by

$$\kappa(\beta_{\mathrm{fb}}, \alpha_{\mathrm{fb}}) \triangleq \max_{\omega \in [0.2\pi, 0.8\pi]} \left| \frac{\Gamma^{\mathrm{T}}(\jmath\omega)\beta_{\mathrm{fb}}}{\Gamma^{\mathrm{T}}(\jmath\omega)\alpha_{\mathrm{fb}} - \omega^2} \right|.$$

Next, define

$$\Lambda \triangleq \left\{ \begin{bmatrix} \alpha_{\mathrm{ff}} \\ \beta_{\mathrm{fb}} \\ \alpha_{\mathrm{fb}} \end{bmatrix} : \alpha_{\mathrm{ff}} \in P, \beta_{\mathrm{fb}} \in Z, \alpha_{\mathrm{fb}} \in P, \kappa(\beta_{\mathrm{fb}}, \alpha_{\mathrm{fb}}) \in K \right\},$$

and note that the elements of Λ satisfy C1)–C4). To construct the candidate pool Φ from the set Λ, consider the elements of Λ that satisfy the closed-loop stability condition C5). Specifically, the candidate pool is defined as

$$\Phi \triangleq \left\{ \phi \in \Lambda \colon \text{if } \tilde{\mathcal{D}}(\lambda, \phi) = 0, \text{ then } \operatorname{Re} \lambda < -0.1 \right\}.$$

Note that Φ can be generated from the superset Λ by using the Hurwitz criteria.

C Details of Candidate Pool used in Chapter 5

We generate potential feedback controllers by constructing a set of potential pole and zero locations in continuous time and then convert these potential pole and zero locations into discrete time by zero-pole matching [123].

Now, C1) is used to construct a set of potential pole locations for the feedback controller. Since $d_{\text{fb}} = 2$, it follows that $\mathcal{D}_{\text{fb}}$ are monic second-order polynomials. If the roots of $\mathcal{D}_{\text{fb}}$ are real, then C1) implies that the roots are on the interval $[-31.5, 31.5]$. Thus, consider the set of potential real pole locations for the feedforward and feedback controller given by

$$P_{\text{r}} \triangleq \{-31.5 + 0.5i\}_{i=0}^{56} \cup \{-3.2 + 0.1i\}_{i=0}^{31} \cup \{0.1i\}_{i=1}^{32} \cup \{3.5 + 0.5i\}_{i=0}^{56}.$$

Note that $P_{\text{r}} \in [-31.5, 31.5]$, and that the elements of P_{r} are more densely spaced near the origin. If the roots of $\mathcal{D}_{\text{fb}}$ are complex, then C1) implies that these roots are given by the roots of $s^2 + 2\zeta\omega_{\text{n}}s + \omega_{\text{n}}^2$, where the natural frequency is $\omega_{\text{n}} \in [0, 31.5]$ and the damping ratio is $\zeta \in (-1, 1)$. Thus, the set of potential natural frequencies for the poles of feedforward and feedback controller is given by

$$P_{\omega_{\text{n}}} \triangleq \{0.05i\}_{i=1}^{64} \cup \{3.3 + 0.1i\}_{i=0}^{87} \cup \{12.5 + 0.5i\}_{i=0}^{18},$$

and the set of potential damping ratios is given by

$$P_{\zeta} \triangleq \{-0.9 + 0.1i\}_{i=0}^{4} \cup \{-0.45 + 0.05i\}_{i=0}^{5} \cup \{-0.18 + 0.02i\}_{i=0}^{18} \cup \{0.2 + 0.05i\}_{i=0}^{5} \cup \{0.5 + 0.1i\}_{i=0}^{4}.$$

Note that $P_{\zeta} \in (-1, 1)$ and $P_{\omega_{\text{n}}} \in [0, 31.5]$. Moreover, note that the elements of P_{ζ} and $P_{\omega_{\text{n}}}$ are more densely spaced near the origin.

Now, the sets P_{r}, $P_{\omega_{\mathrm{n}}}$, and P_{ζ} are used to construct the set of potential denominator coefficients for the feedback controller in discrete-time. Specifically, the set of potential denominator coefficients for the controllers in discrete-time is given by

$$P \triangleq \left\{ \begin{bmatrix} -e^{p_1 T_{\mathrm{s}}} - e^{p_2 T_{\mathrm{s}}} \\ e^{(p_1+p_2)T_{\mathrm{s}}} \end{bmatrix} : p_1, p_2 \in P_{\mathrm{r}} \right\} \cup \left\{ \begin{bmatrix} -2e^{-\zeta\omega_{\mathrm{n}} T_{\mathrm{s}}} \cos(T_{\mathrm{s}}\omega_{\mathrm{n}}\sqrt{1-\zeta^2}) \\ e^{-2\zeta\omega_{\mathrm{n}} T_{\mathrm{s}}} \end{bmatrix} : \zeta \in P_{\zeta}, \omega_{\mathrm{n}} \in P_{\omega_{\mathrm{n}}} \right\}.$$

Now, C2) is used to construct a set of potential numerator coefficients for the feedback controller. Since $n_{\mathrm{fb}} = 2$, it follows that $\mathcal{N}_{\mathrm{fb}}$ is a second-order polynomial. If the roots of $\mathcal{D}_{\mathrm{fb}}$ are real, then C2) implies that the roots are on the interval $[-31.5, 31.5]$. Thus, consider the set of potential real pole locations for the feedforward and feedback controller given by

$$Z_{\mathrm{r}} \triangleq \{-31.5 + 0.5i\}_{i=0}^{56} \cup \{-3.2 + 0.1i\}_{i=0}^{64} \cup \{3.5 + 0.5i\}_{i=0}^{56}.$$

Note that $Z_{\mathrm{r}} \in [-31.5, 31.5]$, and that the elements of P_{r} are more densely spaced near the origin. If the roots of $\mathcal{D}_{\mathrm{fb}}$ are complex, then C2) implies that these roots are given by the roots of $s^2 + 2\zeta\omega_{\mathrm{n}} s + \omega_{\mathrm{n}}^2$, where the natural frequency is $\omega_{\mathrm{n}} \in [0, 31.5]$ and the damping ratio is $\zeta \in (-1, 1)$. Thus, the set of potential natural frequencies for the poles of feedforward and feedback controller is given by

$$Z_{\omega_{\mathrm{n}}} \triangleq \{0.05i\}_{i=1}^{64} \cup \{3.3 + 0.1i\}_{i=0}^{87} \cup \{12.5 + 0.5i\}_{i=0}^{18},$$

and the set of potential damping ratios is given by

$$Z_{\zeta} \triangleq \{-0.9 + 0.1i\}_{i=0}^{4} \cup \{-0.45 + 0.05i\}_{i=0}^{5} \cup \{-0.18 + 0.02i\}_{i=0}^{18}$$

$$\cup \{0.2 + 0.05i\}_{i=0}^{5} \cup \{0.5 + 0.1i\}_{i=0}^{4}.$$

Note that $Z_\zeta \in (-1, 1)$ and $Z_{\omega_\mathrm{n}} \in [0, 31.5]$. Moreover, note that the elements of Z_ζ and Z_{ω_n} are more densely spaced near the origin.

Now, the sets Z_r, Z_{ω_n}, and Z_ζ are used to construct the set of potential denominator coefficients for the feedback controller in discrete-time. Specifically, the set of potential denominator coefficients for the controllers in discrete-time is given by

$$Z \triangleq \left\{ \begin{bmatrix} k \\ -k(e^{z_1 T_\mathrm{s}} + e^{z_2 T_\mathrm{s}}) \\ k e^{(z_1+z_2)T_\mathrm{s}} \end{bmatrix} : z_1, z_2 \in Z_\mathrm{r}, k \in \mathbb{R} \right\} \cup$$
$$\left\{ \begin{bmatrix} k \\ -2k e^{-\zeta\omega_\mathrm{n} T_\mathrm{s}} \cos(T_\mathrm{s}\omega_\mathrm{n}\sqrt{1-\zeta^2}) \\ k e^{-2\zeta\omega_\mathrm{n} T_\mathrm{s}} \end{bmatrix} : \zeta \in Z_\zeta, \omega_\mathrm{n} \in Z_{\omega_\mathrm{n}}, k \in \mathbb{R} \right\}.$$

Now, C3) is used to construct a set of potential peak magnitudes for the feedback controller. Specifically, consider the set

$$K \triangleq \{0.1k\}_{k=0}^{9} \cup \{1.1^k\}_{k=0}^{35} \cup \{30.5\},$$

and note the $K \in [0, 30.5]$. Define $\Gamma \colon \mathbb{C} \to \mathbb{C}^2$ by $\Gamma(z) = \begin{bmatrix} z^2 \\ z \\ 1 \end{bmatrix}$, and define the function $\kappa \colon Z \times P \to [0, \infty)$ by

$$\kappa(\beta_\mathrm{fb}, \alpha_\mathrm{fb}) \triangleq \max_{\omega \in [0,\pi]} \left| \frac{\Gamma^\mathrm{T}(e^{\jmath\omega T_\mathrm{s}})\beta_\mathrm{fb}}{\Gamma^\mathrm{T}(e^{\jmath\omega T_\mathrm{s}})\alpha_\mathrm{fb} + e^{2\jmath\omega T_\mathrm{s}}} \right|.$$

Next, define

$$\Lambda \triangleq \left\{ \begin{bmatrix} \alpha_{\mathrm{ff}} \\ \beta_{\mathrm{fb}} \\ \alpha_{\mathrm{fb}} \end{bmatrix} : \alpha_{\mathrm{ff}} \in P, \beta_{\mathrm{fb}} \in Z, \alpha_{\mathrm{fb}} \in P, \kappa(\beta_{\mathrm{fb}}, \alpha_{\mathrm{fb}}) \in K \right\},$$

and note that the elements of Λ satisfy C1)–C3). To construct the candidate pool Φ from the set Λ, consider the elements of Λ that satisfy the closed-loop stability condition C4). Specifically, the candidate pool is defined as

$$\Phi \triangleq \left\{ \phi \in \Lambda \colon \text{if } \tilde{\mathcal{D}}(e^{\lambda T_{\mathrm{s}}}, \phi) = 0, \text{ then } \operatorname{Re} \lambda < -0.1 \right\}.$$

Note that Φ can be generated from the superset Λ by using the Jury criteria.

Bibliography

[1] S. Brandl, O. Kroemer, and J. Peters. Generalizing pouring actions between objects using warped parameters. In *IEEE-RAS International Conference on Humanoid Robots (Humanoids)*, pages 616–621, Madrid, Spain, November 2014.

[2] A. Frucci. Honda ASIMO can handle stairs like a Pro now. `http://www.gizmodo.com/227489/honda-asimo-can-handle-stairs-like-a-pro-now`, January 2007.

[3] J. Falconer. HERB the robot butler takes part in Oreo cookie challenge. `http://www.gizmag.com/herb-robot-butler-oreo-cookies/26614/`, March 2013.

[4] M. Ito. Neurophysiological aspects of the cerebellar motor control system. *International Journal of Neurology*, 7:162–176, 1970.

[5] R. A. Schmidt. A schema theory of discrete motor skill learning. *Psychological Review*, 82:225–260, 1975.

[6] D. M. Wolpert, R. C. Miall, and M. Kawato. Internal models in the cerebellum. *Trends in Cognitive Sciences*, 2:338–347, 1998.

[7] M. Kawato. Internal models for motor control and trajectory planning. *Current Opinion in Neurobiology*, 9:718–727, 1999.

[8] T. Flash and N. Hogan. The coordination of arm movements: An experimentally confirmed mathematical model. *Journal of Neuroscience*, 5:1688–1703, 1985.

[9] O. Bock. Early stages of load compensation in human aimed arm movements. *Behavioural Brain Research*, 55:61–68, 1993.

[10] R. Shadmehr and F. A. Mussa-Ivaldi. Adaptive representation of dynamics during learning of a motor task. *Journal of Neuroscience*, 14:3208–3224, 1994.

[11] D. L. Weeks, M.-P. Aubert, A. G. Feldman, and M. F. Levin. One-trial adaptation of movement to changes in load. *Journal of Neurophysiology*, 75:60–74, 1996.

[12] F. Gandolfo, F. A. Mussa-Ivaldi, and E. Bizzi. Motor learning by field approximation. *Proceedings of the National Academy of Sciences*, 93:3843–3846, 1996.

[13] S. J. Goodbody and D. M. Wolpert. Temporal and amplitude generalization in motor learning. *Journal of Neurophysiology*, 79:1825–1838, 1998.

[14] R. S. Johansson. *Sensory control of dexterous manipulation in humans*, pages 381–414. Academic Press, San Diego, CA, 1996.

[15] R. S. Johansson and G. Westling. Roles of glabrous skin receptors and sensorimotor memory in automatic control of precision grip when lifting rougher or more slippery objects. *Experimental Brain Research*, 56:550–564, 1984.

[16] R. S. Johansson and K. J. Cole. Sensory-motor coordination during grasping and manipulation actions. *Current Opinion in Neurobiology*, 2:815–823, 1992.

[17] G. Westling and R. S. Johansson. Responses in glabrous skin mechanoreceptors during precision grip in humans. *Experimental Brain Research*, 66:128–140, 1987.

[18] R. S. Johansson and G. Westling. Signals in tactile afferents from the finger eliciting adaptive motor responses during precision grip. *Experimental Brain Research*, 66:141–154, 1987.

[19] V. G. Macefield, C. Häger-Ross, and R. S. Johansson. Control of grip force during restraint of an object held between finger and thumb: Responses of cutaneous afferents from the digits. *Experimental Brain Research*, 108:155–171, 1996.

[20] V. G. Macefield and R. S. Johansson. Control of grip force during restraint of an object held between finger and thumb: Responses of muscle and joint afferents from the digits. *Experimental Brain Research*, 108:172–184, 1996.

[21] C. Hager-Ross and R. S. Johansson. Nondigital afferent input in reactive control of fingertip forces during precision grip. *Experimental Brain Research*, 110:131–141, 1996.

[22] J. R. Flanagan and A. M. Wing. The role of internal models in motion planning and control: evidence from grip force adjustments during movements of hand-held loads. *Journal of Neuroscience*, 17:1519–1528, 1997.

[23] D. A. Nowak, J. Hermsdorfer, S. Glasauer, L. Meyer, and N. Mai. The effects of digital anaesthesia on predictive grip force adjustments during vertical movements of a grasped object. *European Journal of Neuroscience*, 14:756–762, 2001.

[24] D. A. Nowak, S. Glasauer, L. Meyer, N. Mai, and J. Hermsdorfer. The role of cutaneous feedback for anticipatory grip force adjustments during object movements and externally imposed variation of the direction of gravity. *Somatosensory and Motor Research*, 19:49–60, 2002.

[25] D. R. Humphry and D. J. Reed. Separate cortical systems for control of joint movement and joint stiffness: Reciprocal activation and coactivation of antagonist muscles. *Advances in Neurology*, 39:347–372, 1983.

[26] N. Hogan, E. Bizzi, and F. A. Mussa-Ivaldi. Controlling multijoint motor behavior. *Exercise and Sport Sciences Reviews*, 15:153–190, 1987.

[27] N. Hogan. Planning and execution of multijoint movements. *Canadian Journal of Physiology and Pharmacology*, 66:508–517, 1988.

[28] S. J. Blakemore, S. J. Goodbody, and D. M. Wolpert. Predicting the consequences of our own actions: The role of sensorimotor context estimation. *Journal of Neuroscience*, 18:7511–7518, 1998.

[29] M. Kawato, T. Kuroda, H. Imamizu, N. Eri, S. Miyauchi, and T. Yoshioka. Internal forward models in the cerebellum: fMRI study on grip force and load force coupling. *Progress in Brain Research*, 142:171–188, 2003.

[30] J. R. Flanagan and A. M. Wing. Modulation of grip force with load force during point-to-point movements. *Experimental Brain Research*, 95:131–143, 1993.

[31] J. R. Flanagan, J. R. Tresilian, and A. M. Wing. Coupling of grip force and load force during arm movements with grasped objects. *Neuroscience Letters*, 152:53–56, 1993.

[32] J. R. Flanagan and J. R. Tresilian. Grip-load force coupling: A general control strategy for transporting objects. *Journal of Experimental Psychology: Human Perception and Performance*, 20:944–957, 1994.

[33] P. Lennie. The physiological basis of variations in visual latency. *Vision Research*, 21:815–824, 1981.

[34] J. H. R. Maunsell and J. R. Gibson. Visual latencies in striate cortex of the macaque monkey. *Journal of Neurophysiology*, 68:1332–1344, 1992.

[35] M. T. Schmolesky, Y. Wang, D. P. Hanes, K. G. Thompson, S. Leutger, J. D. Schall, and A. G. Leventhal. Signal timing across macaque visual system. *Journal of Neurophysiology*, 79:3272–3278, 1998.

[36] D. A. Robinson. *Basic mechanisms of ocular motility and their clinical implications*, chapter Oculomotor control signals. Oxford: Pergamom, 1975.

[37] L. M. Optican. Sensorimotor transformation for visually guided saccades. *Annals of the New York Academy of Sciences*, 1039:132–148, 2005.

[38] H. Chen-Harris, W. M. Joiner, V. Ethier, D. S. Zee, and R. Shadmehr. Adaptive control of saccades via internal feedback. *Journal of Neuroscience*, 28:2804–2813, 2008.

[39] D. A. Robinson, J. L. Gordon, and S. E. Gordon. A model of the smooth pursuit eye movement system. *Biological Cybernetics*, 55:43–57, 1986.

[40] M. Kawato. A hierachical neural-network model for control and learning of voluntary movement. *Biological Cybernetics*, 57:169–185, 1987.

[41] M. Katayama and M. Kawato. Virtual trajectory and stiffness ellipse during multijoint arm movement predicted by neural inverse models. *Biological Cybernetics*, 69:353–362, 1993.

[42] Y. Wada and M. Kawato. A neural network model for arm trajectory formation using forward and inverse dynamics models. *Neural Networks*, 6:919–932, 1993.

[43] R. C. Miall, D. J. Weir, D. M. Wolpert, and J. F. Stein. Is the cerebellum a smith predictor? *Journal of Motor Behavior*, 25:203–216, 1993.

[44] D. M. Wolpert, Z. Ghahramani, and M. I. Jordan. An internal model for sensorimotor integration. *Science*, 269:1880–1882, 1995.

[45] P. L. Gribble, D. J. Ostry, V. Sanguineti, and R. Laboissiere. Are complex control signals required for human arm movement? *Journal of Neurophysiology*, 79:1409–1424, 1998.

[46] N. Bhushan and R. Shadmehr. Computational nature of human adaptive control during learning of reaching movements in force fields. *Biological Cybernetics*, 81:39–60, 1999.

[47] J. B. Dingwell, C. D. Mah, and F. A. Mussa-Ivaldi. Manipulating objects with internal degrees of freedom: evidence for model-based control. *Journal of Neurophysiology*, 88:222–235, 2002.

[48] J-L. Vercher, F. Sares, J. Blouin, C. Bourdin, and G. M. Gauthier. Role of sensory information in updating internal models of the effector during arm tracking. *Progress in Brain Research*, 142:203–222, 2003.

[49] J. B. Dingwell, C. D. Mah, and F. A. Mussa-Ivaldi. Experimentally confirmed mathematical model for human control of a non-rigid object. *Journal of Neurophysiology*, 91:1158–1170, 2004.

[50] D. Liu and E. Todorov. Evidence for the flexible sensorimotor strategies predicted by optimal feedback control. *Journal of Neuroscience*, 27:9354–9368, 2007.

[51] E. Guigon, P. Baraduc, and M. Desmurget. Computational motor control: redundancy and invariance. *Journal of Neurophysiology*, 97:331–347, 2007.

[52] A. J. Nagengast, D. A. Braun, and D. M. Wolpert. Optimal control predicts human performance on objects with internal degrees of freedom. *PLOS Computational Biology*, 5:e1000419, 2009.

[53] D. J. Ostry and A. G. Feldman. A critical evaluation of the force control hypothesis in motor control. *Experimental Brain Research*, 221:275–288, 2003.

[54] B. Mehta and S. Schaal. Forward models in visuomotor control. *Journal of Neurophysiology*, 88:942–953, 2002.

[55] A. G. Feldman. Once more on the equilibrium-point hypothesis (lambda model) for motor control. *Journal of Motor Behavior*, 18:17–54, 1986.

[56] A. G. Feldman, D. J. Ostry, M. F. Levin, P. L. Gribble, and A. B. Mitnitski. Recent tests of the equilibrium-point hypothesis (λ model). *Motor Control*, 2:189–205, 1998.

[57] T. Flash and I. Gurevich. *Models of motor adaptation and impedance control in human arm movements*, pages 423–481. Elsevier North-Holland, Amsterdam, 1997.

[58] P. L. Gribble and D. J. Ostry. Compensation for loads during arm movements using equilibrium-point control. *Experimental Brain Research*, 135:474–482, 2000.

[59] A. G. Feldman and M. L. Latash. Testing hypotheses and the advancement of science: recent attempts to falsify the equilibrium point hypothesis. *Experimental Brain Research*, 161:91–103, 2005.

[60] Lennart Ljung. *System identification*. Springer, 1998.

[61] Jer-Nan Juang. *Applied System Identification*. Prentice Hall, 1994.

[62] R. Isermann and M. Münchhof. *Identification of Dynamic Systems An Introduction with Applications*. Springer, 2011.

[63] P. M. J. Van den Hof and R. J. P. Schrama. Identification and control–closed-loop issues. *Automatica*, 31(12):1751–1770, 1995.

[64] P. Van den Hof. Closed-loop issues in system identification. *Annual Reviews in Control*, 22:173–186, 1998.

[65] U. Forssell and L. Ljung. Closed-loop identification revisited. *Automatica*, 35:1215–1241, 1999.

[66] E. Itoh and S. Suzuki. Nonlinear approach for human internal models: Feedforward and feedback roles in pilot maneuver. In *IEEE International Conference on Systems, Man and Cybernetics*, volume 3, pages 2455–2462, 2005.

[67] F. M. Nieuwenhuizen, K. A. Beykirch, M. Mulder, and H. H. Bülthoff. Identification of pilot control behavior in a roll-lateral helicopter hover task. In *AIAA Modeling and Simulation Technologies Conference and Exhibit*, page 6799, Hilton Head, SC, 2007.

[68] M. Olivari, F. M. Nieuwenhuizen, J. Venrooij, H. H. Bülthoff, and L. Pollini. Multi-loop pilot behavior identification in response to simultaneous visual and haptic stimuli. In *AIAA Modeling and Simulation Technologies Conference*, page 4795, Minneapolis, MN, 2012.

[69] F. M. Nieuwenhuizen and H. H. Bülthoff. The MPI CyberMotion simulator: A novel research platform to investigate human control behavior. *Journal of Computing Science and Engineering*, 7(2):122–131, 2013.

[70] C. C. Macadam. Understanding and modeling the human driver. *Vehicle System Dynamics*, 40(1-3):101–134, 2003.

[71] J. Steen, H. J. Damveld, R. Happee, M. M. van Paassen, and M. Mulder. A review of visual driver models for system identification purposes. In *IEEE International Conference on Systems, Man, and Cybernetics*, pages 2093–2100, Anchorage, AK, 2011.

[72] E. Hellstrom and M. Jankovic. A driver model for velocity tracking with look-ahead. In *Proc. Amer. Contr. Conf.*, pages 3342–3347, Chicago, IL, 2015.

[73] T. Kiemel, Y. Zhang, and J. J. Jeka. Identification of neural feedback for upright stance in humans: Stabilization rather than sway minimization. *Journal of Neuroscience*, 31(42):15144–15153, 2011.

[74] F. M. Drop, D. M. Pool, H. J. Damveld, M. M. van Paassen, and M. Mulder. Identification of the feedforward component in manual control with predictable target signals. *IEEE Trans. Cybernetics*, 43(6):1936–1949, 2013.

[75] V. A. Laurense, D. M. Pool, H. J. Damveld, M. M. van Paassen, and M. Mulder. Effect of controlled element dynamics on human feedforward behavior in ramp-tracking tasks. *IEEE Trans. Cybernetics*, 45(2):253–265, 2015.

[76] B. Yu, R. B. Gillespie, J. S. Freudenberg, and J. A. Cook. Human control strategies in pursuit tracking with a disturbance input. In *Proc. Conf. Dec. Contr.*, pages 3795–3800, Los Angeles, CA, 2014.

[77] E. Roth, S. Sponberg, and N. J. Cowan. A comparative approach to closed-loop computation. *Current opinion in neurobiology*, 25:54–62, 2014.

[78] A. M. D'Amato, A. J. Ridley, and D. S. Bernstein. Retrospective-cost-based adaptive model refinement for the ionosphere and thermosphere. *Statistical Analysis and Data Mining*, 4:446–458, 2011.

[79] M. Roth, J. Leasage, and L. Litz. Block-box identification of discrete event systems with optimal partitioning of concurrent subsystems. In *Proc. Amer. Contr. Conf.*, pages 2601–2606, Baltimore, MD, June–July 2010.

[80] M. Suzuki, N. Takatsuki, J. Imura, and K. Aihara. Node knock-out based structure identification in networks of identical multi-dimensional subsystems. In *Proc. Euro. Contr. Conf.*, pages 2280–2285, Zurich, Switzerland, July 2013.

[81] J. C. Spall. Identification for systems with binary subsystems. *IEEE Trans. Auto. Contr.*, 59:3–17, 2014.

[82] S. Prakriya and D. Hatzinakos. Blind identification of linear subsystems of LTI-ZMNL-LTI models with cyclostationary inputs. *IEEE Trans. Sig. Proc.*, 45:2023–2036, 1997.

[83] W. Zhao and H. Chen. Recursive identification for Hammerstein system with ARX subsystem. In *Proc. Chin. Contr. Conf.*, pages 473–476, Harbin, China, August 2006.

[84] D. Schmid and G. Enzner. Robust subsystems for iterative multichannel blind system identification and equalization. In *Proc. Pacific Rim Conf. on Communications, Computers and Signal Processing*, pages 889–893, Victoria, Canada, August 2009.

[85] A. Fagergren, O. Ekeberg, and H. Forssberg. Precision grip force dynamics: A system identification approach. *IEEE Trans. Biomedical Engineering*, 47:1366–1375, 2000.

[86] A. Ghoreyshi and H. L. Galiana. Simultaneous identification of oculomotor subsystems using a hybrid system approach: Introducing hybrid extended least squares. *IEEE Trans. Biomedical Engineering*, 57:1089–1098, 2010.

[87] S. Hatakeyama, M. Iwase, and S. Yamaura. Analysis of human operation utilizing closed-loop identification method. In *Proc. IEEE Workshop on Intelligent Data Acquisition and Advanced Computing System: Technology and Applications*, pages 232–236, Sofia, Bulgaria, September 2005.

[88] S. Gillijns and B. D. Moor. Data-based subsystem identification for dynamic model updating. In *Proc. Conf. Dec. Contr.*, pages 3303–3308, San Diego, CA, December 2006.

[89] H. J. Palanthandalam-Madapusi, S. Gillijns, B. D. Moor, and D. S. Bernstein. Subsystem identification for nonlinear model updating. In *Proc. Amer. Contr. Conf.*, pages 3056–3061, Minneapolis, MN, June 2006.

[90] A. V. Morozov, A. A. Ali, A. M. D'Amato, A. J. Ridley, S. L. Kukreja, and D. S. Bernstein. Retrospective-cost-based model refinement for system emulation and subsystem identification. In *Proc. Conf. Dec. Contr.*, pages 2142–2147, Orlando, FL, December 2011.

[91] X. Zhang, S. Wang, T. M. Seigler, and J. B. Hoagg. A subsystem identification technique for modeling control strategies used by humans. In *Proc. Amer. Contr. Conf.*, pages 2827–2832, Portland, OR, June 2014.

[92] X. Zhang and J. B. Hoagg. Frequency-domain subsystem identification with application to modeling human control behavior. *Systems and Control Letters*, 87:36–46, 2016.

[93] R. Beals. *Analysis An Introduction*. Cambridge University Press, Cambridge, 2004.

[94] R. K. Sundaram. *A First Course in Optimization Theory*. Cambridge University Press, Cambridge, 1996.

[95] J. B. Hoagg, X. Zhang, S. Wang, and T. M. Seigler. The roles of feedback and feedforward as humans learn to control unknown dynamic systems. *IEEE Transactions on Cybernetics*, 2015 (under review).

[96] A. J. Bastian. Learning to predict the future: the cerebellum adapts feedforward movement control. *Current Opinion in Neurobiology*, 16:645–649, 2006.

[97] R. Shadmehr, M. A. Smith, and J. W. Krakauer. Error correction, sensory prediction, and adaptation in motor control. *Annual Review of Neuroscience*, 33:89–108, 2010.

[98] P. D. Neilson, M. D. Leilson, and N. J. O'Dwyer. Internal models and intermittency: A theoretical account of human tracking behavior. *Biological Cybernetics*, 58:101–112, 1988.

[99] C. G. Atkeson. Learning arm kinematics and dynamics. *Annual Review of Neuroscience*, 12:157–183, 1993.

[100] R. C. Miall and D. M. Wolpert. Forward models for physiological motor control. *Neural Networks*, 9:1265–1297, 1996.

[101] D. M. Wolpert and M. Kawato. Multiple paired forward and inverse models for motor control. *Neural Networks*, 11:1317–1329, 1998.

[102] E. Todorov and M. I. Jordan. Optimal feedback control theory as a theory of motor coordination. *Nature Neuroscience*, 5:1226–1235, 2002.

[103] S. Schaal, P. Mohajerian, and A. Ijspeert. Dynamic systems vs. optional control – a unifying view. *Progress in Brain Research*, 165:425–445, 2007.

[104] J. Diedrichsen, T. Verstynen, A. Hon, Y. Zhang, and R. B. Ivry. Illusions of force perception: The role of sensori-motor predictions, visual information, and motor errors. *Journal of Neurophysiology*, 97:3305–3313, 2007.

[105] E. Guigon, P. Baraduc, and M. Desmurget. Computational motor control: Redundancy and invariance. *Journal of Neurophysiology*, 97:331–347, 2007.

[106] D. T. McRuer and E. S. Krendel. The human control operator as a servo system element. *Journal of the Franklin Institute*, 6(267):511–536, 1959.

[107] D. T. McRuer, D. Graham, and E. S. Krendel. Manual control of a single-loop system: Part i. *Journal of the Franklin Institute*, 1(283):1–29, 1967.

[108] D. T. McRuer, D. Graham, and E. S. Krendel. Manual control of a single-loop system: Part ii. *Journal of the Franklin Institute*, 2(283):145–168, 1967.

[109] S. Franklin, D. M. Wolpert, and D. W. Franklin. Visuomotor feedback gains upregulate during the learning of novel dynamics. *Journal of Neurophysiology*, 108:467–478, 2012.

[110] X. Zhang and J. B. Hoagg. Subsystem identification of multivariable feedback and feedforward systems. *Automatica*, 2015 (under review).

[111] M. Suzuki and Y. Yamazaki. Velocity-based planning of rapid elbow movements expands the control scheme of the equilibrium point hypothesis. *Journal of Computational Neuroscience*, 18:131–149, 2005.

[112] W. Ford. *Numerical Linear Algebra with Applications: Using MATLAB*. Academic Press, 2014.

[113] X. Zhang, T. M. Seigler, and J. B. Hoagg. Modeling the control strategies that humans use to control nonminimum-phase systems. In *Proceedings of American Control Conference*, pages 471–476, Chicago, IL, July 2015.

[114] J. B. Hoagg and D. S. Bernstein. Nonminimum-phase zeros: Much to do about nothing. *IEEE Control Systems Magazine*, 27(3):45–57, 2007.

[115] B. G. Korenev and L. M. Reznikov. *Dynamic vibration absorbers: theory and technical applications*. John Wiley & Sons, 1993.

[116] L. B. Jemaa and E. J. Davison. Performance limitations in the robust servomechanism problem for discrete-time LTI systems. *IEEE Trans. Automat. Contr.*, 48:1299–1311, 2003.

[117] T. Norimatsu and M. Ito. On the zero non-regular control system. *J. Inst. Elect. Eng. Japan*, 81:566–575, 1961.

[118] T. Mita and H. Yoshida. Undershooting phenomenon and its control in linear multivariable servomechanisms. *IEEE Trans. Automat. Contr.*, 26:402–407, 1981.

[119] M. Vidyasagar. On undershoot and nonminimum phase zeros. *IEEE Trans. Automat. Contr.*, 31:440, 1986.

[120] D. W. Franklin, R. Osu, E. Burdet, M. Kawato, and T. E. Milner. Adaptation to stable and unstable dynamics achieved by combined impedance control and inverse dynamics model. *Journal of Neurophysiology*, 90:3270–3282, 2003.

[121] H. Whitney. *Complex Analytic Varieties*. Addison-Wesley Publishing Company, 1972.

[122] D. S. Bernstein. *Matrix Mathematics*. Princeton University Press, 2nd edition, 2009.

[123] G. F. Franklin, D. J. Powell, and M. L. Workman. *Digital Control of Dynamic Systems*. Prentice Hall, 3rd edition, 1997.

Vita

Xingye Zhang was born in Shenyang, China. After graduating from Shenyang No. 30 High School, he went to the Beihang University, also named as Beijing University of Aeronautics and Astronautics, to study systems and control, where he received a Bachelor of Science Degree in Information and Computation Science in 2009. Continued, he sought a Master of Engineering Degree in General and Fundamental Mechanics at Beihang University with a focus on mechanical vibration control in 2011. He landed in United States in August 2011 to pursue a doctoral degree in Mechanical Engineering at the University of Connecticut at first, then transferred to the University of Kentucky attracted by the human learning project in August 2012, where he is a Ph.D. candidate right now. During the time he is pursing the doctoral degree, he earned a Master of Arts Degree in Mathematics at University of Kentucky in May 2015.